Physically crosslinked thermo-responsive hydrogel nanofibres with tunable hydrophobicity based on poly(*N*-isopropyl acrylamide)-*graft*-poly(dimethyl siloxane)

by

Gestél Christine Kuyler

Thesis presented in fulfilment of the requirements for the degree of
Master of Science
in the Faculty of Science (Polymer Science) at Stellenbosch University

Supervisor: Prof P.E. Mallon

December 2019

Declaration

By submitting this thesis electronically, I declare that the entirety of the work contained therein is my own, original work, that I am the sole author thereof (save to the extent explicitly otherwise stated), that reproduction and publication thereof by Stellenbosch University will not infringe any third party rights and that I have not previously in its entirety or in part submitted it for obtaining any qualification.

December 2019

Abstract

A series of novel physically crosslinked amphiphilic hydrogels based on poly(*N*-isopropyl acrylamide)-*graft*-poly(dimethyl siloxane) (PNIPAM-*g*-PDMS) was synthesized using the simple macromonomer grafting-through technique. The hydrogel materials proved to be both water-insoluble and thermo-responsive. It was shown that the PDMS grafts produce physically crosslinked polymer networks due to intra- and interpolymer hydrophobic interactions of the PDMS side-chains. Structural elucidation and copolymer composition were determined by ATR-FTIR and ^{1}H-NMR spectroscopy. ^{1}H-NMR confirmed the macromonomer incorporation which correlated well with the feed ratios of each reaction. Chromatographic separation by HPLC revealed that the samples consisted of a PNIPAM homopolymer and PNIPAM-*g*-PDMS copolymer fraction. It was noted that the homopolymer fraction diminished with increased PDMS macromonomer in the feed. Increased PDMS content resulted in longer retention times during analysis which related to the increased hydrophobicity of the copolymers as a function of PDMS content. Molecular weight determination of these amphiphilic copolymers proved to be challenging. After analysis on different SEC solvent systems, AF4 allowed the determination of molecular weights ranging between 53 000 and 280 000 g/mol with dispersities of 1.1 to 1.8. The analytical obstacles confirmed the highly amphiphilic nature of these copolymers. The sufficiently high molecular weights and physical crosslinking of the copolymer systems allowed for solution processing from a common solvent. Hydrogel microfibres were fabricated by the electrospinning technique. An array of analytical techniques was utilized to characterize and analyse the copolymers in both thin film and microfibre form. Varying the amount of PDMS incorporated as well as the length of the PDMS side-chains had an observable effect on the physical properties of the material. This was most notable on the swelling of the hydrogel materials, but the relationship between the PDMS content and the lower critical solution temperature (LCST) of the copolymer hydrogels was more complex. Both the film and fibre form of all copolymers exhibited reversible thermo-responsive behaviour in aqueous solution. All samples underwent a phase transition at a specific LCST value. This LCST value was identified by a change from optically transparent to opaque and deswelling of the hydrogel material. PDMS incorporation resulted in a lowered LCST for all copolymers in film and fibre form compared to PNIPAM homopolymer, yet no definitive trend could be established. Conversely, increased PDMS content resulted in reduced equilibrium swelling. In the form of films, the low PDMS content materials swelled significantly in water reaching 50% saturation within 10 to 15 minutes. Microfibres exhibited rapid dimensional swelling, where the 2.9 mol.% 5 000 g/mol PDMS sample reached 115% swelling within 2 minutes. The stability of the materials in water and high humidity environments increased with increasing PDMS content. The films mostly remained structurally stable after repeated swelling cycles. The fibres, however, lost their individual fibrous structure after deswelling. The effect of PDMS incorporation was investigated by calculating the apparent crosslink density. It was shown that shorter PDMS side-chains resulted in a sharp initial increase in apparent crosslink density, after which more gradual increase occurred as a function of PDMS content. Longer PDMS side-chains,

Abstract

on the other hand, displayed a large incremental increase in apparent crosslink density as a function of PDMS content. Notable differences were found when comparing the swelling and LCST behaviour of the graft copolymers in the form of films and electrospun fibres produced from the same material. These differences were ascribed to the amount of incorporated PDMS as well as the differences in the solid-state morphology induced by different sample preparation techniques. These *smart* hydrogel materials proved to be capable of responding to surrounding temperature variations while also presenting the option for tunable hydrophobic character.

Opsomming

‘n Reeks unieke amfifiliese hidrogels gebaseer op poli(*N*-isopropiel akrilamied)-*ent*-poli(dimetielsiloksaan) (PNIPAM-*ent*-PDMS) is gesintetiseer deur middel van die makromonomeer “ent-deur”-tegniek. Die resulterende hidrogel materiaal is beide water-onoplosbaar en temperatuur-responsief. Die insluiting van die PDMS makromonomeer het gelei tot ‘n fisies kruisverbinde netwerk wat ontstaan as gevolg van die hidrofobiese intra- en interpolimeer interaksies tussen die hidrofobiese PDMS sykettings. Strukturele bevestiging en ko-polimeer komposisie is bepaal deur middel van ATR-FTIR en ^{1}H-KMR spektroskopie. ^{1}H-KMR het die makromonomeer inkorporasie, asook die goeie korrelasie tussen die voer verhouding van elke reaksie en die werklik geïnkorporeerde hoeveelheid, bevestig.

Kromatografiese skeiding deur middel van HPLC het aangedui dat die monsters uit ‘n PNIPAM homo-polimeer en PNIPAM-*ent*-PDMS ko-polimeerfraksie bestaan. ‘n Afname in die homo-polimeerfraksie met toename in PDMS makromonomeerinhoud is waargeneem. ‘n Toename in die PDMS inhoud het gelei tot langer retensietye tydens analiese wat ooreenstem met die toenemende hidrofobisiteit van die ko-polimere as ‘n funksie van PDMS inhoud. Die bepaling van die molekulêre massa van hierdie ko-polimere was uitdagend. Na vele analises in verskeie SEC sisteme met verskillende oplosmiddels, kon die molekulêre massa deur middel van AF4 bepaal word en het gewissel tussen 53 000 en 280 000 g/mol met dispersiteite van tussen 1.1 tot 1.8. Die analitiese struikelblokke wat ondervind is, het die hoogs amfifiliese geaardheid van hierdie ko-polimere bevestig. Die hoë molekulêre massa en die fisiese kruisverbinde natuur van die ko-polimeersisteem het toegelaat vir oplossing in ‘n algemene oplosmiddel. Hidrogel mikro-vesels is deur middel van die elekrospintegniek vervaardig. ‘n Verskeidenheid van analitiese tegnieke was onderneem om die ko-polimere in beide film en vesel vorm te analiseer en te karakteriseer. Wisselende hoeveelhede van geïnkorporeerde PDMS, asook die lengte van die PDMS sy-kettings het die fisiese eienskappe van die materiaal waarneembaar beïnvloed. Die effek van die PDMS inhoud was mees oplettend ten opsigte van die materiaal se water-opname eienskappe, alhoewel die effek van PDMS en die laer kritiese oplossings temperatuur (LKOT) van hierdie termo-responsiewe ko-polimeer hidrogels meer kompleks was. Beide die film en die vesel vorm van al die ko-polimere het omkeerbare termo-responsiwiteit vertoon in ‘n waterige oplossing. Al die monsters het by ‘n spesifieke LKOT waarde ‘n fase transisie ondergaan. Die LKOT waarde was geïdentifiseer deur ‘n verandering van opties deursigtig na ondeursigtig, asook deswelling van die hidrogel. PDMS inkorporasie het gelei tot ‘n laer LKOT waardes vir al die ko-polimere in beide film en vesel vorm in vergelyking met die PNIPAM homo-polimeer, alhoewel geen definitiewe tendens bevestig kon word nie. Aan die ander kant het verhoogde PDMS inhoud gelei tot verlaagde ekwilibrium swelling. In die vorm van films, het die lae PDMS inhoud monsters opmerkbare swelling in water vertoon en binne 10 tot 15 min 50% versadigheid bereik. Die mikro-vesels het vinnige dimensionele swelling vertoon, waar die vesels van die 2.9 mol.% 5 000 g/mol PDMS monster 115% swelling bereik het binne 2 min. Die stabiliteit van die vesels in water en hoë humiditeit omgewings, het toe geneem met toenemende PDMS

Opsomming

inhoud. Die films het meestal hul strukturele stabiliteit behou na herhaalde swelling siklusse. Die vesels het wel hul individuele veselagtige struktuur verloor na deswelling. Die effek van PDMS inkorporasie was ondersoek deur die oënskynlike kruisverbinde digtheid te bereken. Dit het getoon dat korter PDMS sy-kettings tot ‘n skerp aanvanklike toename in die oënskynlike kruisverbinde digtheid gelei het, waarna ‘n meer geleidelike toename as ‘n funksie van PDMS inhoud plaas gevind het. Langer PDMS sy-kettings het groot inkrementele toename in die oënskynlike kruisverbinde digtheid as a funksie van PDMS inhoud vertoon. Opmerklike verskille in die swelling en die LKOT van dieselfde ko-polimere in die vorm van films en geëlektrospinde vesels het bestaan wanneer hierdie twee vorme van dieselfde materiaal vergelyk word. Hierdie verskille was toegeskryf aan die geïnkorporeerde hoeveelheid PDMS asook die verskille in die soliede-fase morfologie wat deur verskillende voorbereidings metodes geïnduseer word. Dit was bewys dat hierdie *slim* hidrogels instaat was om op omliggende temperatuur variasies te reageer terwyl dit ook die opsie vir verstelbare hidrofobisiteit bied.

Acknowledgements

I would like to thank the following people for their assistance throughout the course of this project:

Prof Mallon for presenting me with the opportunity to do this project.

Prof Klumperman, Dr Rueben Pfukwa and the free radical group members for all the exciting group meetings.

Dr Helen Pfukwa and the Pasch group members for all their help and patience with HPLC analysis.

Prof Lederer and her team (Susanne Boye, Martin Geisler, Johanna Engelke and Christina Harnisch) for their willingness and assistance with AF4 analysis.

Elsa Malherbe for all the NMR analyses.

The academic staff and personnel in the department for their kind assistance.

MGH and associates for the financial and emotional support.

Hildegard, Mauritz and Annerike: Thank you for the coffees, lunches and cheerful pep-talks.

Lab partners Lambert and Stacey, as well as the occupants of Office 1042.

My family and friends, especially my parents (George and Christél) and two sisters (Chanté and Christéllie). Thank you for your undying support, encouragement and love. Thank you for your enthusiasm and always showing interest in my studies.

Lastly, I would like to thank Ludwig for being there every step of the way.
Thank you for your kind and loving spirit, invaluable support and constant motivation.

Glossary

Abbreviations & Notations

a_o	Contact area
AA	Acetic acid
AF4	Asymmetric flow field flow fractionation
AFM	Atomic force microscopy
AIBN	2,2'-Azobisisobutyronitrile
APCN	Amphiphilic cone network
ATR	Attenuated total reflectance
ATRP	Atom transfer radical polymerization
BHT	Butylated hydroxytoluene
$CDCl_3$	Deuterated chloroform-d
χ	Interaction parameter
DCM	dichloromethane
δ	Chemical shift (NMR)
DMF	Dimethylformamide
EGDMA	Ethylene glycol dimethyl acrylate
ELSD	Evaporative light scattering detector
EtTrp	Tryptophan ethyl ester
FE-SEM	Field emission scanning electron microscopy
FTIR	Fourier transform infrared
FWHM	Full width at half maximum
GEC	Gradient elution chromatography
HMAAM	*N*-hydroxymethyl acrylamide
HPC	Hydroxypropyl cellulose
HPLC	High performance liquid chromatography
IPN	Interpenetrating network
l_c	Critical chain length
LCST	Lower critical solution temperature
MALS	Multi-angle light scattering
MEK	Methyl ethyl ketone
µL	Microliter
µm	Micrometre
M_n	Number average molecular weight
mol.%	Mole percentage
M_w	Weight average molecular weight
MWCO	Molecular weight cut-off
N	Crosslink density (mol/dm^3)

Glossary

*n*BuA	*n*-Butyl acrylate
NIPAM	*N*-isopropyl acrylamide
NMR	Nuclear magnetic resonance
p	Packing parameter
PAA	Poly(acrylic acid)
PAN	Poly(acrylonitrile)
PDMAA	Poly(*N, N'*-dimethyl acrylamide)
PDMAEA	Poly(2-(dimethylamino)ethyl acrylate)
PDMS	Poly(dimethyl siloxane)
PEA	Poly(ethyl acrylate)
PEO	Poly(ethylene oxide)
PHEMA	Poly(2-hydroxyethyl methacrylate)
PMMA	Poly(methyl methacrylate)
PNIPAM	Poly(*N*-isopropyl acrylamide)
PPO	Poly(phenylene oxide)
PPP	Plyphosphazene
PS	Polystyrene
PVA	Poly(vinyl alcohol)
PVME	Poly(vinyl methyl ether)
Q	Q-value (swelling in water)
Q_s	Q-value (swellable fraction PNIPAM)
QELS	Quasi elastic light scattering
R	Gas constant (8.3145 J/mol.K)
r.H.	Relative humidity
r_A	Radical reactivity ratio
RAFT	Reversible addition-fragmentation chain-transfer polymerization
RI	Refractive index
SA	Stearyl acrylate
SCA	Static contact angle
SAXS	Small-angle X-ray scattering
SEC	Size exclusion chromatography
SEM	Scanning electron microscopy
SET-LRP	Single electron transfer living radical polymerization
t.c.d.	Tip-to-collector distance
THF	Tetrahydrofuran
UCST	Upper critical solution temperature
$v_{bb,s}$	Excluded volume parameter for backbone

Glossary

υ_{brs}	Excluded volume parameter for grafts
UV/Vis	Ultraviolet/visible light
υ_p	Polymer volume fraction
w/v	Weight to volume ratio
wt.%	Weight percentage
Z	Z-value (swelling in hexane)
Z_s	Z-value (swellable faction PDMS)

Table of Contents

Table of Contents

Table of Contents

Table of Figures

Chapter 2:

Table of Figures

Table of Figures

Table of Figures

.

Table of Tables

Chapter 4:

Table of Equations

Chapter 2

Chapter 4

Chapter 1

Introduction & Objectives

1.1. Introduction

The design and fabrication of innovative polymeric materials have gained considerable attention in recent years, especially in the field of stimuli-responsive hydrogel materials. Hydrogels can be described as chemically or physically crosslinked polymeric networks with the ability to swell and retain their structure without undergoing complete dissolution.[1] The hydrophilic structures within hydrogels render them capable of retaining large quantities of water within their three-dimensional networks.[2] Some crosslinking mechanism is, however, required to produce a water-insoluble polymeric network. This is commonly done by the introduction of covalent or chemical crosslinks but may also be achieved by non-covalent or physical interactions within the polymer network. In recent years, much focus has been placed on the development of materials that can alter their structure and/or physical properties in response to either chemical or physical external stimuli. These materials are identified as stimuli-responsive, or *smart* polymers. Polymers that specifically respond to surrounding temperature variations by undergoing a reversible phase transition are known as thermo-responsive polymers.[3,4] Hydrogels of these materials have been explored for the development of temperature-triggered intelligent devices applications in areas of photonics, sensors, drug delivery, and optical devices.[1,5] The ability to control the properties of polymer systems by external stimulus is highly desirable in the area of smart material fabrication. This enables the material to be triggered by the alteration of external environmental conditions to perform functions on demand. Achieving both fast response and structural integrity in an aqueous solution during repeated volume changes has, however, been the most significant challenge for thermo-responsive hydrogels.

The focus of the current study is the development of thermo-responsive hydrogel materials by means of non-covalent, physical crosslinking. This may be achieved by the introduction of a hydrophobic comonomer, generating a physically crosslinked inter-polymer network through hydrophobic interactions. These water-insoluble segments form clusters that act as the linkages between the polymeric chains. The physical crosslinking of these materials is not only a simpler crosslinking method as it eliminates the need for additional chemical treatment, but also allow for solution processing from a common solvent for the production of hydrogel nanofibres. This would not be possible in the case of an insoluble chemically crosslinked system unless post-electrospin crosslinking was employed. Thermo-responsive hydrogel nanofibres with large surface-to-volume ratios and nonwoven fibrous structure allow for rapid hydration and dehydration response which is highly desired in many applications.

In an attempt to improve the water-stability of the widely studied thermo-responsive hydrophilic monomer, *N*-isopropyl acrylamide (NIPAM), it will be copolymerized with methacryloxy propyl terminated poly(dimethyl siloxane) (PDMS) macromonomer of varying lengths for the production of graft copolymers through free radical polymerization. To our knowledge, no literature exists on such

an amphiphilic graft copolymer system rendering a physically crosslinked hydrogel material. However, materials of PNIPAM and PDMS synthesized by different techniques have been developed and reported. Some work on interpenetrating polymer networks (IPN's) of PNIPAM and PDMS have been reported for the use of ophthalmic biomaterials.[6] The grafting of PNIPAM chains onto PDMS surfaces is often seen in literature with applications in tissue engineering[7], fluid manipulation in microfluid chips and cell culture.[8,9] Since no work could be found on the production of PNIPAM-*g*-PDMS by the grating-through technique, it is assumed that no reports exist on the production of hydrogel nanofibres from these materials.

The physically crosslinked hydrogel materials developed in this work will be comprehensively characterized and analysed by an array of analytical techniques. The correlation between the PDMS content, side-chain length and swelling behaviour of this material in both thin film and nanofibre form will be extensively explored. Since the crosslinking of these materials is morphology dependent, it is imperative to understand the effect of hydrophobic comonomer incorporation on the material's swelling and thermo-responsive behaviour.

1.2. Objectives

A summary of the key objectives of this work:

- Synthesis of a novel amphiphilic hydrogel with the following requirements:
  - Non-covalent or physically crosslinked system where hydrophobic interactions arising from the presence of the PDMS macromonomer, act as linkages between neighbouring polymer chains.
  - Display amphiphilic behaviour through the ability to swell in both water and non-polar solvents such as hexane without undergoing complete dissolution.
  - Conversely, these materials should still be soluble in certain organic solvents to allow solution processing and analysis.
  - The obtained copolymers should have improved physical properties and water-stability compared to the PNIPAM homopolymer.
  - The copolymers should display thermo-responsive behaviour at temperatures other than that of the PNIPAM homopolymer.
- Structural elucidation of the synthesized hydrogel materials by ATR-FTIR and ^{1}H-NMR.
- SEC, HPLC and AF4 for the determination of molecular weight, molecular weight distributions and chemical composition of the material.
- Production of thin film hydrogels by solvent casting.
- Production of nanofibre hydrogels by the electrospinning technique.

- Full characterization and analysis of both the film and nanofibre form of the obtained copolymers.
  - SEM for the visual investigation of fibre surface morphology.
  - Swelling and water stability studies.
  - LCST measurements and investigation of thermo-responsiveness.
  - Static contact angle measurement of film and fibre surfaces to investigate surface hydrophobicity.

1.3. References

1 J. Maitra and V. K. Shukla, *Am. J. Polym. Sci.*, 2014, **4**, 25–31.

2 E. M. Ahmed, *J. Adv. Res.*, 2015, **6**, 105–21.

3 J. F. Lutz, *J. Polym. Sci. Part A Polym. Chem.*, 2008, **46**, 3459–3470.

4 M. M. Fares and A. A. Othman, *J. Appl. Polym. Sci.*, 2008, **110**, 2815–2825.

5 J. Zhang, L. Y. Chu, C. J. Cheng, D. F. Mi, M. Y. Zhou and X. J. Ju, *Polymer (Guildf).*, 2008, **49**, 2595–2603.

6 L. Liu and H. Sheardown, *Biomaterials*, 2005, **26**, 233–244.

7 J. B. Lin, B. C. Isenberg, Y. Shen, K. Schorsch, O. V. Sazonova and J. Y. Wong, *Colloids Surfaces B Biointerfaces*, 2012, **99**, 108–115.

8 J. Zhou, D. A. Khodakov, A. V. Ellis and N. H. Voelcker, *Electrophoresis*, 2012, 33, 89–104.

9 D. Ma, H. Chen, D. Shi, Z. Li and J. Wang, *J. Colloid Interface Sci.*, 2009, **332**, 85–90.

Chapter 2

Literature Review

2.1. Hydrogel introduction and classification

2.1.1. Introduction to hydrogels

Hydrogels may be described as chemically or physically crosslinked water-insoluble polymeric networks with the ability to swell and retain a substantial fraction of water within their structure without undergoing complete dissolution in aqueous solution.[1–4] The three-dimensional network structure may be achieved by either chemical or physical crosslinking.[5] The hydrophilic structures within hydrogels render these materials capable of retaining large quantities of water in their three-dimensional networks.[1] Over the past few decades, hydrogels have received considerable attention due to exceptional promise in a wide range of applications such as agriculture, hygienic products, sealing and food additives. Significant progress in recent years has led to the development of several biomedical hydrogel applications, including drug delivery systems, pharmaceuticals, tissue engineering and regenerative medicine, wound dressing and biosensors.[1,4,6–11] The use of hydrogel materials in biomedical applications dates back to work done by Wichterle and Lim in 1960, in the development of crosslinked poly(hydroxyethyl methacrylate) (PHEMA). The first synthetic hydrogels for biological use consisted of HEMA with ethylene glycol dimethyl acrylate (EGDMA) crosslinker. These materials were later used in the commercial production of contact lenses, which led to further development of hydrogels in drug release and delivery systems.[12]

2.1.2. Classification of hydrogels by crosslinking

Crosslinking in polymer chemistry is a stabilization process in which a network structure is formed by the multidimensional extension of polymeric chains, where the actual crosslink is a bond linking one polymer chain to another. A liquid polymer can be changed into a gel or solid by crosslinking by restricting the ability of individual polymer chains to move. A polymer's physical properties are affected by the addition of crosslinks. This depends on the degree of crosslinking and whether or not crystallinity is present.[7] The crosslinking mechanism used during hydrogel formation allows for the classification between chemical or physical hydrogels.

The covalent crosslinking of polymers produces chemical or non-reversible hydrogels. This is commonly done by using bifunctional monomers. A network of crosslinked polymeric chains gives rise to an insoluble macromolecular polymer gel. These polymeric hydrogels are synthesized by either step or chain growth reactions of hydrophilic monomers together with functional crosslinkable monomers to assist in network formation. The type and degree of crosslinking employed have a significant influence on hydrogel properties such as elastic modulus, swelling abilities and molecular transport.[5] Chemical or non-reversible crosslinking is widely used to produce hydrogels with excellent mechanical strength due to the covalent linkages between polymeric chains. However, often further chemical processing is required to extract potential toxic crosslinking agents used in the hydrogel synthesis. These potentially toxic crosslinking agents may also result in undesirable

reactions with bioactive substances present in the hydrogel matrix.[2,7] In the case of nanofibre hydrogels produced by electrospinning, the nanofibres require post-electrospin crosslinking since the covalently crosslinked material is not solution processable. The adverse effects of chemical crosslinking may be avoided by the process of physical crosslinking.

The polymeric networks of physical hydrogels are held together by secondary forces. Physical crosslinks include hydrogen bonding, chain entanglement, crystallite formation and hydrophobic interactions.[3] The nature of physical crosslinks may not be permanent but is sufficient in making hydrogels insoluble in aqueous solution. Reversible water-absorbing hydrogels can be produced by physical crosslinking, albeit network defects or inhomogeneities exist since clusters are formed by molecular entanglement, hydrophobic- or ionic-associated domains.[7,9,13] Physical crosslinking of hydrogel materials is also beneficial in terms of solution processing, especially in the case of hydrogel nanofibre production, since no post-electrospin crosslinking or removal of crosslinking agents is required.

In this study, physical crosslinking is used for the production of novel thermo-responsive poly(*N*-isopropyl acrylamide)-*graft*–poly(dimethylsiloxane) (PNIPAM-*g*-PDMS) hydrogel materials. The hydrophobic PDMS domains in this system act as crosslinker by allowing the formation of linkages via hydrophobic interactions that arise from the introduction of the hydrophobic side-chains. These water-insoluble segments form clusters that act as the linkages between the polymeric chains. The physical crosslinking of these materials allowed for solution processing from a common solvent for the production of hydrogel nanofibres. These nanofibre hydrogels are also reversible since redissolution in a common solvent is possible. A potential negative factor in using such hydrophobic interactions as physical crosslinks is that these materials are expected to be less dimensionally stable relative to covalently crosslinked hydrogels, particularly under mechanical deformation.

2.1.3. Factors affecting swelling of hydrogels

One of the most important factors that affect the swelling of hydrogels is the crosslinking ratio. This is defined as the ratio between the mole amounts of crosslinking agent to the mole amount of polymer repeat units. Thus, the higher the crosslinking ratio, the higher the amount of incorporated crosslinking agent in the hydrogel structure, resulting in decreased swelling ability compared to an equivalent hydrogel with a lower crosslinking ratio. Since crosslinking binds polymer chains together, it hinders the mobility of polymer chains and thus lowers the swelling ratio.[14]

Another factor to consider is the chemical structure of the polymer. Hydrogels containing highly hydrophilic polymer and a larger fraction thereof will evidently have a higher swelling ratio compared to hydrogels containing more hydrophobic groups. Hydrophobic groups on the polymeric chains collapse in the presence of water, thus minimizing their exposure to surrounding water molecules

and will consequently swell much less than hydrogels containing more hydrophilic groups within its structure.[14]

When considering stimuli-responsive hydrogels or environmentally-sensitive materials, swelling is affected by specific stimuli.[14] Thermo-responsive hydrogels are, for example, affected by temperature changes in the swelling media.[14,15] Numerous examples of stimuli-responsive hydrogels and the stimuli that affect their swelling exists. Some of these will be discussed in the following sections.

2.2. Stimuli-responsive behaviour and the phase transition phenomenon

2.2.1. Stimuli-responsive polymers

In recent years, much focus has been placed on the development of materials that can alter their own structure and/or physical properties in response to either chemical or physical external stimuli. These materials are known as *intelligent* or *smart* materials, also referred to as *stimuli-responsive* polymers. Stimuli-responsive hydrogel materials may be classified according to the stimuli that render a response. Stimuli include temperature, pH, light, variation in ionic strength, electrical charges and magnetic field variations.[16,17] Stimuli-responsive polymers can further be classified by the physical form they take on after a stimulus is applied, as illustrated in Figure 2-1:

i) Linear free chains in solution, where the individual polymer chains undergo reversible collapse after application of an external stimulus.

ii) Chains adsorbed or grafted onto a surface, where the individual polymer chains adsorb or collapse on the given surface once the external stimulus is applied. This may result in the conversion of a hydrophilic to a hydrophobic interface.

iii) Covalently or physically crosslinked hydrogels, where environmental variations cause a change in either micro- or macroscopic gel networks' swelling behaviour.[18]

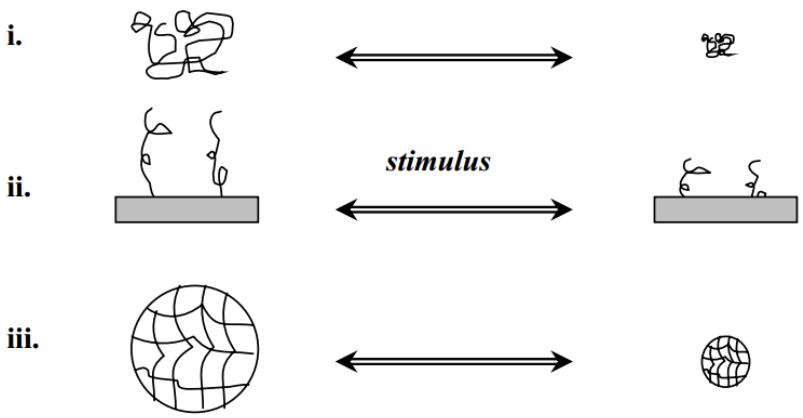

Figure 2-1: Classification of stimuli-responsive polymers according to their physical form.[19]

2.2.2. Thermo-responsive polymers

The focus of this study will be on materials that respond to external temperature stimuli, also known as *thermo-responsive* polymers, and their corresponding hydrogel materials. Thermo-responsive hydrogels are defined as hydrogels capable of responding to variations in its surrounding temperature by swelling and de-swelling in solution.[20] The ability to control the properties of polymer systems by external stimulus is highly desirable in the area of smart material fabrication. This enables the material to be triggered by the alteration of external environmental conditions to perform functions on demand. Smart polymeric hydrogels have been widely studied in the development of temperature-triggered intelligent devices in diverse fields of application such as sensors[21], photonics[22], optical devices[23], actuators[24], tissue engeneering[16] and drug delivery.[8] Significant differences in the swelling and de-swelling kinetics of thermo-responsive hydrogels may be ascribed to differences in structure and chemical composition, as well as its physical assembly. One of the most significant challenges for the synthesis of thermo-responsive hydrogels has been to achieve both structural integrity and rapid response of the hydrogel when exposed to the stimuli.[20,25]

2.2.2.1. Lower and upper critical solution temperatures

Based on the response to temperature variations, thermo-responsive polymers can be categorized as having a lower critical solution temperature (LCST) where the polymer is insoluble above a certain temperature. This is also known as negative temperature-sensitive polymers. Or it can have an upper critical solution temperature (UCST) where the polymer is insoluble below a certain temperature, also known as positive temperature-sensitive polymers. The phase transition phenomena are illustrated in Figure 2-2.

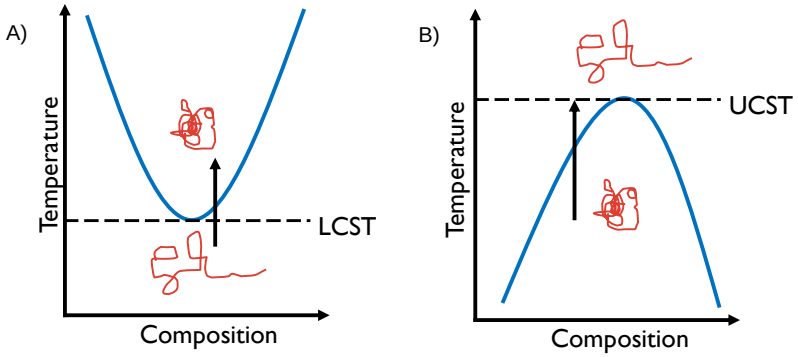

Figure 2-2: Phase transition phenomenon. (A) Lower critical solution temperature (LCST) and (B) upper critical solution temperature (UCST) phase transition behaviour of thermo-responsive polymers in solution.

In the case of polymers with an LCST, the solubility of the polymer in solution decreases with increasing temperature and phase separation occurs above its critical temperature value. Materials exhibiting an LCST undergo a negative volume transition where the polymer chains undergo coil-to-globule transition above its critical temperature. Considering the above phase diagrams, the LCST for polymers in aqueous solution is the point at which the entropy (S) of water in the system increases

due to increased disorder of the water molecules and thus overtakes the enthalpy (H) of the water bonded to the polymer chains by hydrogen bonding. Therefore, the LCST is governed by the entropy of the system.[26] Conversely, the UCST is governed by the enthalpy of the system. In recent studies, it has been shown that the phase transition and the hydrated random coil to hydrophobic globule transition is caused by both hydrophobic interactions and hydrogen bonding in most polymer-solvent systems.[16]

2.2.2.2. Thermodynamics of the temperature-induced phase transition

The thermodynamic feasibility of a process is determined by the Gibbs free energy (ΔG) in:

$$\Delta G = \Delta H - T\Delta S, \text{ where } T \text{ is the temperature.}$$

For the process to be thermodynamically viable, ΔG should be negative at the given reaction conditions. A variety of interactions between the solvent and polymer is involved in the dissolution of the polymer in a specific solvent.

For spontaneous dissolution of a polymer in a solvent to occur and result in a homogenous system, the overall outcome of all interactions involved between the polymer and solvent should result in a negative value for ΔG, which can be achieved by a balance between the enthalpy (ΔH) and the entropy term ($-T\Delta S$). Thus, if ΔH is negative and ΔS increases, $T\Delta S$ will increase and result in decreased ΔG. If a positive value is calculated for ΔG for a given polymer system at a certain temperature, polymer immiscibility in that specific solvent under the specified conditions will occur and result in two different polymer and solvent phases.

The Gibbs free energy is negative for polymers exhibiting LCST behaviour at temperatures below its critical solution temperature, thus these polymers tend to be dissolved in aqueous solutions at those temperatures. The hydrophilic segment of the polymer is hydrated and thus surrounded by a thin layer of water molecules from the aqueous solvent system, resulting in a negative enthalpy for the dissolution process. The hydrophobic segments of the polymer chain causes extensive hydrogen bonding in surrounding water molecules resulting in the formation of a structured arrangement of water molecules around these hydrophobic segments, which in turn is a contributing factor to the negative value of the entropy of the reaction (ΔS).[16] When the temperature of the polymer-aqueous solvent system increases, the system's entropy (ΔS) also increases. As a result of the increased system entropy, hydrogen bonding is broken, leading to the collapse of the polymer chain's hydration shell formed by the surrounding water molecules. The water molecules that form part of the hydration shell is released into the bulk of the solution, causing a further increase in the overall entropy of the system, which is now greater than the negative enthalpy (ΔH) of the reaction, resulting in a positive Gibbs free energy (ΔG) value. The breaking of hydrogen bonds and the consequential loss of the polymer chain's hydration shell results in a significant increase in hydrophobic interaction between the hydrophobic segments of the polymer chain with itself, as well as with surrounding polymer

chains. These intra- and intermolecular hydrophobic interactions result in chain collapse and intermolecular aggregation. This leads to phase separation and ultimately the suppression of conformational changes of polymer chains, causing a decrease in both enthalpy and entropy. Figure 2-3 illustrates the chain collapse in the coil-to-globule transition with increasing temperature of polymers exhibiting LCST behaviour in aqueous solution.

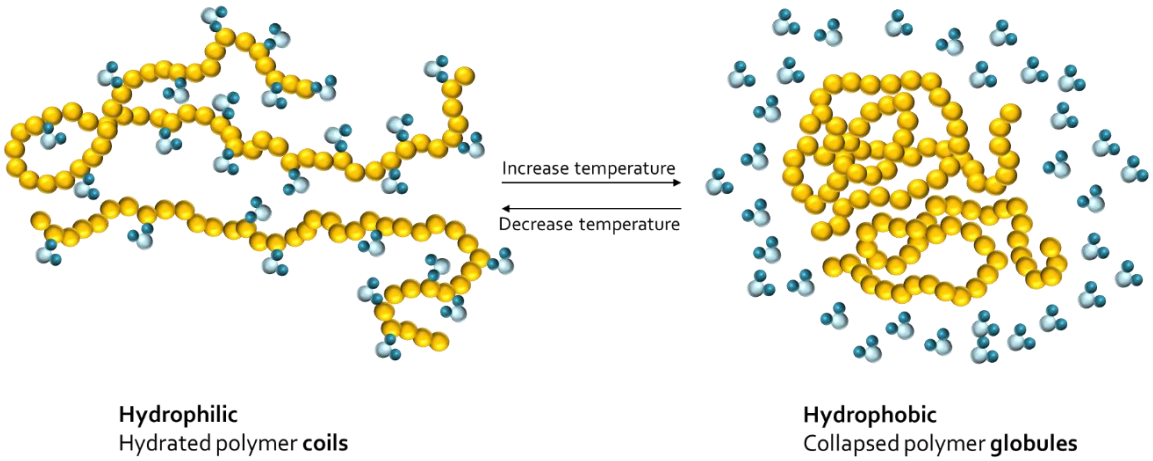

Figure 2-3: Polymer chains exhibiting a lower critical solution temperature (LCST) which undergoes coil-to-globule transition above its critical solution temperature.

For polymers exhibiting UCST behaviour in solution, both enthalpy and entropy are positive below a certain temperature. Opposite behaviour to that shown by polymers exhibiting an LCST is observed since the enthalpy and entropy decreases with increasing temperature in UCST polymer solutions.[16]

2.2.3. PNIPAM-*g*-PDMS as a system of interest

In this study, a series of physically crosslinked amphiphilic hydrogels based on poly(*N*-isopropyl acrylamide)-*graft*-poly(dimethyl siloxane) is synthesized. The thermo-responsive nature of these hydrogels can be attributed to the incorporation of poly(*N*-isopropyl acrylamide) (PNIPAM) which is a widely studied thermo-responsive polymer.[17] The popularity of PNIPAM is not only evident in the biomedical field, but also in other fields as illustrated in Figure 2-4 below.

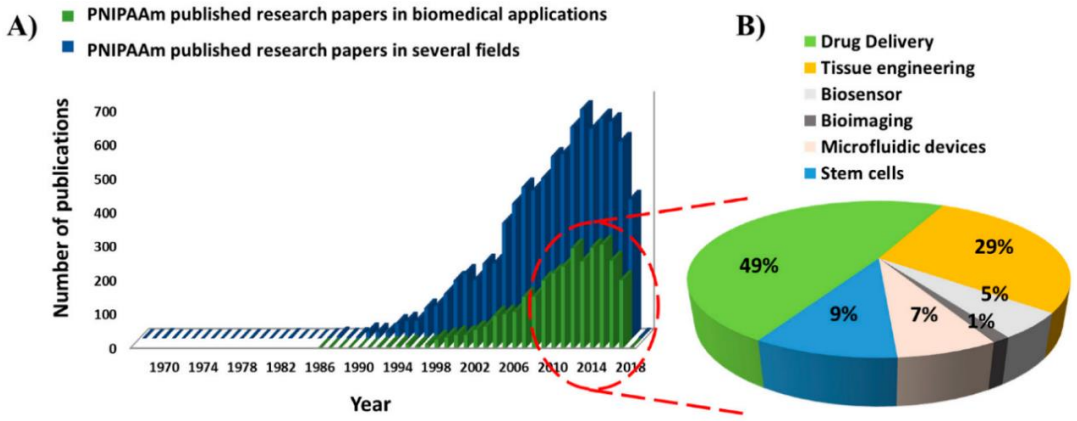

Figure 2-4:(A) Annual evolution of PNIPAM related published research articles, based on its application in biomedical and other fields. (B) Percentage of published research articles based on PNIPAM applications in the biomedical field.[6]

PNIPAM exhibits a lower critical solution temperature (LCST) at around 32 °C in aqueous solution.[6] This phase transition temperature is induced by the balance between the stabilizing hydrogen bonds among the hydrophilic amide group of the NIPAM monomer units and water, and the competitive hydrophobic effect induced by the carbon backbone in addition to the hydrophobic isopropyl segments. Figure 2-5 illustrates the hydrophilic and hydrophobic moieties present within the NIPAM monomer. The thermo-responsive behaviour of the PNIPAM homopolymer is a consequence of the amphiphilicity of the polymer chains.[27,28]

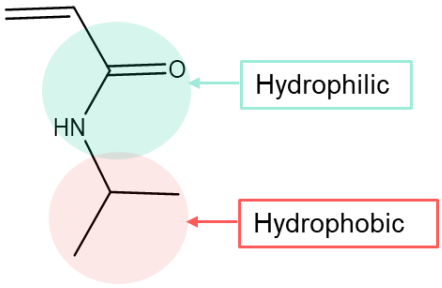

Figure 2-5: Chemical structure of NIPAM monomer and its hydrophilic and hydrophobic moieties.

The homopolymer of PNIPAM is water-soluble below its LCST due to its intra- and intermolecular hydrogen bonding between the NIPAM amide groups and water molecules. These favourable polymer-water interactions cause the polymer chains to exist in solvated, expanded coil conformations resulting in a transparent homogeneous aqueous solution. However, weakened hydrogen bonding between the amide groups and water molecules result from increased temperature. Above the LCST the hydrophobic interactions among the isopropyl groups dominate and result in a sudden transition from hydrophilic to hydrophobic behaviour of the material. This is due to molecular rearrangement and hydrophobic collapse of the polymer chains to globule state. Thus the polymer-polymer interactions are now thermodynamically favoured as compared to the polymer-water interactions.[8,28] Subsequently, the imbibed water within the polymeric structure is expelled as the polymer undergoes a temperature-induced negative volume phase transition, resulting in dehydration and significant shrinkage.[25,29] This signifies the coil-to-globule transition of PNIPAM in aqueous solution.[20,30]

Since the LCST of PNIPAM is between that of room temperature and physiological temperature, its thermo-responsive behaviour may be very useful in biomedical and drug delivery applications. The LCST may be altered by copolymerization of PNIPAM with other monomers resulting in an altered balance between the hydrophobic and hydrophilic interaction within the polymeric network.[28,31]

The hydrogel materials in this study are produced by the copolymerization of NIPAM with PDMS macromonomers of varying lengths to allow tunable hydrophobicity of the materials. PDMS is a silicone elastomer with desirable properties that make it attractive for components in microfluidic devices,[32] biomedical[33] and optical applications.[34] PDMS is widely used due to its potential high

crystallinity, high liquid viscosity and non-flammable, inert nature. PDMS is inherently hydrophobic, however, certain applications require temporary hydrophilicity rendered by surface exposure to oxygen plasma. Long, highly flexible macromolecular chains along with the high flexibility of the siloxane backbone, provide rubber-like elasticity.[35] The combination of very low methyl-methyl interactions among neighbouring chains and high siloxane chain flexibility produces a PDMS elastomer system with exceptionally low glass transition (-123 °C) and melting transitions (dual points at -37 °C and -45 °C). These fundamental characteristics result in other technologically useful consequences such as low surface energy and solubility parameters, and high gas permeability.[35] Thus making PDMS an attractive choice as hydrophobic macromonomer for this amphiphilic copolymer system.

2.3. Synthesis of graft copolymers

2.3.1. Copolymers and polymerization techniques

Copolymers may be described as macromolecules that contain more than one type of monomer unit within its polymeric chain. Figure 2-6 illustrates the many types of copolymer chain topologies that exist, such as statistical, gradient and segmented copolymers (grafts and blocks).[36] Chain architectures can, however, vary between comb, multi-arm stars and dendrimers, or even growth from functionalized surfaces with nearly limitless possibilities for compositional modification.

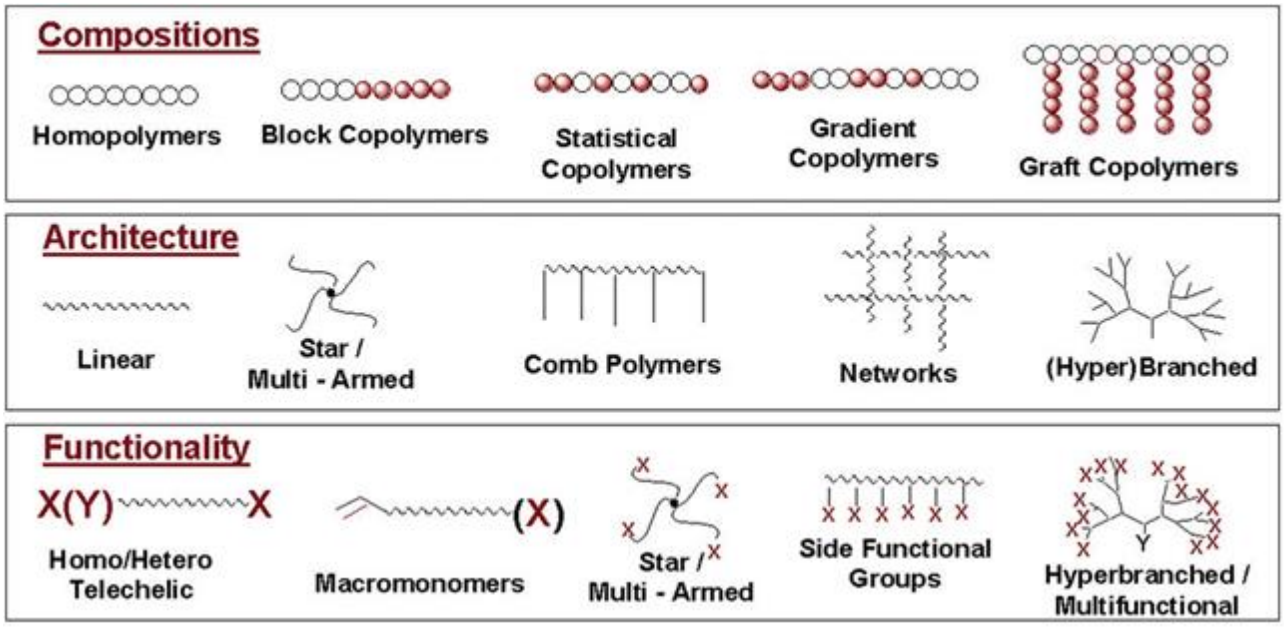

Figure 2-6: Possible molecular structures of polymers with regards to architecture, chain topologies and end-group functionality. Illustration adapted from reference.[37]

Well-defined polymers with structure-property correlation based on chain topology, architecture, or composition may be synthesized with the advent of ionic living polymerization.[38] However, limitations such as available polymerizable monomers do exist. This results from the incompatibility between monomers and the reactive centres. Conversely, free radical polymerizations suffer from fewer

drawbacks since free radicals are less discriminating when reacting to different types of vinyl monomers and can tolerate many functionalities. This is advantageous since it allows for the preparation of statistical and segmented copolymers, especially based on various acrylate and methacrylate monomer combinations which is not possible with ionic methods.[36]

In this study, the focus is on conventional free radical copolymerization making use of the grafting-through technique. This polymerization technique is advantageous due to the ease of polymerization and relative insensitivity towards impurities such as moisture and protic solvents. A drawback, as with many uncontrolled polymerization techniques, is the lack of defined polymer chain architecture and the random distribution of side-chains. This is due to the fact that few polymer chains are initiated at the onset of polymerization and continuous initiation throughout the polymerization reaction occurs when utilizing thermally activated initiators, such as 2,2'-azobisisobutyronitrile (AIBN) with a half-life time of 10 hours at about 64 °C.[39,40] In conventional free radical polymerization, termination by either coupling or disproportionation eventually prevails. The former producing a single dead chain, while the latter will produce both an unsaturated and a saturated chain end. The continuous radical initiation and termination often result in a broad chain length distribution and undefined polymer architecture.

2.3.2. Graft copolymers

Graft copolymers are considered branched molecular structures with polymeric side-chains (grafts) attached to a supposedly linear main chain (backbone). The side-chains usually differ from the main chain in chemical nature and are in most cases randomly distributed along the backbone. The bulk polymer of graft copolymers has a tendency to yield intramolecular phase separation due to interactions that occur between the backbone and grafts. Amphiphilic graft copolymers can be obtained by the copolymerization of grafts and backbone with different solubility behaviours. Rather large compositional heterogeneity is often seen in graft copolymers, however, this has little to no negative effect on most of their applications.[41] Figure 2-7 illustrates the three different approaches that have been developed for the synthesis of graft copolymers, including grafting-though, grafting-from, and grafting-onto.[42]

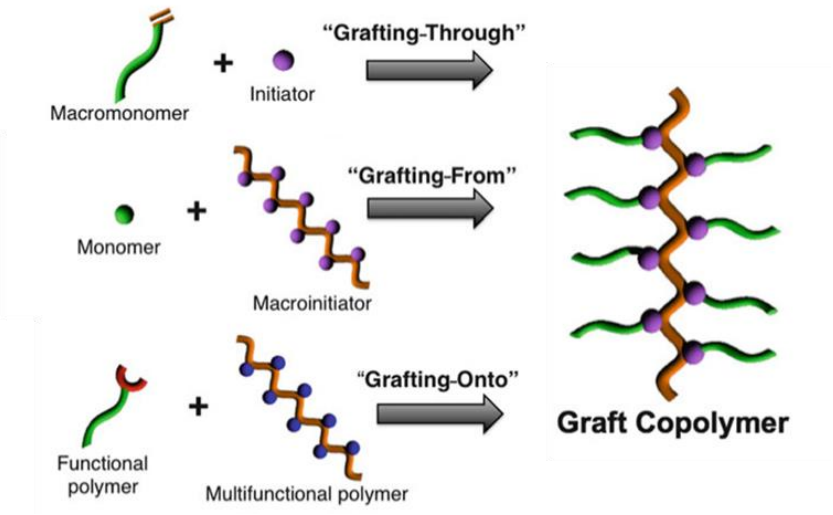

Figure 2-7: Illustration of the three different grafting techniques.[43]

2.3.2.1. Grafting-through

The grafting-through technique utilizes a pre-synthesized macromonomer with a polymerizable chain end-group. This technique allows for relatively facile synthesis with fewer synthetic steps. Since the macromonomer side-chains are pre-synthesized to the desired length, this technique is advantageous as good control over the side-chain length and the characterization thereof can be achieved. This enables the formation of relatively dense grafts. However, obstacles do still exist and may include side reactions and high conversions of the comonomer. This is due to the macromonomer's low reactivity and the large hindrance between the functionalized chain-end of the macromonomer and the reactive site in the propagating graft copolymer.[42] An inherent drawback of both the grafting-through and grafting-from techniques is the high probability of homopolymer formation.[44] This may have an undesired effect on the physical properties of the graft copolymers. Broad chain length distribution and lower molecular weight is often a result of this technique.[44] In work done by Bayley on PAN-*g*-PDMS copolymers synthesized using the grafting-through technique, it was found that a significant fraction of PAN homopolymer was present within the samples.[45] The amount of graft copolymer relative to the amount of PAN homopolymer increased with increasing PDMS in the feed ratio. A similar outcome was attained by Swart, also utilizing the grafting-through method for the preparation of PMMA-*g*-PDMS where homopolymers, as well as copolymers, were present within the samples.[46]

2.3.2.2. Grafting-from

The grafting in the grafting-from technique starts with a pre-synthesized polymer backbone. The backbone precursor acts as multi-functional macroinitiator with initiating sites on it, or functions capable of generating initiating sites. The side-chains are grown from these sites.[41,42] This technique has grown in popularity, especially in the field of controlled radical polymerization, particularity atom-

transfer radical polymerization (ATRP).[47] Coupling and termination reactions are limited by the low concentration of the propagating species. Steric effects are less prominent and allow for increased obtainable side-chain densities since the side-chains are grown *in-situ*. After the completion of the grafting-from reaction, there is no unreacted macroinitiator, thus no separation of ungrafted polymers is needed.[42] One of the general concerns regarding this method is, however, the formation of homopolymers during monomer addition. This may contribute to poor physical properties in the obtained graft copolymer. Well-defined graft copolymers with controlled structure may be obtained using this technique, permitting that the starting polymer is well-defined, and the subsequent grafting reaction proceeds to completion.[44] Nuyken *et al.* used the grafting-from technique and cationic ring-opening polymerization to produce amphiphilic graft copolymers of poly[isobutene-*co*-(*p,m*-chloromethylstyrene)]-*graft*-poly(2-methyl-2-oxazoline).[48] This method was chosen since it enabled the use of macroinitiators and allowed the graft copolymerization of a highly incompatible backbone and graft side-chains.[48] Through a combination of SET-LRP, ATRP and the grafting-from method, Feng *et al.* were able to synthesize a series of PNIPAM-*b*-(PEA-*g*-PDMAEA) double-hydrophilic graft copolymers.[49] Well-defined copolymers with narrow molecular weight distributions were obtained and used for the preparation of stable colloidal gold nanoparticles in aqueous solution. The graft copolymer served as a stabilizer and reducing agent while enabling the tunability of nanoparticle size. The approach may be extended for the development of novel functional materials.[49]

2.3.2.3. Grafting-onto

The grafting-onto technique consists of independently pre-synthesized backbone and side-chains, which are then coupled to form the graft copolymer. The side-chains are attached to the backbone by a coupling reaction, such as hydrosilylation, esterification or the use of click-chemistry. An example of the production of highly functionalized grafted polypeptides would be the synthesis of densely grafted poly(γ-propargyl-L-glutamate)-*g*-poly(ethylene glycol) through a combination of click-chemistry and ring-opening polymerization.[50] Advantages of this technique include the fact that both segments of the copolymer can be pre-synthesized separately which facilitates structural control and detailed individual characterization of both components, resulting in well-defined graft copolymers. However, low graft density is usually achieved with this technique due to steric repulsion of bulky side-chains.[42] Chunzhoa and Benicewicz utilized RAFT polymerization and the grafting-onto technique for the synthesis of well-defined polymer brushes onto silica nanoparticles.[51] A novel RAFT-silane agent allowed for controlled surface graft polymerization of polystyrene (St) and poly(*n*-butyl acrylate) (*n*BuA) homopolymers, as well as poly(St-*b*-*n*BuA) block copolymer brushes from the particle surface. The RAFT agent was directly attached to the surface and thus eliminated the need for additional free RAFT agent, enabling the production of narrow dispersities and predictable molecular weights.[51]

2.3.3. Copolymerization of macromonomers

A relatively simple method to produce graft copolymer is via free radical copolymerization of a macromonomer (M) with a suitable comonomer (A). The key characteristic of this reaction is the large difference in molecular weights between the two involved species. Subsequently, there is always a low mole fraction of macromonomer [M] in the copolymerization mixture ([M] ≤ [A]). Therefore, the classical equation giving the instantaneous copolymer composition can be reduced from the first to the second equation:

$$\frac{d[A]}{d[M]} = \frac{[A]}{[M]} \frac{r_A[A] + [M]}{r_m[M] + [A]} \quad \text{Equation 2-1}$$

$$\frac{d[A]}{d[M]} = r_A \frac{[A]}{[M]} \quad \text{Equation 2-2}$$

Thus, in principle, the radical reactivity ratio (r_A) of the comonomer governs the copolymerization process. The exact determination of the macromonomer's reactivity ratio is difficult in any scenario, due to experimental inaccuracy. There is also ongoing research concerning the influence of the macromonomer's chain length in its ability to copolymerize.[41]

2.4. Amphiphilic copolymers and self-assembly

2.4.1. Amphiphilic copolymers

Amphiphilic copolymers are capable of self-assembling into nanoscale structures in solution, in the bulk, as well as at interfaces.[52] The key element to the determination of self-assembly behaviour is the amphiphilic balance between hydrophilic and hydrophobic moieties within a copolymer.[53] Solution behaviour of amphiphilic copolymers depends on the polarity and solubility of the different copolymer segments in varying solvent systems.[38] This in itself is a critical consideration for the design and fabrication of functional materials.

Amphiphilic copolymers involving a hydrophilic backbone with hydrophobic grafts, or vice versa, have received special interest. Typical examples of hydrophobic polymers include poly(perfluoroalkyl methacrylate) and poly(stearyl methacrylate), whereas poly(hydroxyethyl methacrylate) or poly(vinylpyrrolidone) are non-ionic hydrophilic examples. A number of applications have been found for such graft copolymers, especially as coatings or surface modifiers due to their intramolecular phase separation abilities.[41]

PNIPAM as hydrophilic component is an interesting option for a wide variety of applications, due to it being a widely investigated polymer as well as for its thermo-responsive nature. However, one substantial disadvantage of the water-soluble homopolymer of PNIPAM is its lack of mechanical stability.[54]

Amphiphilic co-networks (APCN) and their corresponding gels have increased mechanical stability compared to their homopolymeric analogues. These materials consist of covalently bonded hydrophilic and hydrophobic polymer components, in a crosslinked macromolecular assembly.[54]

An APCN consists of covalently bonded hydrophobic and hydrophilic chain segments. The incompatibility of these polymer chain segments results in phase separation. Macroscopic demixing is, however, prevented by the covalently crosslinked polymer chains, but results in a phase separated morphology with nanoscale domains.[55] An APCN is capable of swelling in both aqueous and organic solutions without the loss of mechanical stability or undergoing macroscopic phase separation. Bruns *et al.* showed that the nanophase separated polymer domains are interconnected, depending on the composition.[55] Siloxanes are commonly used as the hydrophobic segment due to their biocompatibility, oxygen permeability and low surface energies. The rubber-like nature and low glass transition temperature of siloxanes also contribute to improved physical properties.[56]

2.4.2. Self-assembly of block and graft copolymers

The self-assembly of block copolymers is a well-known and studied phenomenon. These polymers may assume a variety of possible morphologies in bulk and in solution, including spheres, cylinders, bicontinuous structure, vesicles and lamellae.[57] Change in conformation may be induced by exposure to a solvent or environment that only interacts favourably with one segment of a polymer containing two chemically distinct segments. The change in conformation minimizes the number of unfavourable interactions. This behaviour in solution is commonly seen in amphiphilic copolymers but is also evident in any immiscible combination of blocks or segments along the polymer chain. As seen in Figure 2-8, the solution morphology of the aggregates is primarily determined by the packing parameter (p):[57]

$$p = \frac{v}{a_o l_c} \qquad \text{Equation 2-3}$$

Where v is the volume of the hydrophobic segment, a_o is the contact area of the hydrophilic head, and l_c is the critical chain length of the hydrophobic segment. Spheres are formed when $p \leq ⅓$; when $⅓ < p \leq ½$, cylinders are formed; $½ < p \leq 1$, results in the formation of flexible lamellae or vesicles; finally, when $p = 1$, planar lamellae are formed. Inverted structures can be observed if $p > 1$.[57,58]

Three contributions to the free energy system govern the formation of thermodynamically stable block copolymer aggregates of various morphologies. These contributions are:

i) the core-forming block's degree of stretching,
ii) the interfacial tension between the core of the micelle and the solvent surrounding the core,
iii) repulsive interactions between the corona-forming chains.

Therefore, factors affecting any of these three contributions can be manipulated to control the morphologies of aggregates. These factors include the nature of the common solvent, solution water

content, copolymer concentration and composition variations, presence of additives, such as ions or homopolymers, etc.[57]

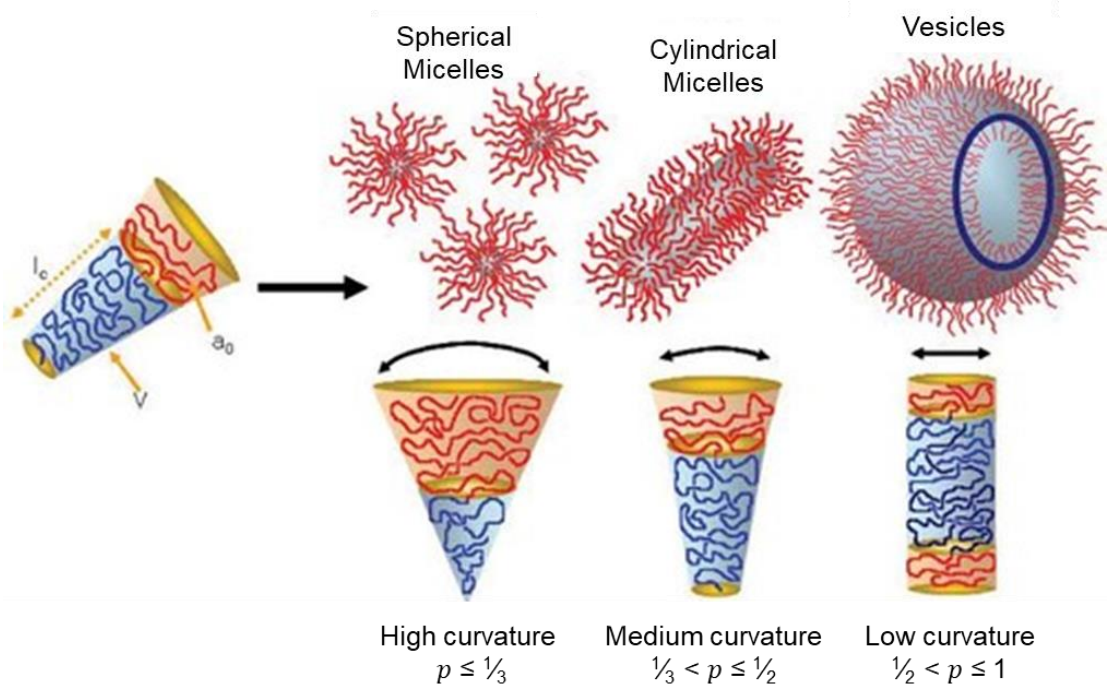

Figure 2-8: Self-assembly of amphiphilic block copolymers in solution may result in various structures. The type of structure formed is determined by the inherent curvature of the molecule, which can be estimated using its packing parameter, p.[58]

The different types of chains in both graft and block copolymers, i.e. the grafts and backbone or the component blocks, are covalently bonded, thus prevents immiscibility and macroscopic phase separation. Conversely, mixing of two different homopolymers may in most cases result in a two-phase blend. The combinatorial entropy of mixing is the main reason for this behaviour since it is very small for chain molecules and miscibility can only be achieved if specific interactions are present.[59] Microphase separation describes the type of chain segregation able to occur in graft and block copolymers in the bulk state and in concentrated solution. Solution behaviour of copolymers undeniably affects the solid-state morphology of the bulk material.

In the late 1950s, Merritt and Bateman presented that graft copolymers with a backbone of natural rubber and graft side-chains of poly(methyl methacrylate) could exist in two physical solid-state forms (soft or hard), depending on the conditions under which it was precipitated.[59] This phenomenon was accounted for by Merritt in terms of domain formation. By this stage in development, it was fully recognized that graft and block copolymers had the ability to form micelles in solution and exist in a microphase-separated state in the bulk.[59] Relatively few studies have been conducted on the microphase separation of graft copolymers compared to block copolymer. This deficiency may be ascribed to the difficulty in the preparation of well-defined graft copolymer. From literature it appears that graft copolymers, depending on homogeneity and their chain structure, can have varying domain morphologies that approaches the morphologies exhibited by the regular AB-, ABA- and $(AB)_nX$-type

systems (where the latter are star-shaped systems with n = 3,4,5, etc.) to those of the segmented multi-block copolymers.

Below are examples of electron micrographs (Figure 2-9 to Figure 2-11) illustrating solid-state microphase separation found in various copolymer systems.[59–61] In Figure 2-9 microphase separation can be observed in a triblock copolymer, polystyrene-*block*-polyisoprene-*block*-polystyrene film, revealing that the specimen has a grainy texture. To "capture" the solution morphology of the copolymer, the specimen has been annealed after casting from a benzene solution, enhancing the periodic regularity of the solid-state structure. The polystyrene cylinders are viewed end-on (white domains) in an osmium tetroxide stained polyisoprene matrix.

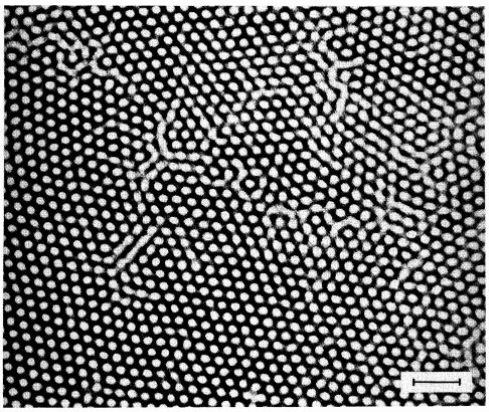

Figure 2-9: Polystyrene-*block*-polyisoprene copolymer film cast from benzene solution. Scale bar indicates 50 nm.[60]

Figure 2-10 illustrates an electron micrograph of a diblock copolymer, a polystyrene-*block*-polyisoprene film, again revealing a grainy solid-state texture. Here the domain morphology consists of end-on viewed polyisoprene cylinders in a polystyrene matrix. The structural regularity of this specimen was enhanced by annealing after casting from a toluene solution in an attempt to "capture" the solution morphology of the copolymer.

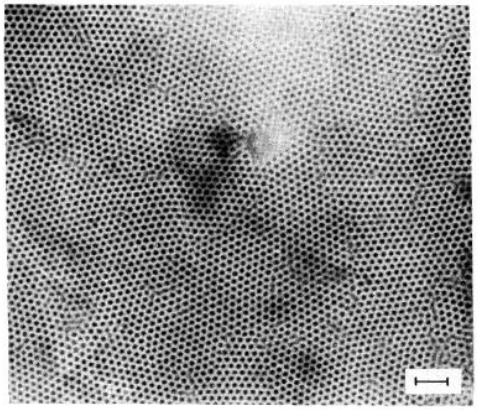

Figure 2-10: Polystyrene-*block*-polyisoprene copolymer film cast from a toluene solution. Scale bar indicates 100 nm.[59]

Figure 2-11 shows the microphase separation in a polystyrene-*graft*-polyisoprene copolymer film.[61] The copolymer film was cast from a hexane solution, showing white polystyrene domains in a dark polyisoprene matrix. Comparing this electron micrograph to the block copolymer systems above, the solid-state microphase separation of this graft copolymer is not as distinct. Slightly more irregular domains are observed, although the specimen was also subjected to careful annealing. This illustrates that, in general, the two components of a graft copolymer are not able to segregate as well as in a block copolymer.

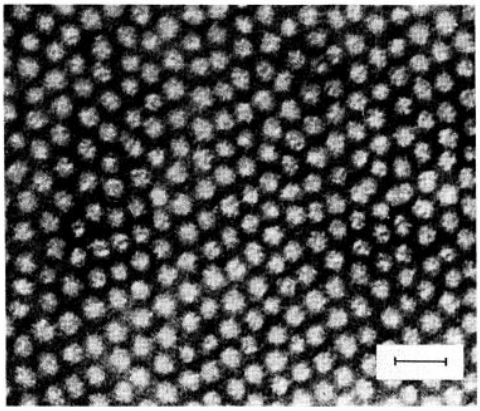

Figure 2-11: Polystyrene-*graft*-polyisoprene copolymer film cast from a hexane solution. Scale bar indicates 50 nm.[61]

2.4.3. Amphiphilic behaviour of graft copolymers in solution

The graft copolymers synthesized in this study are amphiphilic in nature and it is, therefore, essential to understand the solution behaviour of amphiphilic graft copolymers to enable solution processing and electrospinning. Free energy of polymer chains is minimized by the self-assembly of amphiphilic graft copolymers occurring both in solution and at interfaces.

In work presented by Kikuchi and Nose[62,63], amphiphilic graft copolymers of PMMA-*g*-PS were shown to form unimolecular rod-like micelles, as a function of solvent quality with respect to the polymer backbone and grafts, respectively. The solvent system was changed from being a favourable solvent for the backbone and an unfavourable solvent for the graft branches,[62] to an unfavourable solvent for the backbone and a favourable solvent for the graft branches.[63] In their work, they focused on sparsely grafted copolymers with short graft branches. Figure 2-12 illustrates the two different polymer-solvent interactions.

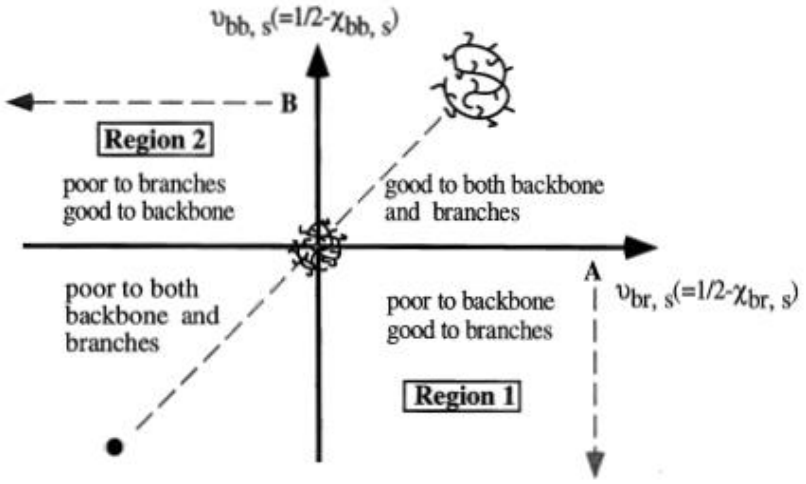

Figure 2-12: Adapted schematic representation from reference[62], illustrating possible micellar structures of graft copolymers with short graft lengths and low branch density as a function of solvent quality.

Solvent quality can be represented by the excluded volume parameters with regards to the backbone and the grafts:

$$\upsilon_{bb,s} = \frac{1}{2} - \chi_{bb,s} \qquad \text{Equation 2-4}$$

$$\upsilon_{br,s} = \frac{1}{2} - \chi_{br,s} \qquad \text{Equation 2-5}$$

Where $\upsilon_{bb,s}$ and $\upsilon_{br,s}$ represent the excluded volume parameters for the backbone and graft branches, respectively, and χ is the monomer-monomer interaction parameter. The dashed line through the origin of the plot represents the non-selective solvent where $\upsilon_{bb,s} = \upsilon_{br,s}$. This is where the coil-to-globule transition for linear polymers may be observed.

Considering Line A, region 1 in Figure 2-13; the solvent quality remains favourable for the graft branches ($\upsilon_{br,s} > 0$), but gradually becomes unfavourable for the backbone of the polymer chain, changing from $\upsilon_{bb,s} = 0$ (also known as theta (Θ) conditions) to $\upsilon_{bb,s} \ll 0$. This causes the chains to initially coil up and gradually transition to rod-like micelles, which eventually collapse to form spheres with the backbone segregated towards the interior as the core and the graft branches as the surrounding corona.

Figure 2-13: Line A in region 1 illustrating the formation of spheres with backbone core and graft branch corona.[62]

In the opposing scenario, considering Line B, region 2 in Figure 2-14; the solvent quality is favourable for the backbone ($\upsilon_{bb,s} > 0$), but becomes increasingly unfavourable for the graft branches changing from $\upsilon_{br,s} = 0$ to $\upsilon_{br,s} \ll 0$. This results in the formation of a string of petal-like micelles as a single polymer chain undergoes coil formation, causing the grafts to segregate towards the interior core of the micelle surrounded by the backbone corona. As the solvent quality becomes more unfavourable for the grafts, the number of petal-like structures decrease until each chain forms a single micelle. The size and number of petal-like structures are determined by the branch-to-branch distance, branching density, as well as solvent quality. As the branching density increases, the number of petal-like loops increases, resulting in more rigid rod-like arrangements of micelle agglomerates.[62]

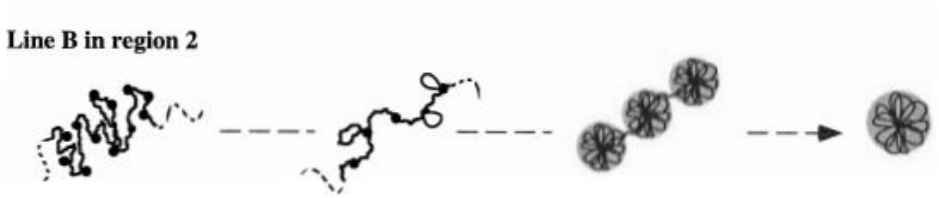

Figure 2-14: Line B in region 2 illustrating the formation of petal-like structure with graft branch core and backbone corona.[62]

Zhang *et al*.[64] studied the self-assembly behaviour of amphiphilic graft copolymers consisting of varying mole ratios of hydrophilic PNIPAM groups to hydrophobic tryptophan ethyl ester (EtTrp) groups with a polyphosphazene (PPP) backbone. They showed that a range of supramolecular aggregates, including network, nanospheres, macrophage-like and high-genus particles, could be produced by modifying the copolymer composition and the organic solvent.[64]

A scaling theory is presented by Borisov and Zhulina[52] for the equilibrium conformations of amphiphilic graft copolymers in dilute solution. The details and thermodynamics of the theory will not be discussed in-depth, but rather a brief overview of their findings will be presented. The model mimics the solution behaviour of water-based copolymers such as PNIPAM-*g*-PEO, PPO-*g*-PAA and PNIPAM-*g*-PAA. They examined intramolecular self-assembly induced by changing the solvent quality from favourable to unfavourable for the backbone on the copolymers, demonstrating that polymers with sufficient grafting density will result in the collapse of the backbone and the formation of a pearl necklace of intrachain micelles, similar to the string of petal-like structures reported by Kikuchi and Nose[62,63], as seen in Figure 2-15.

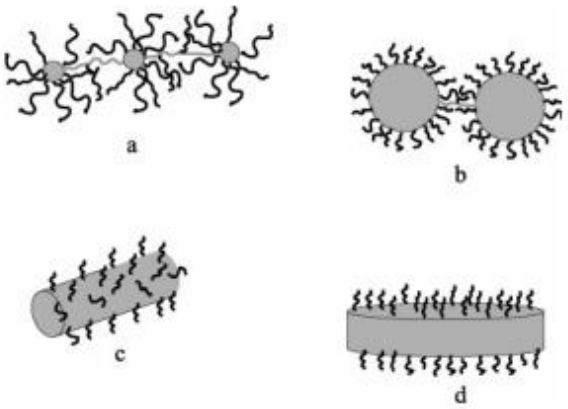

Figure 2-15: Illustration of morphologies of intramolecular micelles in amphiphilic graft copolymers: (a) necklace of star-like micelles, (b) necklace for spherical "crew-cut" micelles, (c) unimolecular cylindrical worm-like micelle, (d) lamellar structure.[52]

Borisov and Zhulina also predicted the formation of spherical as well as cylindrical micelles and lamellar mesophases in the case of sparsely grafted copolymers. These intramolecular morphologies are illustrated in Figure 2-16 in the following diagram:

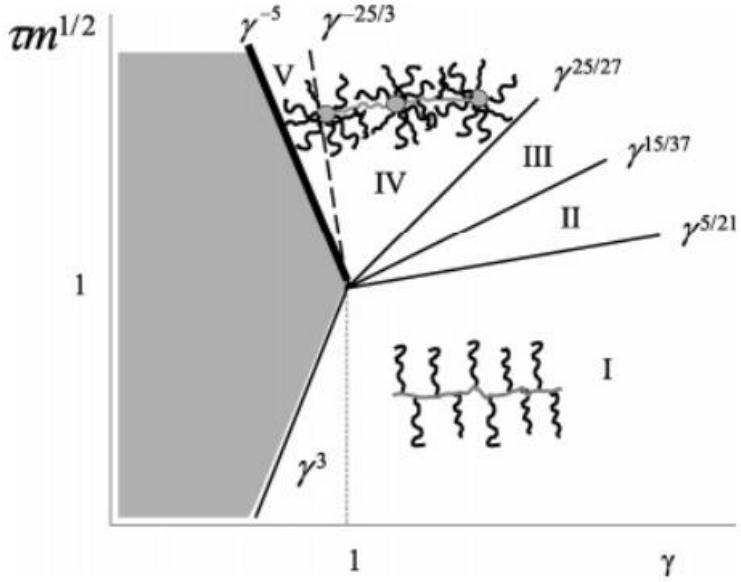

Figure 2-16: States of amphiphilic graft copolymers in dilute solution.[52]

Where γ relates to the degree of branching, and $\tau m^{1/2}$ is the reduced solvent strength (τ representing the uniform polymer density and $m^{1/2}$ the spacer i.e. the backbone length between grafts, under Θ solvent conditions). Each region in the diagram corresponds to different graft copolymer conformations:

I) molecular bottle-brush through a stretched backbone,
II) pearl necklace of globular beads,
III) star-like micelle necklace of overlapping coronas,
IV) star-like micelle necklace of non-overlapping coronas,
V) crew-cut micelle necklace.

The bold line on the diagram defines the stability region for unimolecular cylindrical micelles. The two-phase state of the solution is depicted by the shaded region. The side-chain grafting density (γ) determines the two different potential intramolecular conformational transitions. In the case of densely grafted comb-like copolymers where $\gamma \geq 1$, the pearl necklace of spherical star-like micelles will form. In the case of sparsely grafted copolymers where $\gamma \leq 1$, spherical micelle necklaces are supplemented by unimolecular aggregates of other morphologies, such as cylinders or lamella.[52]

Evidently, there are many possibilities of aggregated structures in solution, depending on the branch-to-backbone length ratio, branching density of graft copolymers, solvent quality and sensitivity of these copolymers. It should be noted that various combinations of the aforementioned morphologies may be present in experimentally obtained structures, thus highlighting the complex solution behaviour of these amphiphilic materials.

2.5. Electrospinning & nanofibre hydrogels

2.5.1. Electrospinning

Many different processing techniques exist for the production of polymer nanofibres, such as template synthesis, self-assembly, drawing, phase separation and electrospinning.[65] In this study, we will primarily focus on the single needle electrospinning technique. Electrospinning is a fibre production technique where electrical forces are used to draw charged polymer solution threads up to nanofibre diameters.[65,66] Electrospinning is highly advantageous due to it being a relatively simple and inexpensive technique. No coagulation chemistry or high temperatures is required by this process to produce solid threads from solution, thus this technique is compatible with a wide range of materials and is particularly suited to produce fibres from large macromolecules.[66] Another advantage of the electrospinning technique is the possibility of upscaling from laboratory to industrial scale. A prime example of laboratory to industry is the establishment of the Stellenbosch Nanofiber Company (SNC). This company is focused on the commercialization and advance of nanofibre technologies established at Stellenbosch University, which includes two processes for high-throughput electrospinning and continuous nanofibre yarn fabrication.

During the electrospinning process, a polymer solution is extruded through a needle or capillary which is placed opposite a collector plate. High voltage is then applied to both the polymer solution and collector plate. Charged ions form in the solution due to the electrical field. The internal charge repulsion counteracts the surface tension of the solution. This phenomenon is known as a Taylor cone, where a hemispherical tip is formed.[25,67,68] The solution is then ejected from the Taylor cone and rapidly undergoes elongation and drying as it travels towards the oppositely charged collector plate. As the jet travels from the Taylor cone to the collector plate, the internal charge densities increase due to the decrease in fibre diameters caused by both the stretching of the fibres and the evaporation of the solvent.[67]

Three main factors affect electrospinning parameters, namely polymer type and solution properties, processing conditions and ambient conditions.[65] The fibre structure and morphology can be determined by the manipulation of one or more of these parameters, depending on the required characteristics for specific applications.[25] Since there are numerous detailed research articles[15,65,68–70] and books[71] available that fully discuss the electrospinning technique and the parameters affecting the produced fibres, it will not be attempted to give a detailed review. Instead, a few of the important electrospinning parameters will be highlighted with the focus being on factors directly affecting the work presented. It should be noted that the interdependence of the various electrospinning parameters is still very complex.

2.5.1.1. Polymer solution parameters – molecular weight, viscosity, conductivity, surface tension

These parameters contribute largely to the final fibre morphology, fibre diameter and the appearance of defects and beading along the fibre axis. As illustrated in (A) in Figure 2-17, very low solution concentration may result in electrospraying instead of electrospinning, where micro- or nanoscale particles are produced due to the low viscosity of the solution.[70] Bead formation (illustrated in (B) and (C) in Figure 2-17) may occur due to low polymer solution concentration or viscosity, reduced molecular weight or low conductivity.[65] Appropriate polymer solution concentration will result in smooth fibres. Fibre diameters, on the other hand, may increase with increasing polymer solution concentration. In general, higher conductivity may result in decreased fibre diameters, except for the known case of polyacrylic acid (PAA) and polyamide-6.[65] Polymer molecular weight is an important factor influencing fibre morphology. If the molecular weight is lowered with enough increase in solution concentration, bead formation will occur. Microfibre formation is favoured by high molecular weight polymers. However, it is worth noting that high molecular weight is not always essential for the production of electrospun fibres, providing that sufficient intermolecular interactions are present amongst oligomers.[70] Another important electrospinning factor to consider is the surface tension as a function of solvent composition in the solution. For example, beaded fibres can be converted into smooth fibres by reducing the surface tension of the solution while keeping the concentration fixed. Surface tension essentially determines the upper and lower boundaries of the electrospinning window, given that all other conditions are kept constant.[70]

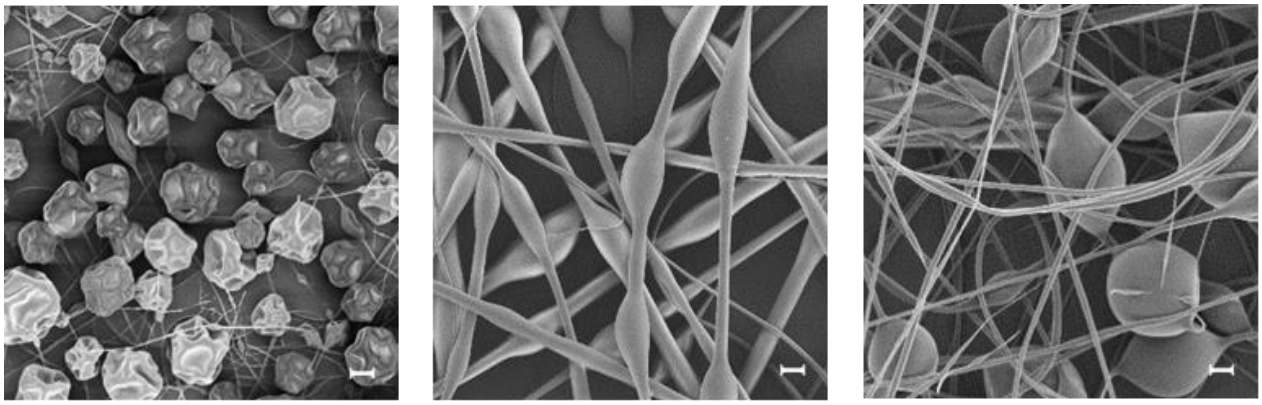

Figure 2-17: SEM images of samples produced in this study with varying solution concentrations. In (A) particles are produced by electrospraying of low viscosity solutions, (B) and (C) illustrate beaded fibres. Scale bars indicate 2, 10 and 2µm, respectively.

2.5.1.2. Processing parameters – voltage, flow rate, distance between the capillary and fibre collector, capillary design and geometry, collector composition

Fibre diameters are greatly affected by processing parameters such as the flow rate and applied voltage. Low flow rate and high voltage may yield small fibre diameters. Fibre drying is largely influenced by the distance between the capillary and the fibre collector and requires a minimum

distance to allow the fibres sufficient drying time before reaching the fibre collector. High flow rates delay solvent evaporation and thus the drying of fibres until it reaches the collector. The surface of the fibres is affected by the composition and geometry of the collector, where a metallic collector may produce smoother fibres and a porous collector more porous fibres. Capillary design influences the structure of the produced fibres, e.g. hollow fibres may be produced by coaxial design.[65]

2.5.1.3. Ambient parameters – temperature and humidity

Ambient conditions refer to external or environmental conditions and have a direct effect on the polymer solution and thus affects the fibre morphology. For example, increased temperature leads to decreased solution viscosity, which consequently reduces fibre diameter. Variations in humidity conditions may result in the appearance of circular pores on the produced fibres.[65] Low humidity conditions may facilitate in faster solvent evaporation during electrospinning, while moisture in surrounding air of high humidity conditions may result in pore formation.[72]

2.5.2. Nanofibre hydrogels

Electrospun fibres are increasingly being used in various applications such as wound dressing material, tissue engineering scaffolds, cosmetic, and drug delivery materials.[65,69,73–75] Electrospinning is considered one of the simplest and most commonly used techniques for the production of nanofibre hydrogels with high surface-to-volume ratios and increased swelling rate and ability, compared to the bulk material.[76] Hydrogel nanofibres are ideal platforms for rapid response systems. Faster response times in stimuli-responsive materials can be ascribed to the smaller diffusion distance of molecules in hydrogel nanofibres compared to macroscopic hydrogels.[76] Figure 2-18 illustrates nanofibre hydrogels produced in this study in their dry and water-swollen state.

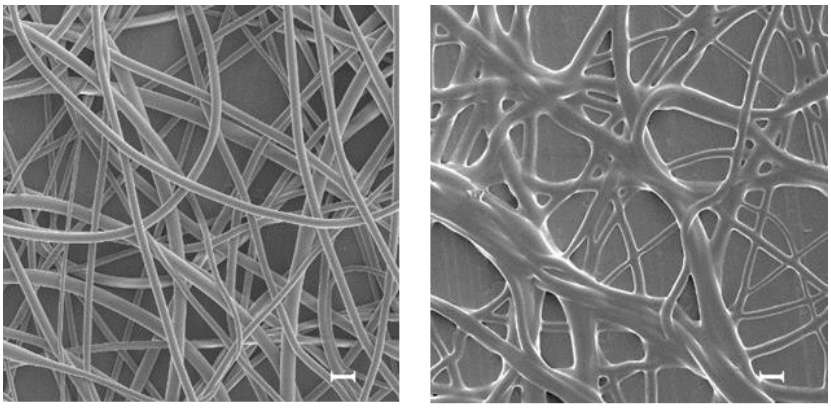

Figure 2-18: PNIPAM-*g*-PDMS (4.3 mol.% 5 000 g/mol PDMS) nanofibre hydrogels produced in this study where (A) illustrates the fibres in the dry state and (B) swollen in water at 20 °C, pH 7 for 24 hours. Scale bars indicate 10 µm.

As discussed in Section 2.1, crosslink density plays a vital role in the hydrogel's swelling ratio. Hydrogels may be either chemically or physically crosslinked polymeric networks, where the crosslinks prevent the flow of the solvated polymer chains. Chemically crosslinked hydrogels and

fibres require post-electrospin crosslinking as the electrospinning process requires the polymer to be in solution. Post-electrospin treatment may comprise of solution or non-solution based crosslinking methods. Solution-based crosslinking may include soaking nanofibre mats in a solution. For example, crosslinking of chitosan fibres with diameters greater than 10 µm are readily achieved by soaking in a glutaric aldehyde solution.[77] However, following the same procedure failed to crosslink the same fibres of diameters less than 100 nm. This highlights one of the risks involved in solution-based crosslinking, where fibre dissolution occurs so rapidly because the minimum time required to form sufficient crosslinks in order to form hydrogel nanofibres is not reached. Therefore, non-solution based chemical crosslinking processes such as thermal and radiation-initiated processes are explored. Thermally annealed crosslinked nanofibres were first reported by Chen and Hsieh.[78] Stable hydrogel nanofibres were obtained by electrospinning poly(acrylic acid) (PAA) and polyvinylalcohol (PVA), followed by thermal annealing at 140 °C. The annealing produced ester linkages between the functional groups on neighbouring polymer chains. Several other research groups have produced chemically crosslinked nanofibre hydrogels by employing similar processes of esterification at elevated temperatures.[79] Some drawbacks of this approach include the degradation of the ester linkage crosslinks after long term water immersion since these linkages are not as water-stable. This approach also only offers a limited range of crosslink densities.[76] Kim et al. produced chemically crosslinked thermo-responsive electrospin nanofibres from poly(NIPAM-*co*-*N*-hydroxymethyl acrylamide) (HMAAM) which showed dynamic and reversible tunable properties, after thermal curing.[15] Chemical crosslinking was achieved by the self-condensation of HMAAM methylol groups upon heating. Another approach to non-solution based crosslinking is based on high energy irradiation, specifically UV radiation, which is widely used to chemically modify or crosslink a wide range of polymeric systems.[79] Considering the work done by Kim et al.,[80] they were able to form poly(2-hydroxyethyl methacrylate) (PHEMA) hydrogel nanofibres by photo-polymerization of oligomers in the presence of a photo-initiator during the electrospinning process, making use of UV radiation. The disadvantage of this approach is that it is undesirable to use photo-initiators in biological applications such as wound dressings, thus neat polymers are preferred.[74,80] Other groups have been able to produce hydrogel films (e.g. films made from PNIPAM, poly(vinyl methyl ether) (PVME), poly(vinyl methyl ether) (PVME), and hydroxypropyl cellulose (HPC)) using crosslinking-agent-free techniques based on UV and electron beam irradiation where the irradiation dose primarily controls the degree of crosslinking.[79]

An alternative to using potentially toxic chemical crosslinkers is to make use of physical crosslinking within the polymer network. This crosslinking approach permits the formation of water-insoluble, mechanical stable crosslinked materials without the need for further purification. Hydrogel nanofibres with physical crosslinks may be advantageous over chemical crosslinking in that stimuli-responsive copolymers with controlled architecture, can be synthesized, e.g. allowing the incorporation of enriched strength imparting monomer segments or enriched responsive monomer segments. The

physical crosslinking of fibres also allow easier processing into thin oriented fibres.[81] Referring to work done by Okuzaki et al.[82] on the production of thermo-responsive PNIPAM-based nanofibre mats that are physically crosslinked via hydrophobic interaction. This group synthesized poly(NIPAM-*co*-stearyl acrylate) by free radical copolymerization, where the stearyl acrylate (SA) acts as the hydrophobic monomer. The nanofibres (seen in Figure 2-19) were produced by electrospinning and exhibited hydrogel properties without dissolution in aqueous solution due to the interpolymer and interfibre physical crosslinks formed via hydrophobic interaction of the long alkyl side-chain of the SA comonomer.

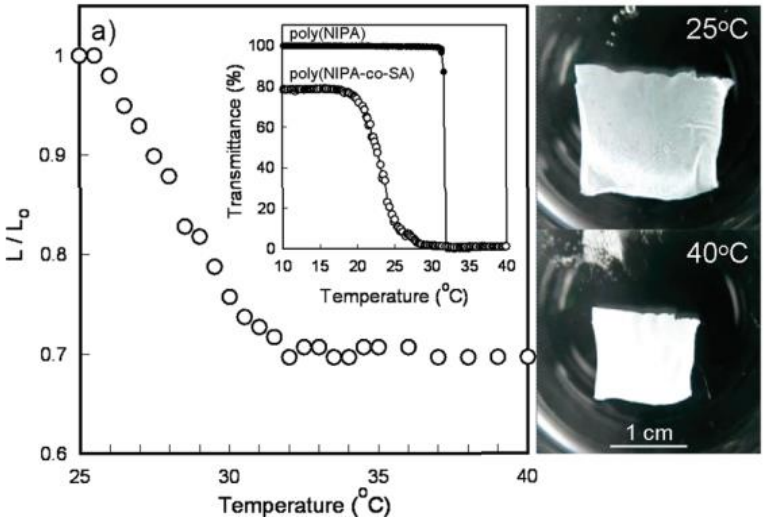

Figure 2-19: The temperature-dependent relative change in length of the poly(NIPAM-*co*-SA) nanofibre mat is plotted in the curve on the left. The change in length of the nanofibre mat (2 cm x 2 cm x 20 µm) is measured in pure water at a heating rate of 0.1 °C/min. Images of the nanofibre mat at 25 and 40 °C can be seen on the right. Temperature dependence of transmittance for PNIPAM and poly(NIPAM-*co*-SA) in aqueous solution with concentrations of 1 wt.% can be seen in the insert.[82]

The behaviour of individual nanofibres was observed by atomic force microscopy (AFM) in a temperature-controlled solution cell, proving that the high surface-to-volume ratios of the fibres allowed for improved drug loading capacity and more effective release. They showed that the LCST of the hydrogel material can be tuned by the incorporation of a hydrophobic comonomer with appropriate alkyl chain length and composition, as well as altering the fibre morphology and fibre diameter by controlling electrospinning conditions.

2.6. References

1 E. M. Ahmed, *J. Adv. Res.*, 2015, **6**, 105–21.

2 M. F. Akhtar, M. Hanif and N. M. Ranjha, *Saudi Pharm. J.*, 2016, **24**, 554–559.

3 C. K. Sudhakar, N. Upadhyay, A. Jain, A. Verma, R. Narayana Charyulu and S. Jain, in *Nanotechnology Applications for Tissue Engineering*, Elsevier Inc., 2015, pp. 77–94.

4 R. A. Green, S. Baek, L. A. Poole-Warren and P. J. Martens, *Sci. Technol. Adv. Mater.*, 2010, **11**, 014107.

5 C. K. Kuo and P. X. Ma, *Biomaterials*, 2001, **22**, 511–21.

6 S. Lanzalaco and E. Armelin, *Gels*, 2017, **3**, 36.

7 J. Maitra and V. K. Shukla, *Am. J. Polym. Sci.*, 2014, **4**, 25–31.

8 T. R. Hoare and D. S. Kohane, *Polymer (Guildf).*, 2008, **49**, 1993–2007.

9 A. S. Hoffman, *Adv. Drug Deliv. Rev.*, 2012, **64**, 18–23.

10 I. Zarzyka, M. L. Di Lorenzo and M. Pyda, *Sci. World J.*, 2014, **2014**, 516076.

11 R. Xue, P. Behera, M. S. Viapiano and J. J. Lannutti, *Mater. Sci. Eng. C*, 2013, **33**, 3450–3457.

12 O. Wichterle and D. Lím, *Nature*, 1960, **185**, 117–118.

13 K. T. Nguyen and J. L. West, *Biomaterials*, 2002, **23**, 4307–14.

14 N. A. Peppas, P. Bures, W. Leobandung and H. Ichikawa, *Eur. J. Pharm. Biopharm.*, 2000, 50, 27–46.

15 Y. J. Kim, M. Ebara and T. Aoyagi, *Sci. Technol. Adv. Mater.*, 2012, **13**, 064203.

16 A. K. Teotia, H. Sami and A. Kumar, in *Switchable and Responsive Surfaces and Materials for Biomedical Applications*, Woodhead Publishing, 2015, pp. 3–43.

17 D. Roy, W. L. A. Brooks and B. S. Sumerlin, *Chem. Soc. Rev.*, 2013, **42**, 7214–7243.

18 B. Jeong and A. Gutowska, *Trends Biotechnol.*, 2002, 20, 305–311.

19 M. Panayiotou, Université Polytechnique, 2005.

20 J. Wang, A. Sutti, X. Wang and T. Lin, *Soft Matter*, 2011, **7**, 4364–4369.

21 A. Richter, G. Paschew, S. Klatt, J. Lienig, K. F. Arndt and H. J. P. Adler, *Sensors*, 2008, 8, 561–581.

22 J. D. Debord and L. A. Lyon, *J. Phys. Chem. B*, 2002, **104**, 6327–6331.

23 L. Dong, A. K. Agarwal, D. J. Beebe and H. Jiang, *Adv. Mater.*, 2007, **19**, 401–405.

24 L. Ionov, *Mater. Today*, 2014, 17, 494–503.

25 S. Maeda, T. Kato, H. Kogure and N. Hosoya, *Appl. Phys. Lett.*, 2015, **106**, 171909.

26 M. Heskins and J. E. Guillet, *J. Macromol. Sci. Part A - Chem.*, 1968, **2**, 1441–1455.

27 G. Roshan Deen, *Polymers (Basel).*, 2012, **4**, 32–45.

28 J. F. Lutz, *J. Polym. Sci. Part A Polym. Chem.*, 2008, **46**, 3459–3470.

29 S. Sun, J. Hu, H. Tang and P. Wu, *J. Phys. Chem. B*, 2010, **114**, 9761–9770.

30 G. Zhang and C. Wu, *J. Am. Chem. Soc.*, 2001, **123**, 1376–1380.

31 S. Ida, T. Kawahara, Y. Fujita, S. Tanimoto and Y. Hirokawa, *Macromol. Symp.*, 2015, **350**, 14–21.

32 D. Bodas and C. Khan-Malek, *Sensors Actuators, B Chem.*, 2007, **123**, 368–373.

33 A. Mata, A. J. Fleischman and S. Roy, *Biomed. Microdevices*, 2005, **7**, 281–293.

34 A. S. C. Félix, A. Santiago-Alvarado, F. Iturbide-jiménez and B. Licona-morán, *Int. J. Eng. Sci. Innov. Technol.*, 2014, **3**, 563–571.

35 M. J. Owen, in *Encyclopedia of Materials: Science and Technology*, Elsevier, 2004, pp. 2480–2482.

36 K. A. Davis and K. Matyjaszewski, *Advances in Polymer Sciences: Statistical, Gradient, Block and Graft Copolymers by Controlled/Living Radical Polymerizations*, Springer Berlin Heidelberg, 2002, pp. 191.

37 K. Matyjaszewski and J. Spanswick, *Mater. Today*, 2005, **8**, 26–33.

38 M. I. Malik and H. Pasch, *Prog. Polym. Sci.*, 2014, 39, 87–123.

39 A. Székely and M. Klussmann, *Chem. - An Asian J.*, 2019, **14**, 105–115.

40 H. Rau, in *Photochromism: Molecules and Systems*, John Wiley & Sons, Inc., Hoboken, NJ, USA, 2003, pp. 165–192.

41 P. F. Rempp and P. J. Lutz, in *Comprehensive Polymer Science and Supplements*, Pergamon, 2012, pp. 403–421.

42 Y. Deng, S. Zhang, G. Lu and X. Huang, *Polym. Chem.*, 2013, 4, 1289–1299.

43 S. Uchida, in *Encyclopedia of Polymeric Nanomaterials*, 2013, pp. 1–4.

44 Y. Kawakami, *Prog. Polym. Sci.*, 1994, **19**, 203–232.

45 G. M. Bayley and P. E. Mallon, *Polymer (Guildf).*, 2012, **53**, 5523–5539.

46 M. Swart and P. E. Mallon, in *Pure and Applied Chemistry*, 2009, vol. 81, pp. 495–511.

47 M. Ejaz, S. Yamamoto, K. Ohno, Y. Tsujii and T. Fukuda, *Macromolecules*, 1998, **31**, 5934–5936.

48 O. Nuyken, J. R. Sanchez and B. Voit, *Macromol. Rapid Commun.*, 1997, **18**, 125–131.

49 C. Feng, Z. Shen, Y. Li, L. Gu, Y. Zhang, G. Lu and X. Huang, *J. Polym. Sci. Part A Polym. Chem.*, 2009, **47**, 1811–1824.

50 A. C. Engler, H. Il Lee and P. T. Hammond, *Angew. Chemie - Int. Ed.*, 2009, **48**, 9334–9338.

51 C. Li and B. C. Benicewicz, *Macromolecules*, 2005, **38**, 5929–5936.

52 O. V. Borisov and E. B. Zhulina, *Macromolecules*, 2005, **38**, 2506–2514.

53 Y. Wang, J. A. Finlay, D. E. Betts, T. J. Merkel, J. C. Luft, M. E. Callow, J. A. Callow and J. M. Desimone, *Langmuir*, 2011, **27**, 10365–10369.

54 G. Kali, S. Vavra, K. László and B. Iván, *Macromolecules*, 2013, **46**, 5337–5344.

55 N. Bruns, J. Scherble, L. Hartmann, R. Thomann, B. Iván, R. Mülhaupt and J. C. Tiller, *Macromolecules*, 2005, **38**, 2431–2438.

56 J. Xu, M. Qiu, B. Ma and C. He, *ACS Appl. Mater. Interfaces*, 2014, **6**, 15283–15290.

57 Y. Mai and A. Eisenberg, *Chem. Soc. Rev.*, 2012, **41**, 5969.

58 A. Blanazs, S. P. Armes and A. J. Ryan, *Macromol. Rapid Commun.*, 2009, 30, 267–277.

59 R. A. Brown, A. J. Masters, C. Price and X. F. Yuan, in *Comprehensive Polymer Science and Supplements*, Pergamon, 1989, pp. 155–198.

60 C. Price, T. P. Lally, A. G. Watson, D. Woods and M. T. Chow, *Br. Polym. J.*, 1972, **4**, 413–425.

61 C. Price, R. Singleton and D. Woods, *Polymer (Guildf).*, 1974, **15**, 117–118.

62 A. Kikuchi and T. Nose, *Macromolecules*, 1996, **29**, 6770–6777.

63 A. Kikuchi and T. Nose, *Polymer (Guildf).*, 1996, **37**, 5889–5896.

64 J. X. Zhang, L. Y. Qiu and K. J. Zhu, *Macromol. Rapid Commun.*, 2005, **26**, 1716–1723.

65 M. H. A. Zanin, N. N. P. Cerize and A. M. de Oliveira, in *Nanocosmetics and Nanomedicines*, Springer, Berlin, Heidelberg, 2011, pp. 311–332.

66 A. Ziabicki, *New York Wiley*, 1976, 488.

67 L. Sfakis, A. Sharikova, D. Tuschel, F. X. Costa, M. Larsen, A. Khmaladze and J. Castracane, *Biomed. Opt. Express*, 2017, **8**, 1025–1035.

68 A. Frenot and I. S. Chronakis, *Curr. Opin. Colloid Interface Sci.*, 2003, 8, 64–75.

69 M. Zamani, M. P. Prabhakaran and S. Ramakrishna, *Int. J. Nanomedicine*, 2013, **8**, 2997–3017.

70 A. R. Unnithan, R. S. Arathyram and C. S. Kim, *Electrospinning of Polymers for Tissue Engineering*, Elsevier Inc., 2015.

71 S. Ramakrishna, K. Fujihara, W.-E. Teo, T.-C. Lim and Z. Ma, in *An Introduction to Electrospinning and Nanofibers*, 2005, pp. 341–382.

72 S. Megelski, J. S. Stephens, D. Bruce Chase and J. F. Rabolt, *Macromolecules*, 2002, **35**, 8456–8466.

73 A. R. Unnithan, R. S. Arathyram and C. S. Kim, in *Nanotechnology Applications for Tissue Engineering*, Elsevier Inc., 2015, pp. 45–55.

74 J. M. Rosiak, P. Ulański, L. A. Pajewski, F. Yoshii and K. Makuuchi, *Radiat. Phys. Chem.*, 1995, **46**, 161–168.

75 X. J. Loh, P. Peh, S. Liao, C. Sng and J. Li, *J. Control. Release*, 2010, **143**, 175–182.

76 A. Gestos, P. G. Whitten, G. M. Spinks and G. G. Wallace, *Soft Matter*, 2010, **6**, 1045–1052.

77 G. M. Spinks, S. R. Shin, G. G. Wallace, P. G. Whitten, S. I. Kim and S. J. Kim, *Sensors Actuators, B Chem.*, 2006, **115**, 678–684.

78 H. Chen and Y. Lo Hsieh, *J. Polym. Sci. Part A Polym. Chem.*, 2004, **42**, 6331–6339.

79 I. Tokarev and S. Minko, *Soft Matter*, 2009, 5, 511–524.

80 S. H. Kim, S. H. Kim, S. Nair and E. Moore, *Macromolecules*, 2005, **38**, 3719–3723.

81 A. K. Agrawal and M. Jassal, *Functional smart textiles using stimuli-sensitive polymers*, Woodhead Publishing Limited, 2011.

82 H. Okuzaki, K. Kobayashi and H. Yan, *Macromolecules*, 2009, **42**, 5916–5918.

Chapter 3

Experimental Section

3.1. Materials used

N-isopropyl acrylamide ≥99% (Sigma-Aldrich, South Africa) was used as received. Mono methacryloxypropyl terminated poly(dimethyl siloxane) with varying chain lengths, 1 000 g/mol (MCR-11), 5 000 g/mol (MCR-220), 10 000 g/mol (MCR-41), was used as received from Gelest, USA.

Tetrahydrofuran (THF) (Sigma-Aldrich, South Africa) was dried by refluxing over sodium/benzophenone and distilled prior to use. 2,2‟-Azobisisobutyronitrile (AIBN) (ChemLab) was purified by recrystallization from dry methanol (Sigma-Aldrich, South Africa). A saturated solution of excess amount of AIBN in 100 mL of methanol was heated to 50 °C. The methanol was rapidly decanted and filtered before being cooled in an ice bath to precipitate the crystals, after which the precipitate was dried under vacuum at room temperature.

Chromatography grade THF and methanol were obtained from Sigma-Aldrich and used as received for HPLC analysis. THF stabilized with BHT was used for SEC and AF4 analysis. Chloroform-d ($CDCl_3$ 99.8% atom D), was obtained from Sigma-Aldrich and used as analysis solvent for ^{1}H-NMR. MilliQ Millipore deionized water was used for water stability, swelling and LCST measurements (pH 7).

3.2. Synthesis

N-isopropyl acrylamide (1.116 g/mL) and PDMS (0.955 g/mL) with varying chain lengths (1 000, 5 000 and 10 000 g/mol, respectively) were copolymerized via the macromonomer grafting-through technique. The amount of PDMS in the feed was varied to obtain a series of each copolymer with varying chain-lengths. Copolymerizations were performed at a solids content of 20% w/v. NIPAM and PDMS was dissolved in 15 mL dried THF and degassed with dry nitrogen for 30 minutes while stirring in a 50 mL single neck round bottom flask. 1 mol.% AIBN, dissolved in 1 mL THF was added to the solution, followed by a further 15 min of degassing. The sealed reaction vessel was allowed to react for 24 hours at 65 °C while stirring. Thereafter, the samples were cast in aluminium pans, allowing solvent evaporation under ambient conditions (22 °C, 40% r.H.). After significant solvent evaporation, any residual volatiles were removed under vacuum at room temperature for several hours. Samples were extracted in MilliQ water for 2 days to allow the removal of unreacted NIPAM monomer and any PNIPAM homopolymer that may have formed. Hexane extraction was unsuccessful to aid in the removal of unreacted PDMS, thus dialysis (Sigma-Aldrich, MWCO 14 000 g/mol) in hexane for 2 days was the subsequent option. The same synthetic procedure was followed for the homopolymerization of PNIPAM, with the exclusion of the PDMS macromonomer. PNIPAM was purified by dialysis (Sigma-Aldrich, MWCO 7 500 g/mol) in water for 2 days, after which the dry polymer was obtained by lyophilization.

Kinetic studies: the general synthesis procedure was followed with the addition of 10 µL of DMF as an internal reference standard. Samples were periodically removed with a degassed glass syringe. The crude samples were exposed to atmospheric oxygen, cooled and added to 0.7 mL $CDCl_3$ for ^{1}H-NMR analysis to allow the monitoring of monomer consumption throughout the reaction.

3.3. Electrospinning

Nanofibres were produced using an in-house built setup via the single needle electrospinning process. This setup consisted of a Genie Plus Model Kent Scientific syringe pump, and a voltage supply which was able to produce electrical potentials in the range of 1 to 30 kV. The positive electrode was attached to the syringe needle, and the negative electrode to the collector plate, which was a heavy-duty aluminium foil-covered glass petri dish of 15 cm diameter. Copolymer to solvent ratios and electrospinning parameters were determined on a trial-and-error basis until stable, bead-free fibres were obtained. For PNIPAM-*g*-PDMS samples containing 5 000 g/mol PDMS and 10 000 g/mol PDMS, 55% w/v and 50% w/v polymer solutions, respectively, were prepared in dried THF. The dried copolymer easily dissolved in the solvent with no need for aggressive stirring or sonification. The polymer solutions were loaded in 1 mL syringes of 4.6 mm diameter, with blunt needles. Smooth, bead-free fibres were obtained at a flow rate of 5 µL/min, a tip-to-collector distance of 15 cm and a voltage supply of 5 kV. Ambient conditions (24 °C, 40% r.H.) were maintained throughout the electrospinning process. Fibre mats were dried under vacuum to remove any residual THF and/or moisture before analysis.

3.4. Characterization

3.4.1. Attenuated total reflectance (ATR) Fourier transform infrared (FTIR) spectroscopy

Samples were characterized by ATR-FTIR using a Thermo Niclolet iS10 Smart iTR spectrometer with diamond/ZnSe internal reflection crystal ATR accessory. Spectra were recorded from 600 – 4000 cm^{-1} with a spectral resolution of 4 cm^{-1}, utilizing 64 individual scans. Omnic computer software (V 8.1) was used for data acquisition and processing.

3.4.2. Liquid state nuclear magnetic resonance (NMR)

Liquid state NMR analysis was performed on a Varian VXR-Unity (600 MHz) at 25 °C to obtain ^{1}H NMR spectra. Deuterated chloroform ($CDCl_3$) was used for the analysis of monomers, homopolymers and all copolymer series. Approximately 30 mg of each sample was dissolved in 0.7 mL of deuterated solvent.

3.4.3. High Performance Liquid Chromatography (HPLC)

Separation of polymers according to chemical composition was achieved by varying solvent composition in a methanol/THF gradient as mobile phase. This technique was performed using an Aligent Technologies 1200 series with the following components, solvent organizer, degasser,

quaternary pump, autosampler, temperature-controlled column compartment, fraction collector with Aligent Technologies 1260 Infinity ELSD detector, interfaced with PSS WinGPC UniChrom (Build 2827) software used for instrument handling and data accusation. A Waters Symmetry300 C_{18} column of dimensions 4.6 × 250 mm and particle size of 5 µm with 300 Å pore size was used as stationary phase. The column was held isothermally at 30 °C during analysis with an analysis flow rate of 0.5 mL/min and injection volume of 30 µL. Samples were thoroughly dried under vacuum, prepared at a concentration of 0.5 mg/ml in HPLC grade THF and filtered through 0.45 µm RC membrane filters prior to analysis.

3.4.4. Size exclusion chromatography (SEC)

THF SEC system: Molecular weight and molecular weight distributions of the synthetic graft copolymers were obtained by a Breeze system equipped with a Waters 1515 Isocratic pump, Waters AF degasser, a Waters 717 Plus auto-sampler and a Waters 600E system controller. HPLC grade THF (0.125 % BHT stabilized) was used as eluent. An 8 x 50 mm PSS GRAM precolumn with 10 µm particles and an 8 x 300 mm, 100 Å pore size PSS GRAM analytical column was used. Waters 410 Refractive Index and Waters 2487 dual-wavelength UV detectors were used, interfaced with Breeze SPA software (v3.3). THF (0.125% BHT stabilized) prepared sample solutions (2 mg/mL) were filtered through 0.45 µm RC membrane filters prior to analysis. The column was held isothermally at 30 °C during analysis with an analysis flow rate of 1.0 mL/min and injection volume of 100 µL. The system was calibrated using poly(styrene) (PS) molecular weight standards. The molecular weights were reported relative to these standards.

THF/Acetic acid SEC system:

Aligent system with Aligent 1260 quaternary pump, interfaced with PSS WinGPC UniChrom, (Build 2830). THF stabilized with 0.125 % BHT and 5% v/v acetic acid was used as eluent. THF (0.125% BHT stabilized) sample solutions (2 mg/mL) were filtered through 0.45 µm RC membrane filters prior to analysis. The column was held isothermally at 30 °C during analysis with an analysis flow rate of 1.0 mL/min and injection volume of 100 µL. The system was calibrated using poly(styrene) (PS) molecular weight standards. The molecular weights were reported relative to these standards.

Aligent Mixed B guard column with two Aligent Mixed B analytical columns.

THF SEC (Dresden):

Analysis was completed by the *Institute of Macromolecular Chemistry* in Dresden on Aligent Technologies system with isocratic pump 1200, PLgel mixed column of 4.6 mm internal diameter and 5 µm particle size. THF (stabilized with 0.025% BHT) mobile phase with the following detectors, UV-detector VWD VL 1260 (Agilent Technologies), light scattering detector HELEOS II (Wyatt Technology), ViscoStar III (Wyatt Technology), RI-detector Optilab T-rEX (Wyatt Technology) were used for analysis. Sample concentrations of 2 mg/mL with a 1.0 mL/min flow rate was used.

3.4.5. Asymmetric flow field flow fractionation (AF4)

Experiments were conducted by the *Institute of Macromolecular Chemistry* in Dresden in THF (stabilized with 0.025% BHT) on an Aligent Technologies system with the following detectors, UV-detector VWD VL 1260 (Agilent Technologies), light scattering detector HELEOS II (Wyatt Technology), ViscoStar III (Wyatt Technology), RI-detector Optilab T-rEX (Wyatt Technology). A detector flow of 0.90 mL/min, focus flow of 3.00 mL/min and injection flow of 0.20 mL/min was used with a RC 10 000 Da membrane. Injection volumes were 100 and 200 µL, respectively, at sample concentrations of 2 mg/mL.

3.5. Analysis

3.5.1. Swelling and water stability studies

To investigate the viability of these copolymers as hydrogel materials, swelling and water stability experiments were conducted on both the film and fibre form of all copolymer samples. Swelling measurements of the film samples were done by immersing samples of 5 x 5 mm in deionized water for various time intervals while monitoring gravimetrically. Equilibrium swelling was measured after 24 hours of water immersion. For the deswelling studies, the fully swollen film samples were removed from the water, dabbed with filter paper to remove excess water from the surface and weighed at regular time intervals.

Thermo-reversibility of the films was investigated by gravimetric recording of the water swelling ratios of different film samples in 20-minute intervals at temperature below (at 20 °C) and above (at 60 °C) its lower critical solution temperature (LCST) in repeated cycles. The swelling and deswelling behaviour of the hydrogel was monitored over 400 minutes, undergoing 4 temperature cycles of 100 minutes each.

The effect of moisture on the fibre morphology was investigated by subjecting fibre samples of both copolymers to varying humidity conditions of 45, 85 and 95% r.H., respectively. The humidity environments were created within desiccators by preparing saturated aqueous solutions of potassium carbonate (K_2CO_3), potassium chloride (KCl) and potassium nitrate (KNO_3), respectively. All fibre samples were placed in the varying humidity environments for 7 days after being dried under vacuum and visualized by SEM.

For fibre water stability experiments, a 1 x 1 cm sample of each fibre sample were submersed in deionized water for 5 minutes and 1 hour, respectively. Excess water was removed after which the fibres were kept at 95% r.H. for 24 hours before drying and analysing by SEM.

Slow precipitation by dialysis was achieved by creating highly concentrated polymer solutions in THF, placing in dialysis tubing (Sigma-Aldrich, MWCO 3 500 g/mol) and dialyzing in deionized water for 48 hours while changing the dialysis water regularly. Swollen gel structures were removed from

the tubing and analysed gravimetrically. Samples were dehydrated under vacuum, weighed and rehydrated to allow gravimetric comparison of swelling ratios.

MilliQ deionized water with pH 7 was used for all experiments while swelling and water stability studies were conducted at ambient conditions (22 °C, 40% r.H.).

3.5.2. Field Emission Scanning Electron Microscopy (FE-SEM)

A Zeiss Merlin Field Emission Gun (FEG) SEM with an in-lens detector (Oxford Instruments), as well as secondary detector (Oxford Instruments) set to a working distance of approximately 4 mm, spot size of 100 pÅ and an EHT of 3.00 kV was used for the analysis of fibres. Samples were dried under vacuum at room temperature for several hours to remove any residual moisture, placed on double-sided conducting tape on a sample holder and then gold coated before analysis. Gold coating was necessary for enhanced surface conductivity. Zeiss AxioVision LE software was used for digital fibre diameter measurements.

3.5.3. Static contact angle (SCA) measurements

The hydrophobic nature of the film and fibre surfaces of all samples were investigated using static contact angle measurements. Krüss Drop Shape Analyzer 25 (DSA 25) equipped with a 500 µL glass syringe and sessile drop needle, was used to accurately deposit deionized water in a 10 µL sessile drop at a rate of 0.3 mL/min on the material's surface. Allied Vision technology and Krüss Advance software was used to image and determine the contact angles on the material's surface at a view angle of +2°. In average instantaneous static contact angle measurements, a minimum of 10 measurements were taken at different positions on the material surfaces. For time-based experiments, the SCA contact angle decay was imaged as a function of time. For the films and high PDMS content fibres, images were recorded in 15-second intervals over 9 minutes. For the low PDMS content fibres, images were recorded in 1-second intervals over 90 seconds since rapid contact angle decay was observed for these samples. The experiments were repeated 3 times for each sample. MilliQ deionized water with pH 7 was used for all experiments which were conducted at ambient conditions (22 °C, 40% r.H.).

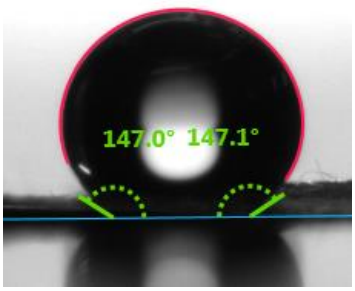

Figure 3-1: Image of a 10 µL water droplet recorded using the Krüss Drop Shape Analyzer 25 and Allied Vision technology with software-generated baseline, tangent and contact angle on a fibre sample surface (22 °C, 40% r.H.).

3.5.4. Optical microscope for fibre visualization

Due to operational limitations and the high vacuum employed during conventional SEM, dry and wetted fibres were visualized at temperatures below and above the material's LCST to establish dimensional swelling ratios of all fibres. An Olympus CX31 optical microscope attached with a JVC digital colour video camera at 10 X/0.25 magnification and Compro X-series computer software was used for digital image recording. The optical microscope was fitted with a Pike Technologies temperature controller and recirculater to allow visualization of the fibres at varying temperatures. Fibres were removed from the aluminium foil backing, placed on a glass microscope slide, imaged while dry and then wetted with deionized water. The analysis temperature of the wetted fibres was raised from 25 °C to 45 °C. MilliQ deionized water with pH 7 was used for all experiments which were conducted at ambient conditions (22 °C, 40% r.H.).

3.5.5. Lower critical solution temperature (LCST) determination

Since traditional turbidity measurements are not suitable for LCST determination of water-insoluble hydrogel materials and accurate gravimetric analysis of swollen hydrogels at exact temperatures are often challenging and unreproducible, a new approach was taken. Two methods were employed, were the first method proved to be extremely labour and time-intensive, although the results were reproducible and correlated well with the method to follow. The second approach involved the use of the OptiMelt apparatus, an automated melting point system with digital image processing technology (Stanford Research Systems) and SRS OptiMelt V.1.107 (Stanford Research Systems 2006) computer software. Film and fibre samples of all copolymers were placed in 1 mm glass capillary tubes, filled with water. Samples were allowed to swell within the capillary tubes at ambient conditions (22 °C, 40% r.H.) for 24 hours before analysis. Samples were digitally recorded as a function of temperature from 18 to 40 °C at a heating rate of 1.0 °C/min.

Chapter 4

Results & Discussions

4.1. Synthesis

Synthesis of hydrogel materials often occur in water-based systems at moderate temperatures. Due to the large differences in polarity and hydrophobicity of the two monomers and other reaction components employed in the system, solvent selection proves to be challenging, especially since the solubility of the hydrophobic poly(dimethyl siloxane) (PDMS) macromonomer changes with the increasing side-chain length and amount. In some cases, monomers and reaction components may be soluble in the selected solvent, but the product itself may be insoluble, resulting in precipitation and a reduction in reaction control. An advantage of the chosen polymerization technique is the relative ease at which the grafting-through copolymerization technique is done. This technique allows for the development of a one-pot synthesis procedure, where all reaction components are added to the reaction vessel at the onset of the reaction and requires no further synthetic steps. *N*-isopropyl acrylamide (NIPAM) is a strongly hydrophilic monomer and acts as both the hydrophilic and thermo-responsive component of the amphiphilic system.[1] NIPAM and similar acrylamide derivatives are generally more soluble in high polarity solvents and water, however, it remains soluble in less polar solvents such as THF and toluene, making these types of monomers ideal candidates for hydrophilic components of amphiphilic copolymer systems. Siloxanes, specifically liquid PDMS macromonomers, are readily soluble in low polarity solvents such as pure aliphatics, including pentane and hexane, but also in solvents such as toluene, THF and chloroform.[2]

Different solvents were investigated as appropriate polymerization solvents, ensuring solubilisation of all reaction components as well as having a moderately high boiling point allowing for elevated reaction temperatures for the effective decomposition of the thermal free radical initiator. NIPAM, mono methacryloxy propyl terminated PDMS of varying lengths (1 000, 5 000 and 10 000 g/mol), and the 2,2'-azobisisobutyronitrile (AIBN) thermal initiator were all found to be soluble in THF. This is a versatile aprotic solvent with moderate polarity, low dielectric constant and a boiling point of 66 °C, at which AIBN has a half-life of 10 hours.[3] THF is capable of dissolving a wide range of polar and nonpolar chemical compounds. This solvent does, however, require careful drying, since it is highly hydroscopic.

Polymerization reactions were performed at a solids content of 20% w/v. Copolymer series of 3, 5, 8, 10 and 12 mol.% PDMS of molecular weight 1 000 g/mol in the feed and 1, 2, 3, 4 and 5 mol.% PDMS of molecular weights 5 000 g/mol and 10 000 g/mol, respectively, in the feed, were synthesized. Figure 4-1 shows the general reaction scheme.

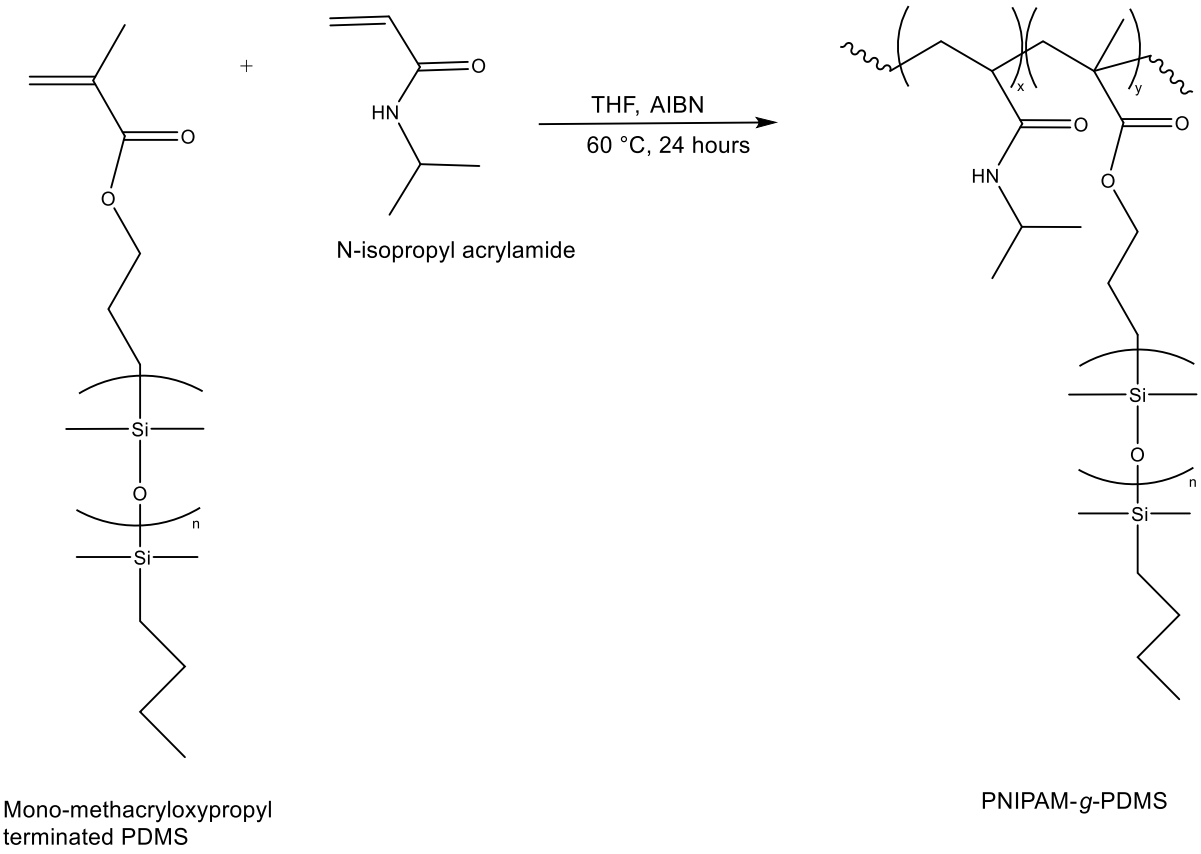

Figure 4-1: Reaction scheme for the synthesis of PNIPAM-*g*-PDMS.

The 1 000 g/mol PDMS series produced polymers that were very brittle, making these materials difficult to handle and analyse for swelling behaviour. On the other hand, the 5 000 g/mol and 10 000 g/mol PDMS series produced materials with better physical properties as well as exhibiting thermo-responsive hydrogel behaviour. Both hydrogel series containing the 5 000 and 10 000 g/mol PDMS, respectively, were analysed. This served as a comparative study in which the effect of hydrophobic PDMS inclusion on the material's hydrogel and physical properties were investigated. Preliminary swelling and water stability studies showed that all materials, including at least 1 mol.% of PDMS in the feed with molecular weight of either 5 000 g/mol or 10 000 g/mol, displayed hydrogel properties. However, when the PDMS content was above 8 mol.% in the feed, the materials were tacky to the touch, very hydrophobic and did not easily form proper films. Based on this, a series of samples with 1 to 5 mol.% PDMS content were synthesized and investigated as part of this study. Table 4-1 summarizes the details of the PNIPAM homopolymer and the copolymer series. These results will be discussed in later sections.

Table 4-1: Feed ratios from polymerizations and PDMS content determined by ^{1}H-NMR [a], molecular weight and dispersity data determined by THF/AA SEC [b].

		mol.% PDMS in feed	mol.% PDMS[a]	wt.% PDMS	M_n x 10^3 (g/mol)[b]	M_w x 10^3 (g/mol)[b]	Đ[b] (M_n/M_w)
	PNIPAM	0	0	-	19.1	36.3	1.9
PDMS chain length	1 000 g/mol	3	3.4	22.3	19.8	30.0	1.5
		5	4.7	32.9	19.6	33.3	1.7
		8	8.1	44.7	26.5	44.1	1.7
		10	10.2	50.9	30.2	51.5	1.7
		12	13.5	56.0	35.6	56.5	1.6
	5 000 g/mol	1	1.7	30.9	18.2	26.8	1.5
		2	2.3	47.4	24.8	32.3	1.3
		3	2.9	57.7	42.5	71.1	1.7
		4	3.0	64.8	29.4	41.5	1.4
		5	4.3	69.9	61.0	113.0	1.9
	10 000 g/mol	1	1.2	47.2	20.2	36.2	1.8
		2	2.5	64.3	35.7	50.2	1.4
		3	2.9	73.2	81.7	197.0	2.4
		4	3.8	78.6	50.3	80.5	1.6
		5	4.1	82.3	117.0	498.0	4.3

The general procedure for the synthesis of PNIPAM-*g*-PDMS copolymers were adapted from work done by Wagenaar and allowed for one-pot synthesis using THF as reaction solvent and AIBN as thermal free radical initiator.[4] The amount of hydrophilic monomer, NIPAM, was kept constant with respect to the mole amount of initiator used, while the amount of hydrophobic PDMS macromonomer was varied. The reaction was run for 24 hours while stirring at 65 °C, after which the reaction mixture was cast into films and allowed to dry under ambient conditions. Dried films were then purified by water extraction, followed by dialysis against hexane to remove any unreacted monomers and homopolymer fractions that may have formed during synthesis. Samples were redissolved and cast from THF to yield optically transparent films, ranging from brittle to rubber-like with increasing PDMS content, as seen in Figure 4-2 below.

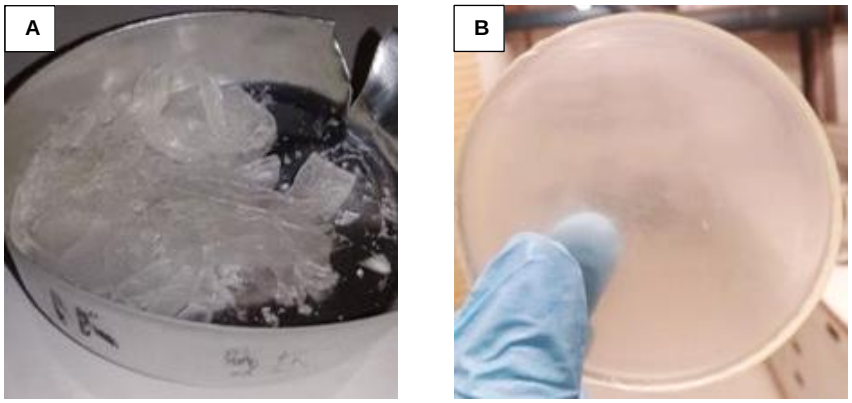

Figure 4-2: An illustration of the effect of PDMS chain length on the physical properties of the hydrogel materials, where (A) illustrated the brittle film of 4.7 mol.% 1 000 g/mol PDMS inclusion compared to (B) rubber-like film of 4.3 mol.% 5 000 g/mol PDMS inclusion.

The variation of PDMS incorporation, as well as the chain length, had an observable effect on the physical properties of the copolymers in terms of their brittleness and appearance. The inclusion of PDMS resulted in physically crosslinked hydrogel materials that were processed into thin films and electrospun nanofibres as will be discussed in later sections.

4.2. Copolymer analysis

4.2.1. Attenuated total reflectance (ATR) Fourier transform infrared (FTIR) spectroscopy

ATR-FTIR spectroscopy was used to determine the success of the copolymerization and whether the PDMS macromonomer was incorporated or not. Figure 4-3 shows the spectra of the PNIPAM homopolymer and the 5 000 g/mol PDMS macromonomer. From the spectra, the characteristic O-Si-O peak at around 1000 cm^{-1} and the two sharp Si-CH_3 peaks at 790 and 1260 cm^{-1} can be seen. Figure 4-4 shows the spectra of the 5 000 g/mol PDMS copolymer series. Since these materials were purified to remove residual monomers and/or homopolymers before analysis, the presence of the characteristic macromonomer peaks confirmed the successful synthesis and incorporation of the macromonomer. An increase in peak intensity with increasing PDMS feed ratio during synthesis further confirmed the increased incorporation of the macromonomer within the copolymer series.

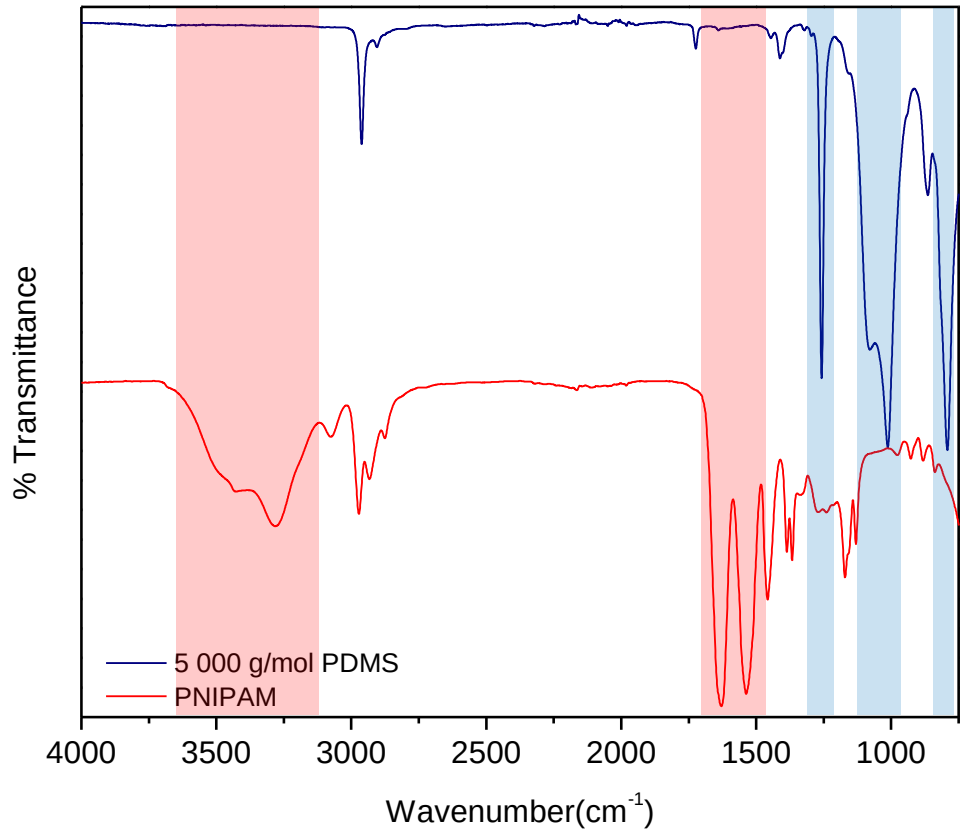

Figure 4-3: ATR-FTIR spectra of 5 000 g/mol PDMS macromonomer with characteristic peaks at 790, 1000, and 1260 cm^{-1} highlighted in blue, and PNIPAM homopolymer with characteristic peaks at 1600 and 3600 cm^{-1} highlighted in red.

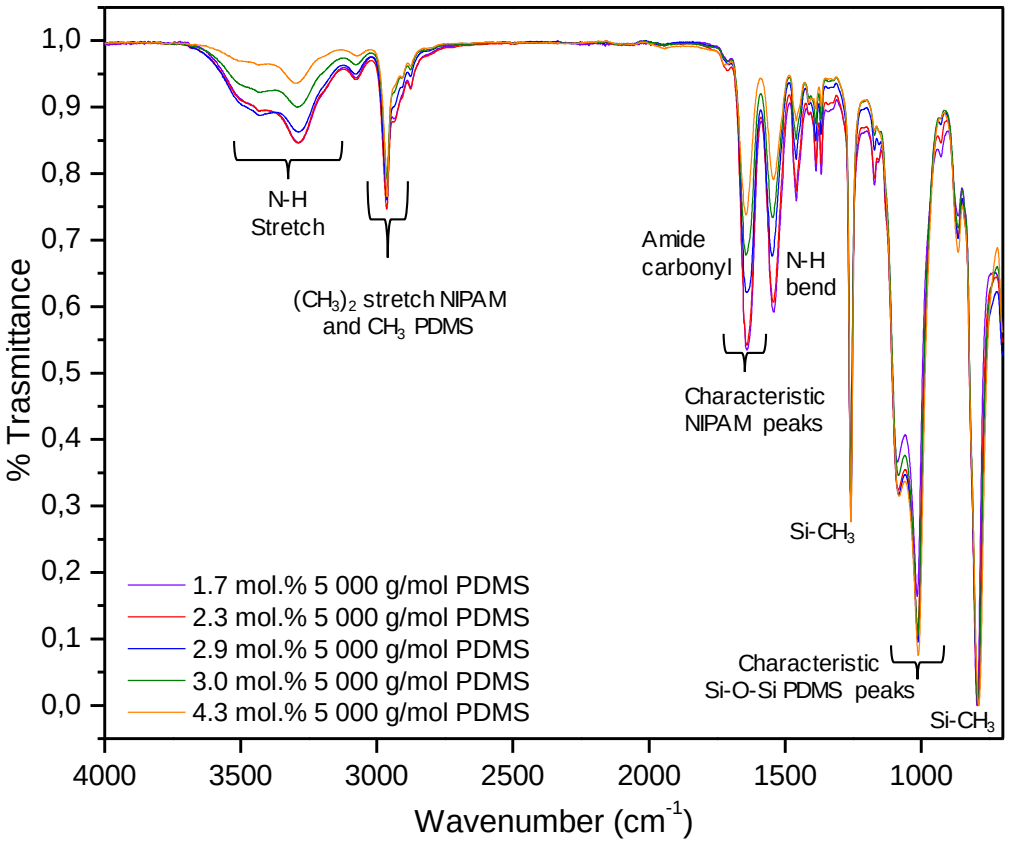

Figure 4-4: ATR-FTIR spectra of PNIPAM-*g*-PDMS copolymers with varying amounts of PDMS inclusion, ranging from 1.7 to 4.3 mol.% PDMS (5 000 g/mol).

4.2.2. ^{1}H-nuclear magnetic resonance (NMR)

^{1}H-NMR spectroscopy is a very powerful analytical technique, enabling quantitative analysis and chemical structure elucidation. It complements the ATR-FTIR findings presented above and provides further evidence of successful PNIPAM-*g*-PDMS copolymer synthesis. This technique confirms the incorporation of the PDMS macromonomer while also allowing the determination of actual incorporated PDMS amounts within the graft copolymers. Table 4-1 reports the good correlation that exists between the feed ratios and the calculated amount of incorporated PDMS. The noted deviations and higher calculated values can be ascribed to the loss of PNIPAM homopolymer during the purification step via water extraction which may indirectly result in the sample being enriched with PDMS.

Figure 4-5 and Figure 4-6 show the ^{1}H-NMR spectra of the two individual monomers used during the copolymer synthesis. In Figure 4-5 the six protons of the NIPAM isopropyl group (a) attached to the amide can be seen around 1.2 ppm as a doublet. At 4.2 ppm the single proton (b) on the secondary carbon appears as a septet. The single proton on the amide nitrogen (c) can be seen as a slightly broadened peak at 5.9 ppm. The three doublet of doublets at 5.6, 6.1 and 6.3 ppm represent the three respective vinyl peaks (d, e', e'').

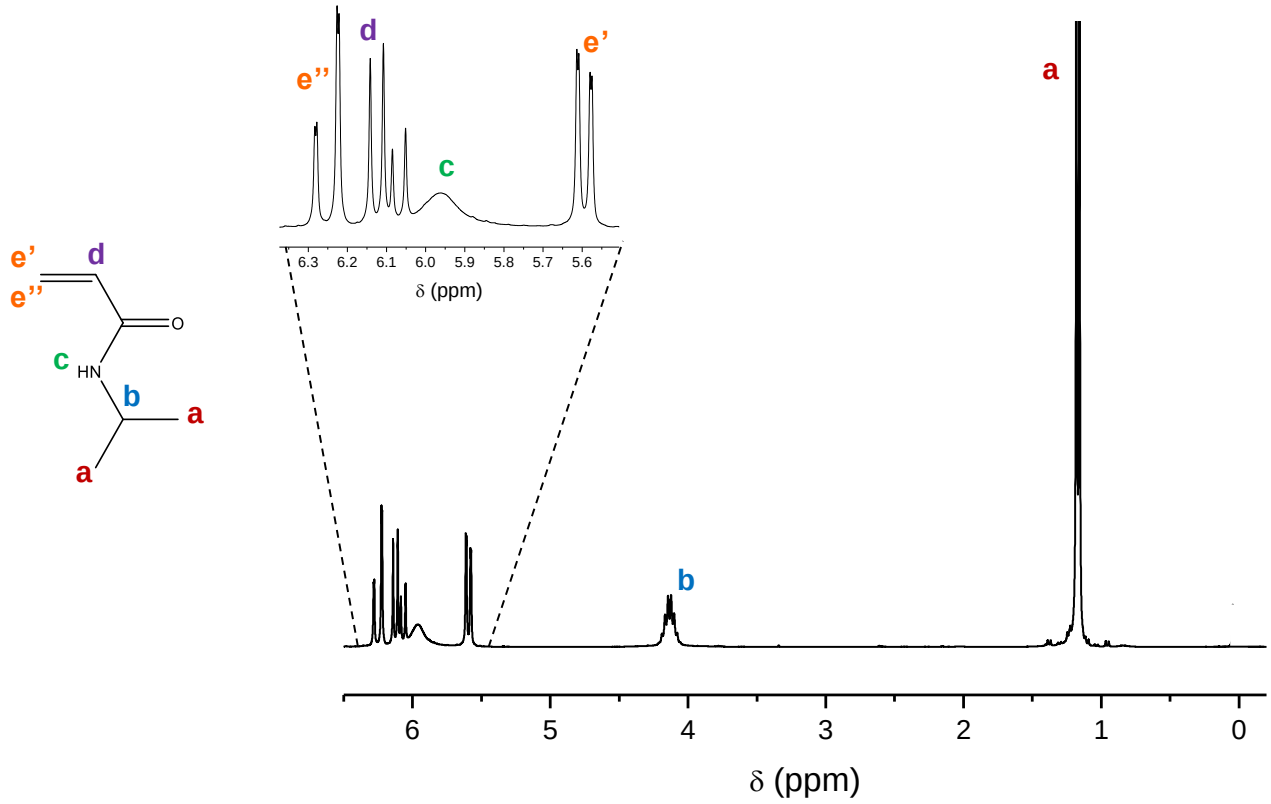

Figure 4-5: ^{1}H-NMR (600 MHz, $CDCl_3$) spectrum of the NIPAM monomer.

Figure 4-6 shows the PDMS macromonomer spectrum where the two respective vinyl protons (a', a'') can be seen at 5.5 and 6.1 ppm. The peak around 1.9 ppm corresponds to the three protons (b) of methyl group attached to the acrylate group. At 4.1 ppm the peak represents the two protons (c) on the carbon of the propyl group adjacent to the acryloxy group. Overlap of the propyl and butyl chains attached to the siloxane group occur in the downfield region between 0.4 and 1.8 ppm. The methyl protons (f) directly attached to the siloxanes give rise to a distinctive cluster of signals at 0.1 ppm.

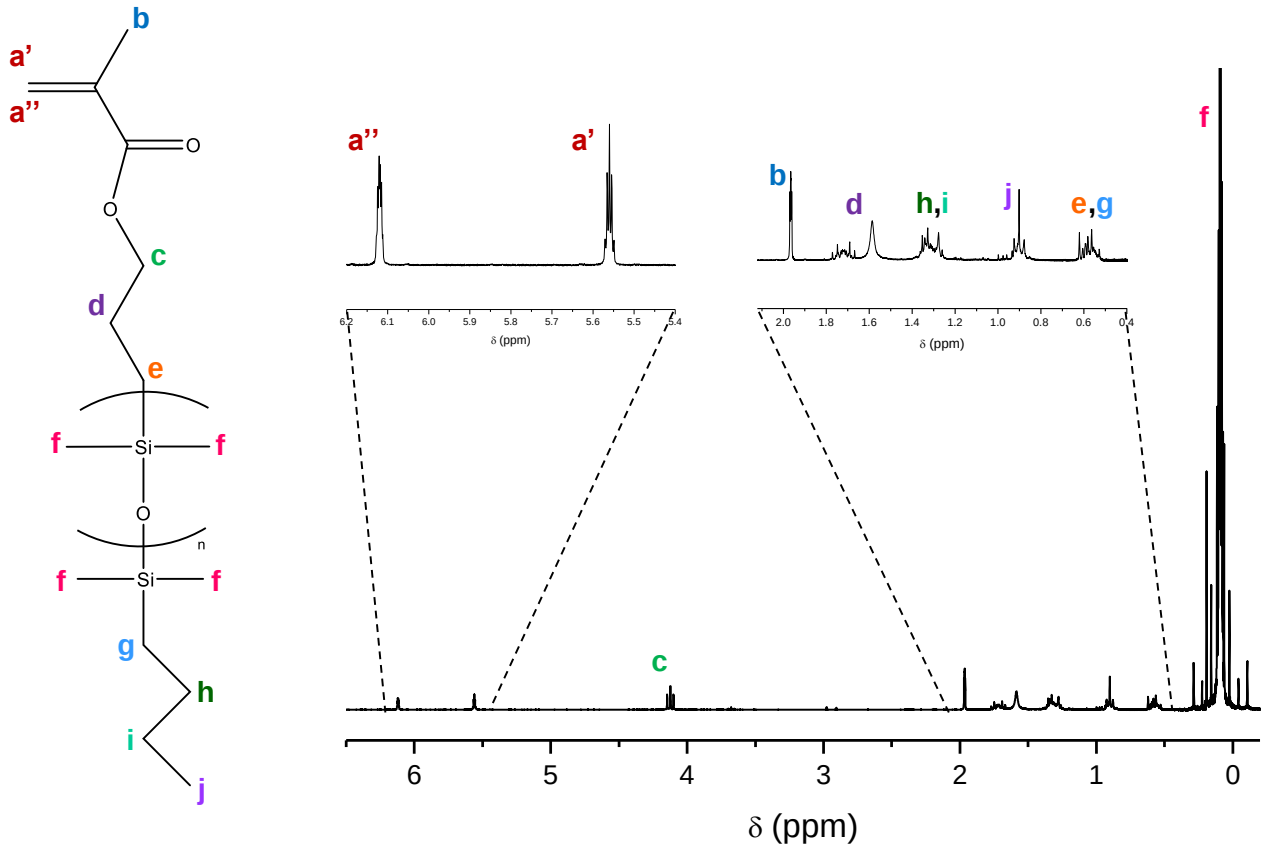

Figure 4-6: ^{1}H-NMR (600 MHz, $CDCl_3$) spectrum of the PDMS macromonomer.

As an example, the ^{1}H-NMR spectrum of the PNIPAM-*g*-PDMS copolymer with 2.9 mol.% PDMS (5 000 g/mol) in the feed is shown in Figure 4-7. The six protons of the isopropyl group (a) appear as a large peak at around 1.2 ppm. The methyl protons attached to the siloxanes (b) give rise to a distinctive peak at 0.1 ppm. As the PDMS content increases, so does the intensity of the peak at 0.1 ppm. As expected, no vinyl peaks are present in the upfield region, which is indicative of successful purification and extraction of residual unreacted monomer. Appropriate peak integrals allow the determination of the ratio between NIPAM and PDMS monomers in each sample. This was done by taking the ratio of the integration of the peak at 1.2 ppm (a), and the integration of the siloxane methyl protons (b) at 0.1 ppm. Further details can be found in the Appendix. Table 4-1 summarizes the actual mol.% PDMS incorporated as determined by ^{1}H-NMR.

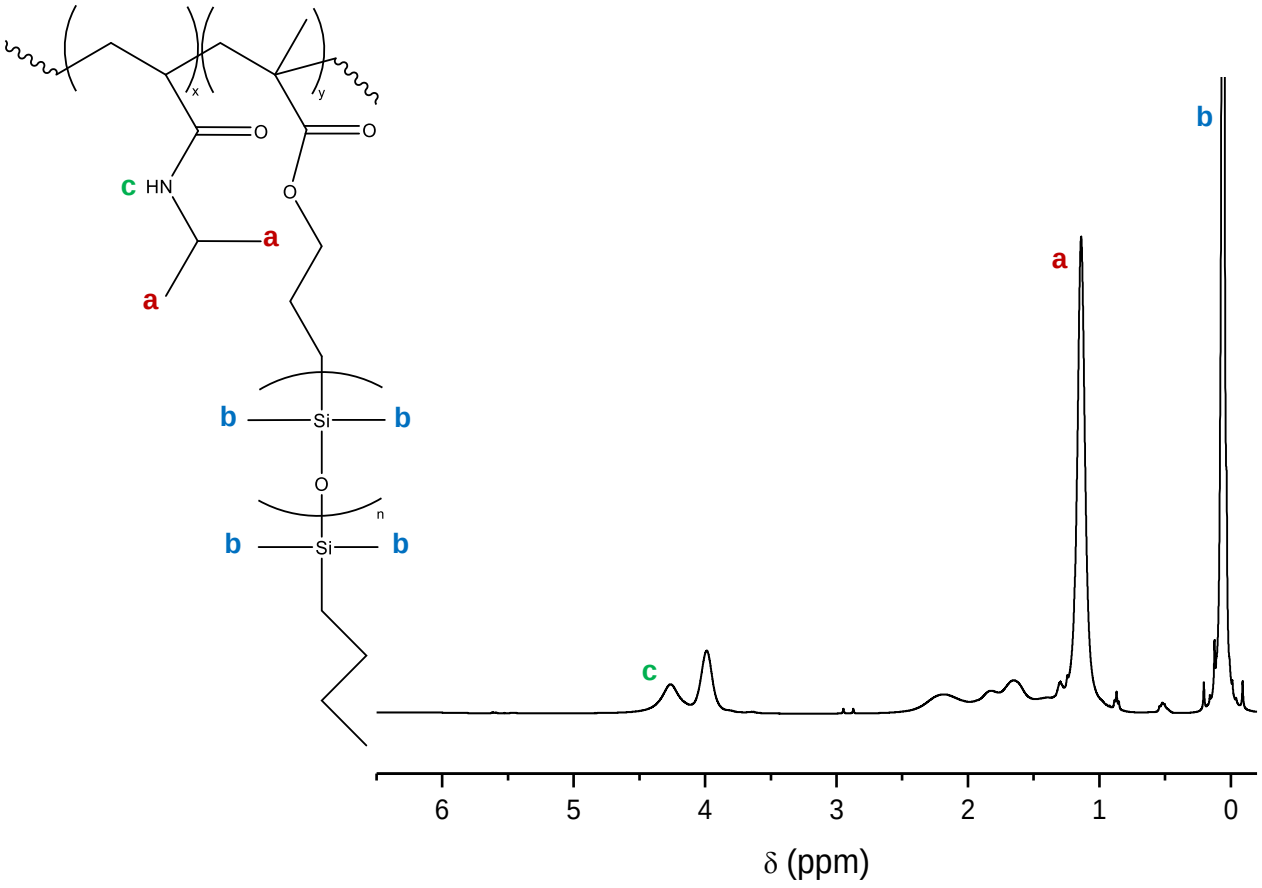

Figure 4-7: ^{1}H-NMR (600 MHz, $CDCl_3$) spectrum of PNIPAM-*g*-PDMS copolymer with 2.9 mol.% PDMS (5 000 g/mol) in the feed.

The PDMS incorporation determined by ^{1}H-NMR for all copolymer samples correlate fairly well with the feed ratios of the comonomers. There is an apparent decrease in the incorporation amount of the longer 5 000 g/mol and the 10 000 g/mol macromonomers compared to the 1 000 g/mol PDMS samples. These deviations may be ascribed to the viscosity effect of the comonomers in solution, brought on by slow diffusion of the long, bulky PDMS macromonomers in the reaction medium. The increasing viscosity of the larger macromonomers impede chain movement, thus reducing the effective end-group concentration available to react.[5] The higher feed ratios of PDMS result in a larger number of bulky macromonomers in solutions competing with much smaller NIPAM monomers to add to the growing polymer chain. This subsequently leads to lower incorporation of PDMS than reactions with lower PDMS feed ratios.

Comonomer incorporation is reliant on the reactivity ratios of the individual monomers in the reaction medium as previously discussed in Section 2.3. Conventional free radical polymerization of comonomers with large differences in molecular weight is employed in this study. It has been reported that copolymerizations involving macromonomers are governed by the reactivity ratio of the comonomer. The exact determination of the macromonomer's reactivity ratio is, however, difficult due to experimental inaccuracy.[6] Yet, it is reasonable to assume that the bulky nature of the PDMS macromonomer would have a significantly lower reactivity ratio than that of the NIPAM monomer.

The decreased incorporation of PDMS with an increasing feed ratio and the size of the macromonomer support this hypothesis.

Reaction kinetics can give some insight into the reactivity of the two monomers in the reaction medium. The reaction kinetics was determined by monitoring the rate of monomer consumption by analysing the decrease in the vinyl peaks of the individual monomers during homopolymerization, using ^{1}H-NMR on samples at different time intervals in the reaction. This study allows for the investigation of monomer concentration change as a function of time over the course of the reaction and assists in the rationalization of homopolymer formation.

Figure 4-8 shows the conversion plot of the two monomers. From the figure, it can be seen that after 24 hours, NIPAM monomer reached nearly 98.1 % conversion whereas the 5 000 g/mol PDMS macromonomer only reached about 25.0 % conversion under the same reaction conditions. It should be noted that high conversion (nearly 90 %) is reached within the first 6 hours of the NIPAM reaction. This finding supports the previously stated hypothesis and thus it may be deduced that the NIPAM is the more reactive monomer of the two.

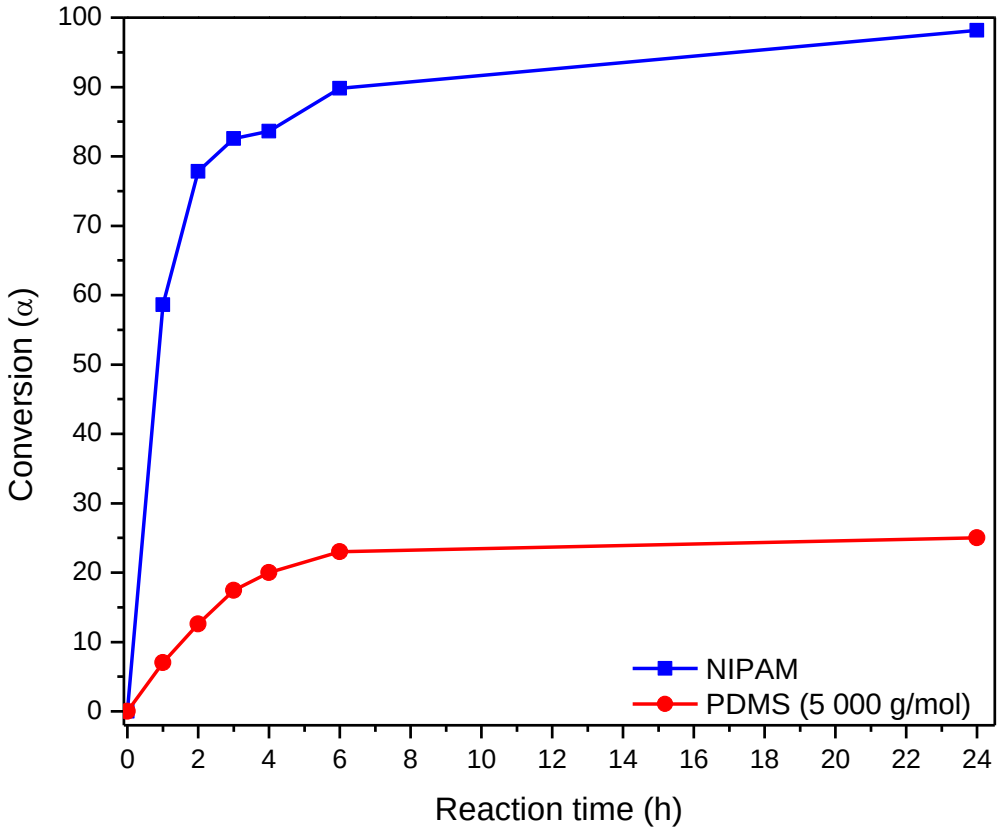

Figure 4-8: Conversion plots of the homopolymerizations of NIPAM and 5 000 g/mol PDMS, over time.

A similar kinetic study was done using 3 mol.% of the 5 000 g/mol PDMS macromonomer in the feed to monitor the macromonomer incorporation in the copolymer. Once again, the vinyl regions of the samples were examined by ^{1}H-NMR. Figure 4-9 shows a stacked plot of the vinyl regions of the NMR spectra at the different time intervals in the copolymer reaction. The relative integral of the

NIPAM monomer vinyl peak (a) at 6.1 ppm and the PDMS macromonomer vinyl peak (b) at 5.4 ppm was monitored over 24 hours using dimethylformamide (DMF) as the internal reference standard at 65 °C in THF. Figure 4-10 shows the PDMS incorporation over the time of the reaction. It was determined that after the 24-hour reaction period, 2.9 mol.% of PDMS was incorporated within the copolymer. This correlated very well with the 3.0 mol.% PDMS available in the feed.

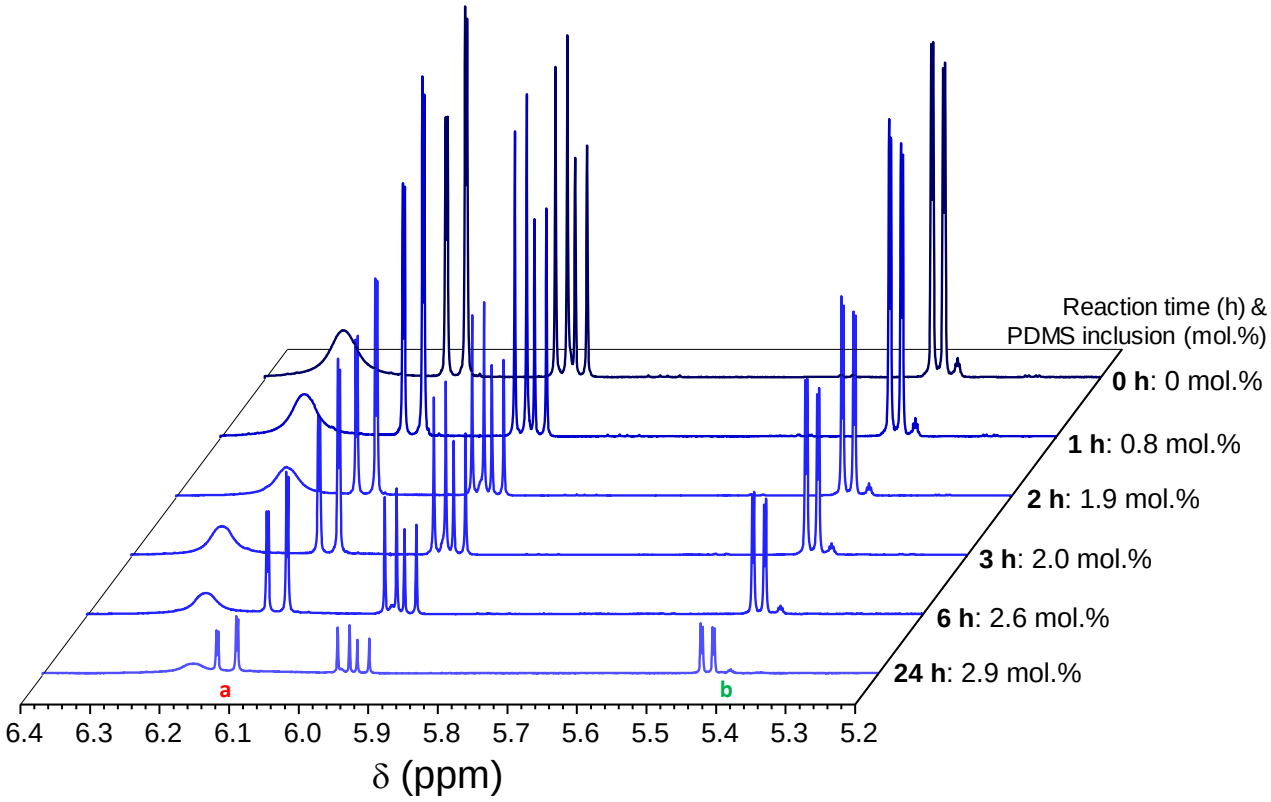

Figure 4-9: ^{1}H-NMR (600 MHz, $CDCl_3$) spectra to monitor the disappearance of the comonomer peaks in the vinyl region over reaction time (prior to purification) for 3 mol.% of the 5 000 g/mol PDMS macromonomer in the feed. Reaction time (hours) and PDMS incorporation (mol.%) can be seen on the right-hand-side of the plot.

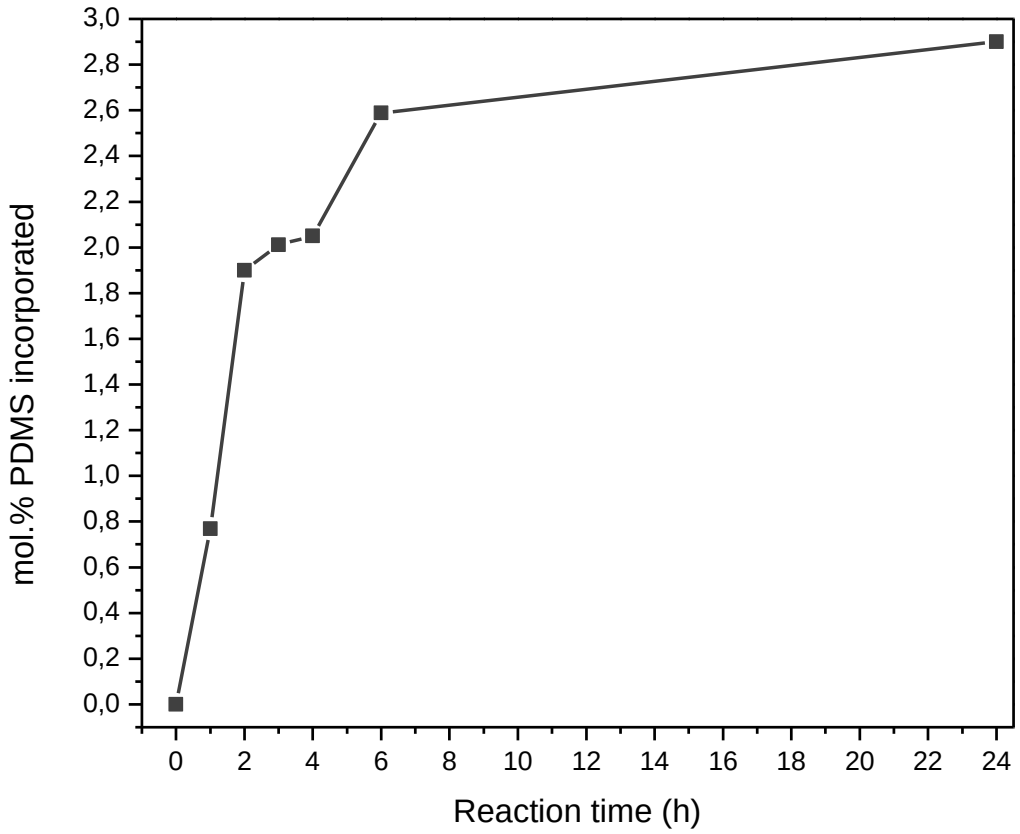

Figure 4-10: 5 000 g/mol PDMS incorporation as a function of reaction time with 3 mol.% PDMS macromonomer available in the feed.

4.2.3. High performance liquid chromatography (HPLC)

Column based separation based on chemical composition allows for definitive confirmation of successful synthesis of PNIPAM-*g*-PDMS copolymers with increasing PDMS content as well as providing information regarding composition and distributions within the samples. Copolymers produced by free radical polymerization techniques are known to be complex and may possibly contain homopolymer, copolymer and even residual monomers.[7] A previous analysis of PDMS graft copolymers by gradient elution chromatography (GEC) proved useful to characterize the graft copolymers. This included PDMAA-*g*-PDMS[4], PAN-*g*-PDMS[8], PS-*g*-PDMS[9] and PMMA-*g*-PDMS[10]. However, in the current study, method development proved to be challenging, due to the complex solution behaviour of these amphiphilic copolymers. Several different analysis options were investigated using a variety of different gradient profiles and solvent combinations. It was found that a suitable solvent gradient profile consisting of methanol and THF (Figure 4-11) gave the best results and allowed for sufficient separation of two distinct peaks in the copolymer analysis. Figure 4-12 shows the analysis of the 5 000 g/mol PDMS series using this gradient profile.

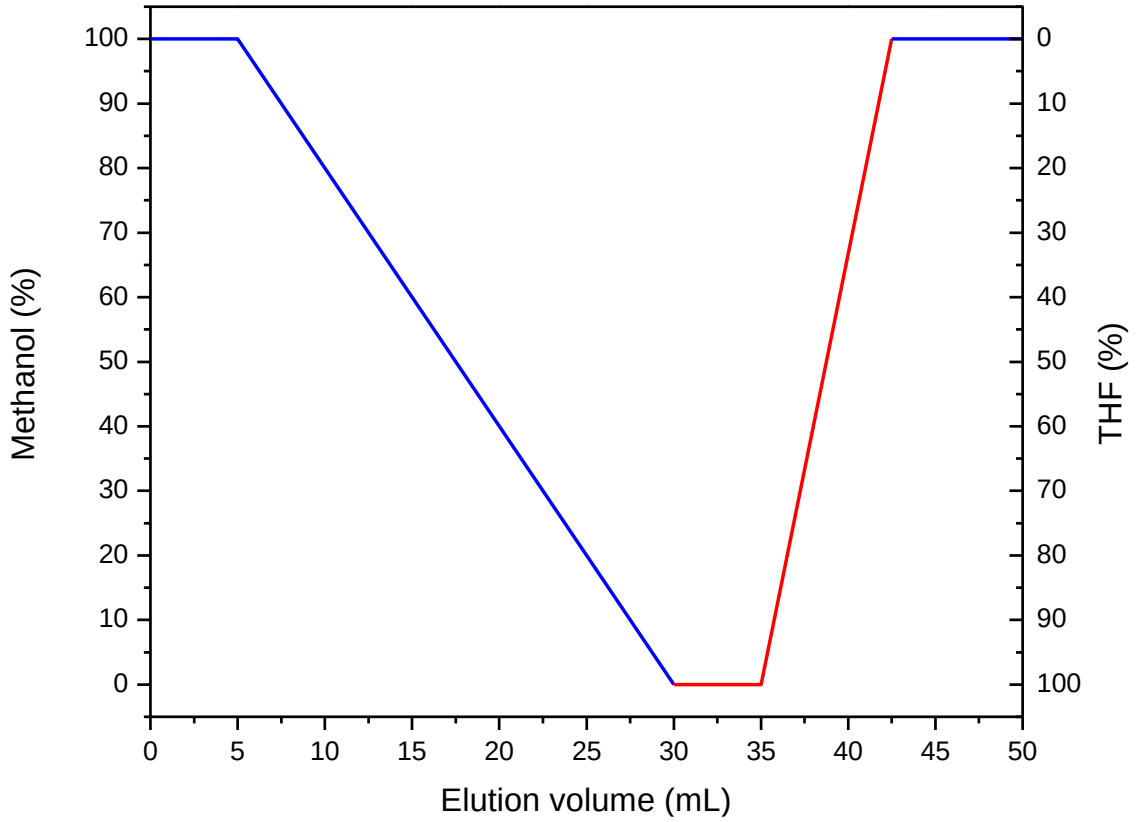

Figure 4-11: Gradient profile of methanol:THF mobile phase vs elution volume for the separation of PNIPAM-*g*-PDMS copolymers. (Methanol/THF mobile phase, C-18, 250 x 4.6 mm, 5 µm, 0.5 ml.min^{-1}, 30 °C).

In Figure 4-12 the first peak eluting at around 3.1 mL in the 100% methanol step, was speculated to be pure PNIPAM homopolymer, as the homopolymer of the same sample concentration and analytical parameters eluted at the exact same position. PNIPAM is fully soluble in methanol, whereas the PDMS containing copolymers are not, causing adsorption to the stationary phase in the first step of the gradient profile. After 5 mL, the linear gradient of the mobile phase gradually changed from 100% methanol to 100% THF, during which the copolymer started to elute according to PDMS content relative to the PNIPAM content in the copolymer. The second peak eluting within the methanol/THF gradient from 17 to around 24 mL was therefore assigned to the PNIPAM-*g*-PDMS copolymer. A shift in the peak position was observed with increasing PDMS content. The mobile phase was effectively becoming less polar, thus samples with increased hydrophobic PDMS content took longer to solubilize and elute through the column. This was due to increased adsorption to the column and thus increased retention time was to be expected, causing the more hydrophobic copolymers to elute later in the gradient.

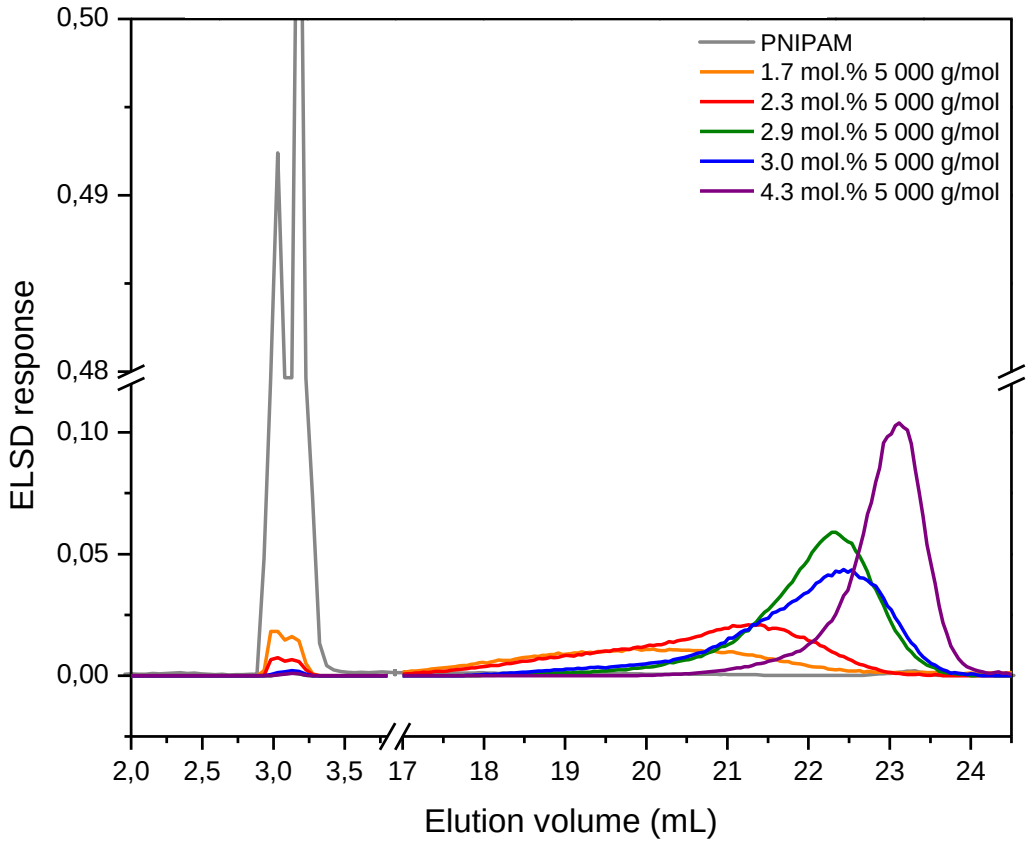

Figure 4-12: HPLC chromatogram of PNIPAM and five samples with varying 5 000 g/mol PDMS contents. A 100-minute gradient of methanol and THF at 30 °C was selected for analysis. (Methanol/THF mobile phase, C-18, 250 x 4.6 mm, 5 µm, 0.5 ml.min^{-1}, 30 °C).

Peak broadening is to be expected for uncontrolled free radical polymerizations with increased copolymer dispersities. In this case, copolymers with lower PDMS content had much broader peaks than the higher PDMS content equivalents. It should also be noted that samples with low PDMS content had a significantly larger fraction of PNIPAM homopolymer (seen at 3.1 mL). Since the reactivity of the NIPAM monomer is much higher than that of the large PDMS macromonomer, homopolymer formation of NIPAM is to be expected. The less PDMS in the feed, the higher the probability of NIPAM homopolymerization, as well as an increased probability of forming gradient type copolymers with only a few PDMS grafts. As the amount of incorporated PDMS macromonomer increased, the second peak visibly increased in intensity and sharpness. This is indicative of a more uniform chemical composition and may indicate a more uniform graft distribution on the polymer backbone. The intensity of the corresponding PNIPAM peak of these samples drastically diminished as the relative amount of NIPAM in the feed decreased with an increasing PDMS content.

Figure 4-12 shows that the 2.9 mol.% 5 000 g/mol PDMS and 3.0 mol.% 5 000 g/mol PDMS sample elute approximately at the same time with slight differences in peak intensity. The ^{1}H-NMR data presented in Table 4-1 shows that the actual PDMS incorporation of these two samples are very similar, thus supporting the fact that the retention time of the two samples are virtually the same.

The HPLC chromatograms and intuition alone cannot verify that the peaks are separated as homopolymer and copolymers. Fractionation and collection of the two separate peaks allow for further analysis by ATR-FTIR spectroscopy to confirm the chemical composition and prove that the two peaks are indeed PNIPAM homopolymer (at 3.1 mL) and PNIPAM-*g*-PDMS copolymer (from 16 mL). Although care was taken to remove unreacted PDMS macromonomers and potential PDMS homopolymer during the purification step, the peaks at > 17 mL may be overlapped with some of the unreacted PDMS macromonomer and copolymer. The 1.7 mol.% 5 000 g/mol PDMS sample was selected as the representative sample since it contained a relatively large PNIPAM fraction and a broad copolymer peak. A total of 4 fractions were collected at 2.6-3.7 mL, 8.0-11.0 mL, 13.5-19.5 mL, and 19.5-25.0 mL, respectively. The first fraction potentially being PNIPAM, second fraction a blank, the third and fourth fractions from 13.5-25 mL potentially represented the broad chemical composition distribution of the copolymer and possibly overlapping PDMS macromonomer. The peak at 3.1 mL, however, proved to be pure PNIPAM, since no silicone contributing signals were observed in the ATR-FTIR spectra, thus any PNIPAM contributing signals in peak > 17 mL must be that of the graft copolymer.

The single ELSD detector used for this analysis was not quantitative, therefore this experiment did not allow the quantification of incorporated PDMS. However, this analysis undoubtedly confirmed successful graft copolymerization of the copolymers consisting of hydrophilic PNIPAM backbone and hydrophobic PDMS side-chains.

It should be noted that the column-based separation achieved in the case of PNIPAM-*g*-PDMS copolymers was not as trivial as the other PDMS containing graft copolymers mentioned. Despite the investigation of several different gradient options, it was not possible to achieve better separation in this case. A possible reason for this may be the longer 5 000 g/mol and 10 000 g/mol PDMS side-chains used in the current system, compared to the other PDMS copolymers which mostly utilized 1 000 g/mol PDMS side-chains. Broader separation peaks were also seen for the current study, compared to the PAN-*g*-PDMS and other copolymers.[8] This is indicative of the difficulty to achieve column-based fractionation when the copolymers contain much longer PDMS grafts. Nevertheless, an in-depth study could be conducted to further optimize the separation conditions to allow for separation of PNIPAM homopolymer, copolymer, as well as any unreacted or homopolymerized PDMS that may still be present within the sample. However, for the purpose of this study within the respective timeframe, it was satisfactory to be able to qualitatively confirm that a copolymer consisting of PNIPAM and PDMS was successfully synthesized. This further supports the ^{1}H-NMR and ATR-FTIR results, suggesting that the PDMS graft content increased with increasing PDMS in the feed.

4.3. Molecular weight

4.3.1. Size exclusion chromatography (SEC)

Characterization and molecular weight determination are critically important in the design and fabrication of new functional materials. The aim of this study was to produce a physically crosslinked system with sufficiently high molecular weight to enable the production of nanofibres through the electrospinning technique. Although SEC is one of the most common analytical techniques used for the determination of molecular weight and molecular weight distribution, the analysis of these copolymers proved to be very challenging since contradicting results were found in different SEC solvent systems. Variations are to be expected when using different solvent systems and calibration standards, but the extent of variation cannot just be explained by the hydrodynamic volume effect. The solution behaviour of these amphiphilic thermo-responsive graft copolymers is much more complex than initially anticipated, since a variety of aggregation morphologies may be present in a single sample, as previously discussed Section 2.4.

Low molecular weights were initially determined by a 100% THF SEC system, utilising a RI detector and polystyrene calibration standards. The low molecular weight data obtained with this system may be due to enhanced hydrogen bonding between the hydrophilic NIPAM functional groups of the copolymer and the stationary phase.

In an attempt to determine the molecular weight of these perplexing amphiphilic copolymers, isolation of the polymer backbone via hydrolysis, as well as amidation was attempted.[11,12] The idea was to cleave off the PDMS grafts and isolate the polymer backbone. Then use SEC analysis to determine the backbone molecular weight. Although this would not provide a definitive copolymer molecular weight, it would provide a general indication of the molecular weights produced. After isolation and purification of the cleaved product characterization by ATR-FTIR and ^{1}H-NMR, as well as THF SEC was done. Unfortunately, the characteristic PDMS peaks were still observed in the FTIR and ^{1}H-NMR spectra, indicating that the side-chain cleavage was unsuccessful. The reason for this is unclear. An alternative approach of changing the SEC mobile phase from 100% THF to 95:5 THF/Acetic acid (AA) was used. This allowed for a more accurate molecular weight determination. The molecular weight data obtained from the THF/Acetic acid SEC system is presented in Table 4-1 on page 45.

The addition of acetic acid to the THF mobile phase resulted in an acidic pH. This decreased the copolymer interaction with the stationary phase of the SEC column and provided more accurate results. It is essential to limit polymer-column interactions to allow purely size-based (hydrodynamic volume) separation. The absolute molecular weight data will most likely vary from these results since the data reported is relative to the polystyrene standards used for calibration. The molecular weight of the copolymers increased as the feed ratio of PDMS increased. Broadening dispersities ranging from 1.3 to 2.4 are observed and is expected for typical uncontrolled free radical polymerizations.

The large dispersity value of 4.3 for the 4.1 mol.% 10 000 g/mol PDMS sample can be explained by examining the SEC chromatogram where a shoulder peak and tailing can be seen and may be indicative of some column interaction.

In addition to the THF/AA SEC results, the samples were analysed by SEC coupled to a range of molecular weight detectors. This analysis was done at the *Institute of Macromolecular Chemistry* in Dresden. Their SEC system was coupled to a variety of detectors, including UV/Vis, RI, MALS and differential viscometer. This allowed for the direct determination of the molecular weight of the copolymers. The obtained data are shown in Table 4-2.

Table 4-2: Feed ratios from polymerization and PDMS content determined by ^{1}H-NMR [a], molecular weight and dispersity data determined THF SEC [b] coupled to a range of molar mass detectors.

		mol.% PDMS in feed	mol.% PDMS [a]	wt.% PDMS	M_n x 10^3 (g/mol)[b]	M_w x 10^3 (g/mol)[b]	Đ[b] (M_n/M_w)
	PNIPAM	0	0	-	61.4	68.3	1.1
PDMS chain length	1 000 g/mol	3	3.4	22.3	26.9	29.8	1.1
		8	8.1	44.7	36.3	41.5	1.2
		12	13.5	56.0	43.8	56.8	1.3
	5 000 g/mol	1	1.7	30.9	-	-	-
		3	2.9	57.7	-	-	-
		5	4.3	69.9	73.2	83.1	1.1
	10 000 g/mol	1	1.2	47.2	54.4	63.7	1.2
		3	2.9	73.2	-	-	-
		5	4.1	82.3	-	-	-

It should be noted that although the molecular weight data presented in Table-4-2 is expected to be closer to the true value, the refractive index increment (d_n/d_c) could not be determined for each individual sample. The 1.7 mol.% 5 000 g/mol PDMS sample formed large aggregates and showed no reproducible light scattering data. The 2.9 mol.% 5 000 g/mol PDMS sample could also not be calculated due to large fluctuation in the refractive index. In the case of the 10 000 g/mol PDMS samples, neither the 2.9 mol.% nor the 4.1 mol.% samples could be calculated since huge fluctuations in the refractive index occurred. These fluctuations may be the result of the increasing chain length of PDMS within the copolymers since the refractive index of PDMS in THF approaches zero.[13]

Of the molecular weights obtained, it can be seen that these results are significantly higher with smaller dispersity values than the THF/AA SEC results previously presented in Table 4-1. This is a probable outcome since those results were obtained using only a RI detector and calculated according to calibration standards. The multitude of detectors used by our Dresden colleagues allows for absolute characterization and molecular weight determination. It should be noted that although the current analysis was done on a premium SEC system with a multitude of excellent detectors and good molecular weight data could be obtained, not all samples could be analysed and proved the analysis of these copolymers to be very challenging. Thus, it is evident that alternative characterization techniques are needed.

4.3.2. Asymmetric flow field flow fractionation (AF4)

Although SEC is one of the most commonly reported molecular weight determination methods, it is not always the most suitable, especially due to the limited range of calibration standards available and the possibility of column interactions. Column base chromatography also present challenges where large aggregates may form in solution. Although satisfactory molecular weight data was obtained from the THF/AA system, and improved results were obtained using a THF SEC system coupled with an array of detectors, further analysis was done using AF4. This technique uses channel-based fractionation and does not utilize a stationary phase such as in SEC and HPLC. This eliminates the possibility of the solute interacting with the stationary phase and allows for evaluation of the solute's solution behaviour, specifically its size i.e. hydrodynamic volume in solution, which is used to calculate the molecular weight of the polymer. The lack of stationary phase, together with a multitude of detectors such as UV-Vis, quesi elastic light scattering (QELS), differential viscometer, and refractive index (RI) detectors; enabled greatly detailed chemical characterization.

Table 4-3 shows the results of the comprehensive AF4 analysis. It is clear from the data that this analytical technique not only provides more insight into the molecular weight, but also provides detailed information on the solution characteristics of these copolymers. The molecular weights prove to be much greater than those determined by any of the SEC analyses. Again, an increase in copolymer molecular weight with increasing PDMS content is seen.

The intrinsic viscosity in solution ($[\eta]_w$) could be obtained through this analytical technique coupled to a differential viscometer. This value is an indication of a solute's contribution to the solution viscosity and can be related to copolymer molecular weight through the Mark-Houwink relationship. As expected, there is a distinct correlation between increasing intrinsic viscosity and increased molecular weight of the copolymers. The viscosity hydrodynamic radius $R_h(v)$ could also be determined using the viscometer. The radius is calculated using the intrinsic viscosity and the Flory-Fox equation, assuming a sphere model. The value is reported as the z-average since a scaling calculation is used. All radii are averaged over the entire sample distribution.

Table 4-3: Actual PDMS content (mol.%) determined by ^{1}H-NMR[a], molecular weight and dispersity data, apparent average hydrodynamic radius and intrinsic viscosity obtained by AF4 coupled to UV/Vis, RI, differential viscometer and QELS detectors.

PDMS chain length		mol.% PDMS in feed	mol.% PDMS [a]	$M_n \times 10^3$ (g/mol)	$M_w \times 10^3$ (g/mol)	Đ (M_w/M_n)	Uncertainty (%)	$[\eta]_w$ (mL/g)	Uncertainty (%)	$R_h(v)z$ (nm)	Uncertainty (%)
	PNIPAM	0	0	47.6	60.05	1.3	1.8	13.3	2.3	6.4	2.4
	1 000 g/mol	3	3.4	81.5	95.0	1.2	2.3	6.1	0.4	5.3	1.1
		8	8.1	53.4	60.7	1.1	2.0	6.8	0.7	4.4	0.9
		12	13.5	57.6	72.1	1.3	1.9	10.5	0.6	6.2	1.3
	5 000 g/mol	1	1.7	60.6	67.3	1.1	2.5	5.0	0.3	3.8	0.5
		3	2.9	91.2	126.7	1.4	1.9	10.4	0.6	10.0	1.7
		5	4.3	97.2	141.0	1.5	2.6	11.7	1.1	11.6	2.6
	10 000 g/mol	1	1.2	138.4	173.0	1.3	2.3	4.5	0.5	5.9	2.0
		3	2.9	201.1	283.1	1.5	2.6	20.4	28.5	10.9	12.6
		5	4.1	279.4	508.3	1.8	4.0	20.1	6.7	11.0	4.0

From Table 4-3 it can be seen that the size in solution of these copolymers generally increased with increasing PDMS content as a function of molecular weight. This may be rationalized by the fact that increased PDMS content within the copolymer results in a greater number of PDMS graft side-chains on the PNIPAM backbone. Self-assembly in the solution may occur, resulting in intra-polymer interactions between neighbouring PDMS side-chains. The more PDMS side-chains within the graft copolymer, the larger the size (hydrodynamic volume) of the copolymer in solution.

In general, the analysis of the 10 000 g/mol PDMS samples were challenging, since the elution peaks occasionally overlapped with the delay reservoir volume of the viscometer, which complicated peak range determination. Preliminary experiments were conducted in THF as mobile phase. Future work on these copolymers may be investigated using different solvents, preferably with higher boiling point solvents to allow more efficient separation between the delay volume peak and sample peak.

It is clear that the highly amphiphilic nature of these graft copolymers present immense challenges in terms of their characterization using solution-based chromatography. Despite these challenges, the channel-based AF4 fractionation provides the most reliable data on the copolymers particularly with regards to molecular weight. In all cases, the molecular weights are sufficient to allow for the

electrospinning of these copolymers. It should be noted that the complex solution behaviour of the copolymers may have a dramatic influence on the solid-state morphology of the materials since they are processed from solution. This point will be discussed in more detail in later sections.

4.4. Swelling behaviour

A material's ability to swell and retain water, not only serves to define whether a material can be considered a hydrogel, but also influences several physical properties of the material. For example, the material's degree of swelling determines the maximum drug loading capacity of the material and thus influences the efficiency of the material in the field of drug release.[14] Figure 4-13 shows an example of a dry and swollen hydrogel film produced in this work.

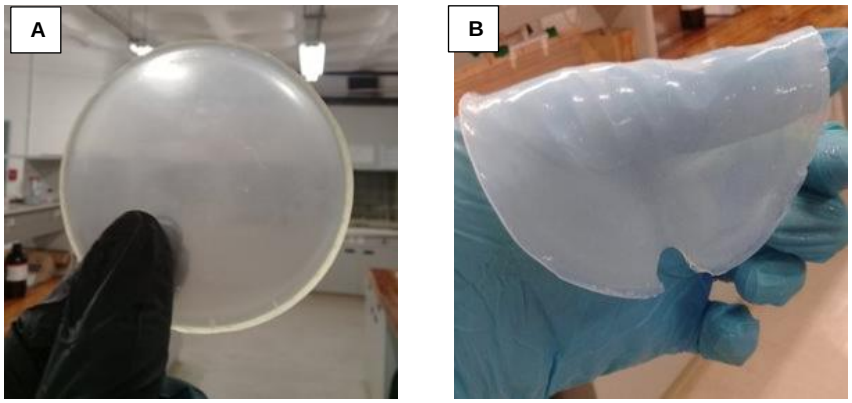

Figure 4-13: Film of 2.9 mol.% 10 000 g/mol PDMS (A) dry and (B) swollen in water at 20 °C, pH 7.

The swelling results in water will be presented as a gravimetric ratio of the swollen mass to the initial dry mass of the hydrogel, also known as the Q-value, where Q = 1 is indicative of no swelling. The Q-value can be calculated using the equation below:

$$Q = \frac{(swollen\ mass)_{water}}{(mass)_{dry}} \qquad \text{Equation 4-1}$$

Swelling in a non-polar solvent (hexane) will be denoted as the Z-value and can be calculated using the equation below:

$$Z = \frac{(swollen\ mass)_{\ hexane}}{(mass)_{dry}} \qquad \text{Equation 4-2}$$

Homopolymers of the hydrophilic, thermo-responsive NIPAM are completely soluble in water unless crosslinked and hence not considered a hydrogel. Therefore, only the swelling of physically crosslinked PNIPAM-*g*-PDMS hydrogels with varying PDMS content are reported and compared.

4.4.1. General swelling behaviour

Table 4-4 shows the swelling results of the 5 000 g/mol and the 10 000 g/mol PDMS hydrogel series. Swelling studies of the copolymer series containing 1 000 g/mol PDMS could not be successfully performed due to the lack of adequate film formation. Previous work done on PDMS containing graft copolymers did, however, utilize the 1 000 g/mol PDMS macromonomer for hydrogel synthesis.[4,8] Unlike the other studies, the copolymerization of NIPAM and the 1 000 g/mol PDMS macromonomer produced very brittle materials lacking stability, making these materials very difficult to accurately quantify, especially for their swelling and thermo-responsive behaviour.

To gain an understanding of possible sample morphology, it is important to consider the PNIPAM fraction of the copolymer in isolation, since the imbibed water is almost exclusively retained within these fractions. This can be achieved by independently calculating the swellable PNIPAM segments within the copolymer network, based on the weight percentage included, denoted as Q_s. Conversely, the independent hexane swellable PDMS segments can be calculated and denoted as Z_s, since PNIPAM undergoes negligible swelling in hexane. Calculation details can be found in the Appendix. The swelling data of the two copolymer series in water and hexane are summarized in Table 4-4. It is evident from the swelling data that the addition of the PDMS significantly influences the equilibrium swelling of the material. The hydrophilic or water-swellable fraction of PNIPAM (Q_s) decreased with increasing PDMS content. This is to be expected as the ratio of PNIPAM to PDMS is decreased in the feed during synthesis and has been confirmed by a variety of analytical techniques such as ^{1}H-NMR, discussed in previous sections. Thus, a systematic reduction in equilibrium swelling in water is observed with increasing PDMS content. The opposite is true for the hexane-swellable fraction (Z_s) where the amount of incorporated PDMS is directly related to the degree of swelling in hexane.

Table 4-4: Swelling data of films after 24 hours in pH 7 water (Q) and in hexane (Z), respectively, at 20 °C.

PDMS chain length		mol.% PDMS in feed	mol.% PDMS (^{1}H-NMR)	wt.% PDMS	Q	Q_s	Z	Z_s
	5 000 g/mol	1	1.7	30.9	-	-	-	-
		2	2.3	47.4	2.79	4.40	-	-
		3	2.9	57.7	2.15	3.72	-	-
		4	3.0	64.8	1.97	3.70	1.92	2.42
		5	4.3	69.9	1.80	3.66	2.00	2.43
	10 000 g/mol	1	1.2	47.2	-	-	-	-
		2	2.5	64.3	2.65	5.63	1.81	2.26
		3	2.9	73.2	2.11	5.14	2.12	2.53
		4	3.8	78.6	1.73	4.42	2.32	2.68
		5	4.1	82.3	1.52	3.94	2.61	2.96

Figure 4-14 shows the rate of swelling in water for both sample series. It is evident from the plotted data that the low PDMS content samples of both the 5 000 g/mol and the 10 000 g/mol PDMS series reached 50% saturation within the first 10 to 15 minutes of water exposure. The high PDMS content

film samples of both PDMS series reached almost 50% saturation between 1 and 2 hours of water exposure. The swelling rate of the low PDMS samples of both copolymer series was much faster than that of the high PDMS content samples. The low PDMS content samples have less hydrophobic PDMS domains present within the copolymer structure. This results in lower apparent crosslinking density, posing less obstruction to water diffusion in the swellable fraction of the copolymer network, ultimately resulting in a faster swelling rate in water.

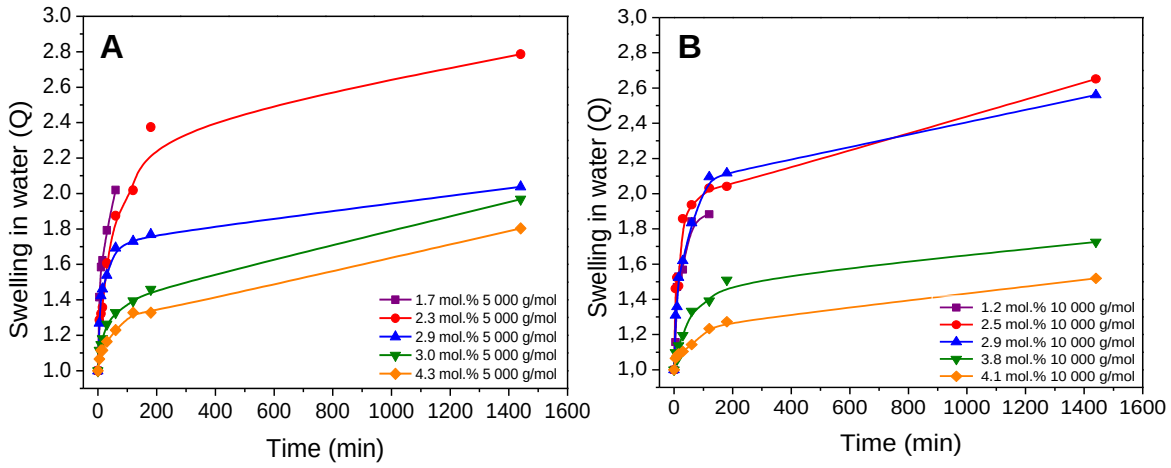

Figure 4-14: (A) 5 000g/mol PDMS film series and (B) 10 000 g/mol film series swelling in water (Q) (20 °C, pH 7).

On the other hand, the Z-value, or swelling in the non-polar hexane, increases with an increasing PDMS content, as seen in Table 4-4. This is due to the increase in the incorporated hydrophobic fraction within the copolymer, which is able to swell in the non-polar solvent. Figure 4-15 presents the swelling rate of both film sample series in hexane. Since PNIPAM undergoes virtually no swelling in hexane, the swelling in this solvent can be ascribed to the presence of the hydrophobic PDMS domains within the copolymer network. The plotted data shows that the low PDMS content samples of the 5 000 g/mol PDMS series fractured after the first hour in hexane and did not undergo swelling to the same extent as the high PDMS content samples. Respectively, the 1.7, 2.3 and 2.9 mol.% 5 000 g/mol PDMS samples only reached 40%, 65% and 70% saturation before fracturing. Both the 3.8 and 4.1 mol.% samples of that series reached about 75% saturation within 30 minutes of hexane submersion. The 10 000 g/mol PDMS samples displayed more systematic swelling in hexane, with the 3.8 and 4.1 mol.% samples, reaching 95 and 100% swelling within the first 5 minutes of hexane exposure. The rapid swelling behaviour of these samples in hexane may be indicative of continuous PDMS domains present within the copolymer network. It should be noted that these samples all formed relatively weak gels in hexane. These had to be handled with care as the films disintegrated readily when handled while swollen.

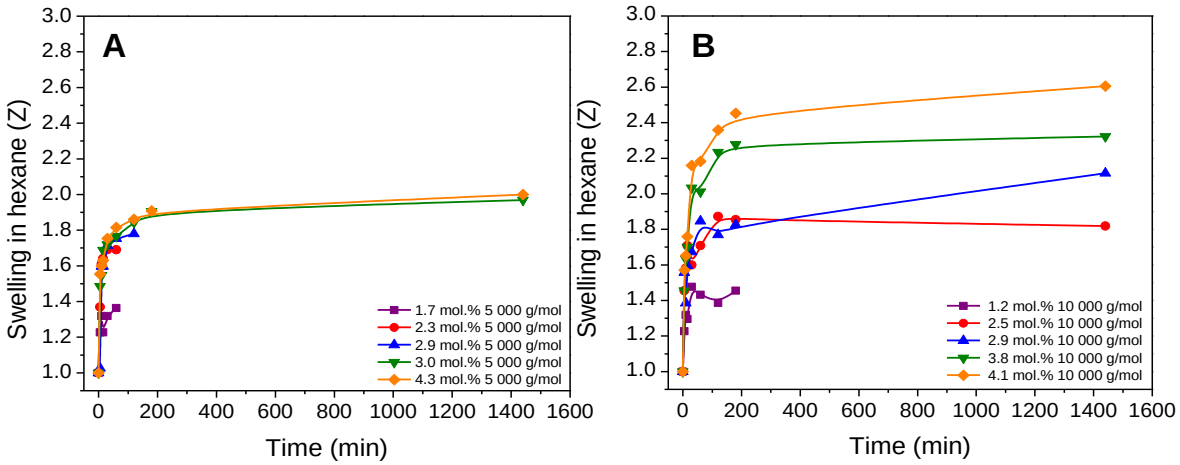

Figure 4-15: (A) 5 000g/mol PDMS film series and (B) 10 000 g/mol film series swelling in hexane (Z) at 20 °C.

The behaviour of these films can be explained in terms of the chain length as well as the amount of incorporated PDMS within the respective samples. Longer and higher amount of PDMS grafts may result in larger, more efficient hydrophobic domain formation and thus higher crosslink density. This is essential in the production of water-insoluble physically crosslinked polymer networks. Less effective crosslinking is a possible reason for the fracturing of low PDMS content samples in water after 1 to 2 hours. The hydrophobic domains of these samples are most likely much smaller and do not provide sufficient crosslink density during the rapid swelling of the PNIPAM fraction, compared to the high PDMS content samples. PDMS itself is, however, soluble in hexane, thus the larger the hydrophobic domains, the greater the extent of swelling in a non-polar solvent such as hexane. The low PDMS content samples display initial swelling in hexane, after which the samples displayed very weak physical properties, causing the swollen films to fracture. To rationalize why low PDMS inclusion samples fractured after some time in hexane, the efficiency of secondary interactions within the polymer network should be investigated. When the PDMS chains swell in hexane, the physical crosslinks provided by the secondary interactions of the hexane-insoluble PNIPAM segments, are not sufficient to hold the network together and consequently result in material fracture.

Figure 4-16 shows the deswelling rates from water for the films of both copolymer series. The plotted data shows that there is a much more gradual decrease in the swelling ratio when left to deswell at ambient conditions (22 °C, 40% r.H.) compared to the rapid swelling presented in (A) and (B) in Figure 4-14. The films of the 5 000 g/mol PDMS series initially deswelled quite rapidly in the first 10 minutes, after which gradual, almost linear deswelling was observed for most of the copolymers. The same observation is true for the 10 000 g/mol PDMS series, where rapid deswelling occurred within the first 10 minutes.

The rate of water loss can be associated with the amount of incorporated PDMS within the copolymers where the rate of water loss increased with increasing PDMS content. This can be rationalized by considering the composition of the hydrogel material. Increased PDMS content

consequently resulted in a decreased water-swellable fraction, Q_s (as seen Table 4-4), thus less water was retained within the structure.

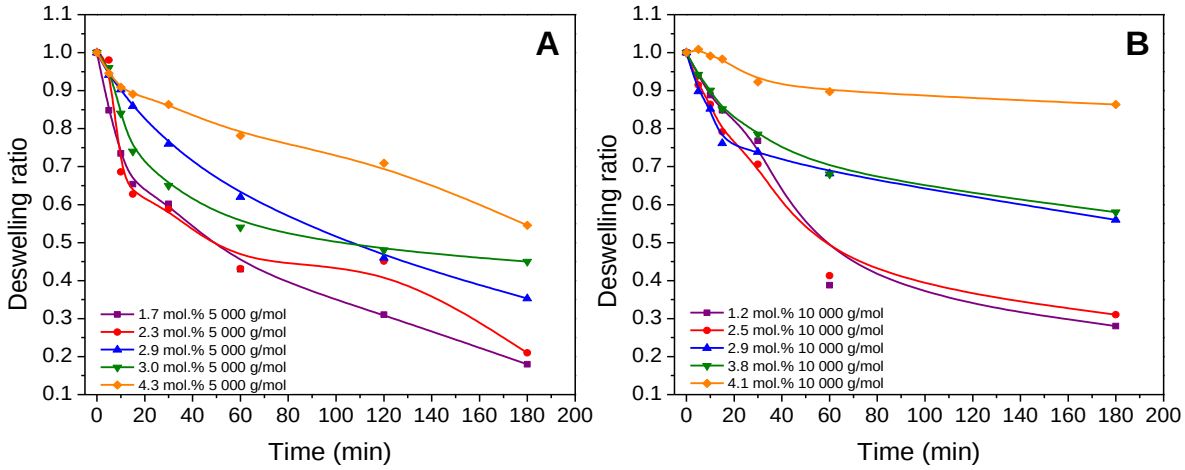

Figure 4-16: Deswelling ratios from water for (A) the 5 000 g/mol PDMS film samples and (B) the 10 000 g/mol PDMS films, as a function of time (min).

Figure 4-17 shows the deswelling rates of the 10 000 g/mol PDMS series in hexane. All samples underwent rapid deswelling at ambient conditions (22 °C, 40% r.H.). Contrary to the water deswelling results, the high PDMS content samples swelled to a greater extent in hexane, due to the large PDMS fraction within the copolymer (Z_s). These samples, therefore, deswelled at a higher rate than the low PDMS containing samples. The 4.1 mol.% 10 000 g/mol PDMS sample deswelled by about 70% within the first 10 minutes of deswelling, whereas the 1.2 mol.% sample lost about 40% of its hexane content within the same time.

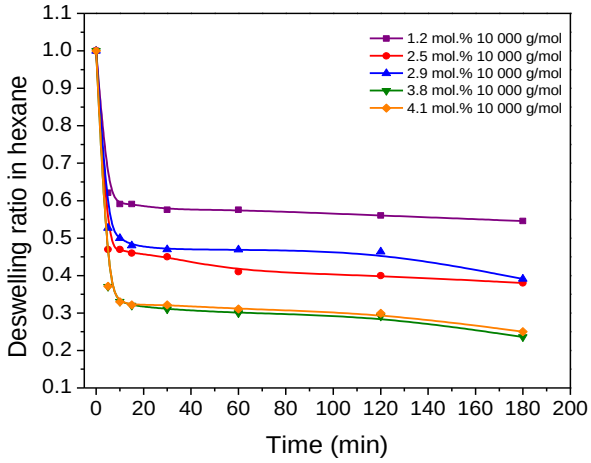

Figure 4-17: The deswelling ratios from hexane for the 10 000 g/mol PDMS series.

4.4.2. Crosslink density

The swelling degree of polymer networks are influenced by several factors, however, without adequate crosslinking, dissolution of the hydrogel materials will occur in suitable solvents and form a uniform solution. Crosslinking prevents the polymer network from disintegrating in solution. Effective or overall crosslinking consists of both physical and chemical crosslinks within the polymer network. The physical and mechanical properties of the hydrogel material, as well as the physical integrity of the hydrogel, is largely maintained by the effective crosslinks.[15] Accurate determination of crosslinking density proves to be challenging and thus many different methods exist for calculating the crosslinking density of polymer networks. Since physical hydrogels are the focus of this study, the Flory-Rehner theory is considered:

$$-\left[\ln(1-v_p)+\ v_p+\ \chi v_p^2\right]=NV_s\left[v_p^{1/3}-\frac{v_p}{2}\right] \qquad \text{Equation 4-3}$$

Where v_p is the polymer volume fraction, χ is the polymer-solvent interaction parameter, N is the crosslinking density (mol/dm^3) of the polymer network, and V_s the molar volume of solvent. It is worth noting that the polymer-solvent interaction parameter (χ) quantifies the exchange interaction between the polymer chains and the pure solvent, and therefore represents the polymer's tendency to dissolve in a specific solvent. This is based on the Flory-Huggins theory, where the free energy of mixing (ΔG) is a function of the interaction parameter (χ) and the polymer volume fraction (v_p) in:

$$\Delta \mathrm{G}=\mathrm{RT}\left\{\ln(1-v_p)+\ v_p+\ \chi v_p^2\right\} \qquad \text{Equation 4-4}$$

For the copolymers in this study, the Flory-Rehner model can be used to calculate an estimated crosslink density which cannot be directly compared to literature values, since the current system is a completely physically crosslinked system, where crosslinking is induced by hydrophobic interaction instead of the traditional covalent crosslinking as used in the development of this model. In covalently crosslinked systems, randomly distributed inter-polymer linkages exist and yield an insoluble three-dimensional network. In the current system, phase segregation gives rise to large, intermittent domain formations. Therefore, the purpose of the work presented in this section is to highlight the effect of hydrophobic PDMS inclusion as physical crosslinking mechanism within the system on the crosslink density of the materials.

An estimation of the apparent crosslink density (N) of the PNIPAM domains was calculated for all samples using the Flory-Rehner equation. Listed Q_s values and PNIPAM density (ρ_{polymer}) of 1.116 g/cm^3 is used in the calculation of the polymer volume fraction (v_p) with an interaction parameter (χ) of 0.518 for PNIPAM and water[16]. Calculation details for v_p may be found in the Appendix.

Figure 4-18 presents an estimation of the apparent crosslink density within the copolymer networks that could be calculated according to the Flory-Rehner model. The results are generally in agreement with findings presented throughout this work. The apparent crosslink density of the lowest PDMS content sample of both copolymer series could not be calculated since these materials formed weak

hydrogels that fractured after the first 1 to 2 hours in water. Only hydrogel materials that lasted 24 hours in water were considered. In both the 5 000 and 10 000 g/mol PDMS copolymer series an apparent trend of increased crosslink density exists as a function of PDMS content. This is to be expected since the PDMS side-chains of the graft copolymer form hydrophobic clusters within the copolymer network, which acts as physical crosslinks among polymer chains yielding a water-insoluble hydrogel material. Therefore, the higher the incorporated amount of PDMS within the copolymer, the greater the number of possible crosslinks within the network.

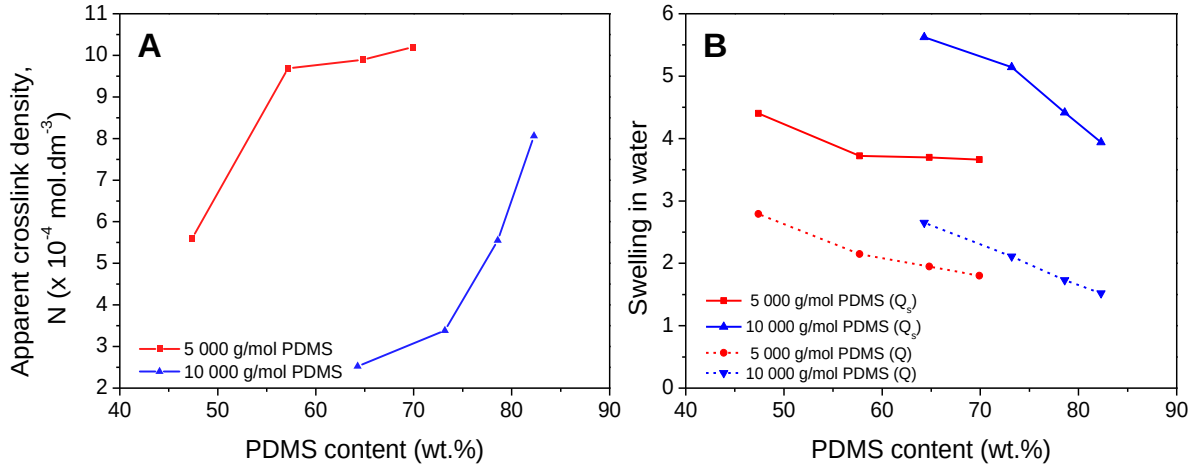

Figure 4-18: (A) Apparent crosslink density (N) as a function of PDMS content (wt.%) calculated according to the Flory-Rehner model and (B) plotted swelling data (Q and Q_s values) of the corresponding samples.

An interesting observation in (A) in Figure 4-18 is the sharp increase in crosslink density between the 47.4 and 57.7 wt.% 5 000 g/mol PDMS samples, after which a slight but gradual increase with increasing PDMS is observed. This observation agrees with the properties and appearance of the hydrogel materials where the 47.4 wt.% sample is still quite brittle compared to the more rubber-like 57.7 wt.% sample. As discussed in previous sections, the amount of incorporated PDMS and thus the effective number of crosslinks within the copolymer network, have a significant effect on the physical appearance and brittleness of the materials. A slight but gradual increase in crosslink density is observed for the last three samples in the 5 000 g/mol PDMS series, which can be related to the very similar swelling ratios ((B) in Figure 4-18) and more rubber-like appearance of these samples.

The 10 000 g/mol PDMS series, on the other hand, display a large incremental increase in crosslink density with increasing PDMS content. This is a likely outcome since increasing the feed with only 1 mol.% of 10 000 g/mol PDMS has a large effect on crosslinking density due to the large size of the macromonomer. This reiterates the effectiveness of the macromonomer as physical crosslinker and can again be related to the change in swelling capabilities and physical appearance of these materials, ranging from brittle to more rubber-like with increasing PDMS.

The nature of the Flory-Rehner model should be considered when interpreting the results. The model is based on the equilibrium swelling of randomly coiled polymer chains in a solvent, providing a correlation between the degree of swelling and the crosslink density. The model is based on chemical crosslinking, but also includes a certain fraction of physical crosslinks such as chain entanglement within the polymer network. Since the current system consists only of physical crosslinks, all crosslinks may not be attributed for in this model. Another important factor is the polymer-solvent interaction parameter (χ). Upon expansion of the natural log term of the Flory-Rehner equation, it can be shown that $\Delta G < 0$ when $\chi < 0.5$ for all values of v_p, which indicates that the polymer and the solvent are miscible in all proportions, resulting in the polymer being soluble in the particular solvent. When $\chi > 0.5$, the value of v_p is the condition for limited or equilibrium swelling, and thus determines where $\Delta G = 0$.[17] In this case, χ is 0.518 and therefore the volume fraction of polymer is the determining factor for solvent miscibility. Considering the volume fraction of incorporated polymer within the system to further rationalize the results; only the PNIPAM fraction of the polymer is taken into consideration, therefore the crosslink density is expressed in terms of PNIPAM content and not necessarily in terms of the actual comonomer which gives rise to the crosslinking mechanism.

Nevertheless, the given model highlights the effect of hydrophobic PDMS inclusion on the apparent crosslink density of the materials. PDMS proved to provide an effective physical crosslinking mechanism by means of phase segregated hydrophobic domains for the production of water-insoluble, yet solution-processable, hydrogel materials.

4.5. Sample preparation and its effect on morphology and swelling behaviour

4.5.1. Changing the casting solvent

The thermo-responsive materials produced in this study rely on the physical crosslinks induced by the hydrophobic PDMS domains. Since this is the case, it is expected that the solid-state morphology will have a dramatic influence on the swelling behaviour of the materials. In order to investigate the solid-state morphology induced by different sample preparation methods, films of the same sample were cast from different solvents to determine whether induced morphologies are the consequence of solvent effects or drying process kinetics of the different preparation methods. The chosen solvents had different polarities and volatilities and may, therefore, affect the morphology. Figure 4-19 shows the swelling results of the 4.3 mol.% 5 000 g/mol PDMS films casted from low boiling point solvents (high volatility), DCM (39.6 °C), THF (66.4 °C) and ethanol (78.5 °C) as well as higher boiling point (lower volatility) solvents such as dioxane (101.1 °C) and methyl-ethyl ketone (79.6 °C). It can be seen that the films cast from lower boiling point solvents generally produced lower swelling ratios than the higher boiling point equivalents. These results can be explained by considering the rate of evaporation. For example, less volatile solvents will essentially evaporate at a slower rate than highly volatile solvents, allowing more time for molecular rearrangement and phase segregation to occur. Enhanced phase segregation may result in larger, more defined non-swellable, hydrophobic PDMS domains. Although differences in equilibrium swelling do exist, it is not as notable as when comparing swelling behaviour of samples prepared by different techniques, i.e. film casting vs electrospinning (as discussed in detail later). The fact that there is a difference between the swelling behaviour of films cast from ethanol and methyl ethyl ketone, with very similar boiling points, also supports the fact that solvent effects may not be the only contributing factor to a material's swelling behaviour. In the following sections, sample preparation methods and the effect thereof on the material's swelling behaviour will be further investigated.

The polarity of the processing solvent has a major effect on solution behaviour of the copolymers and thus may affect the solid-state morphology thereof. Arranging the solvents according to increasing polarity indexes; DCM (3.1), THF (4.0), MEK (4.7), dioxane (4.8), and ethanol (5.2). The copolymer used in this experiment is highly soluble in THF, MEK and dioxane. It did, however, take longer to dissolve in DCM and ethanol. This may be due to polarity differences. If the solvent favours one component of the amphiphilic copolymer more than the other, it may result in solution self-assembly. For instance, the low polarity DCM may favour the hydrophobic PDMS side-chains more than the PNIPAM backbone, resulting in varying solution morphologies. The opposite may be true for more polar ethanol, where the PNIPAM backbone may be favoured over the PDMS side-chains, also potentially giving rise to solution morphologies. Therefore, considering that both segments of the copolymer are potentially not fully soluble in these two solvents, varying solution morphologies

may have caused altered solid-state morphologies, which directly influenced the swelling behaviour of the material.

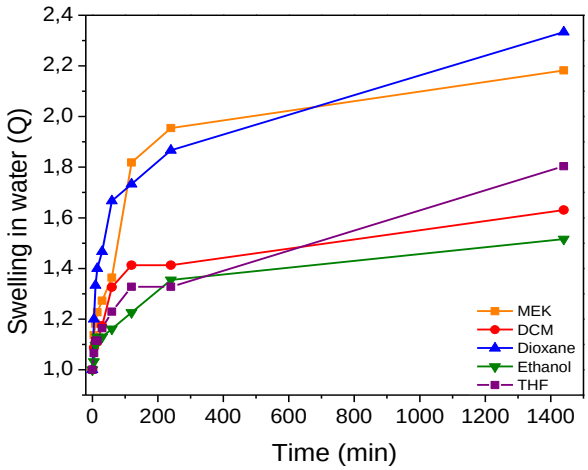

Figure 4-19: Swelling of films of the same sample (PNIPAM-*g*-PDMS, with 4.3 mol.% 5 000 g/mol PDMS inclusion) that were cast from different solvents (20 °C, pH 7).

An in-depth study on solution morphology of these complex amphiphilic copolymers should be conducted to confirm and further investigate the assumptions made here. A multitude of variables exist, with solvent composition and temperature effects almost certainly being the most significant morphology-inducing factors. For the purpose of the current study, it is, however, sufficient to note that solvent effects do affect the solid-state morphology of the samples, but the drying kinetics and sample preparation methods are most prominent. This can be concluded from the investigations done in this study and presented in the following sections.

4.5.2. Slow precipitation by dialysis

Since the film and fibre samples (discussed in Section 4.5.3 to follow) were both processed from THF, it can be assumed that the morphological differences that exist do not solely arise from solvent effects. Thus, varying morphologies must be related to the kinetics of the drying process and the sample preparation technique, rather than the nature of the solvent alone. To support this concept, the swelling behaviour of differently prepared samples were compared. Differences between films cast from solvent and fibres made by electrospinning of the same solvent will be thoroughly discussed in the following sections of this work. However, it was attempted to induce new morphologies in the samples by preparing samples by alternative methods such as slow precipitation via dialysis. The objective was to precipitate the sample in a more polar solvent, such as water, to favour the hydrophilic PNIPAM segment of the copolymer and so induce greater swelling capabilities in water. This was achieved by dissolving samples in THF and dialysing (3500 MWCO) against water for 2 days, resulting in slow precipitation of the hydrogel materials. Table 4-5 shows the swelling data of the differently prepared samples compared to that of films prepared by slow solvent evaporation. The data shows that this preparation method produced highly swollen hydrogel structures with greatly enhanced swelling capabilities compared to the films. After initial dehydration, however, the

slow precipitated hydrogels did not rehydrate to the same extent as to which it initially had swollen and only exhibited normal swelling behaviour. Wagenaar observed a similar effect for PDMAA-*g*-PDMS copolymers.[4] It is proposed that the solution morphologies induced in these hydrogels are only stable under aqueous conditions, thus suggesting that these gels should be considered a dense emulsion in water, rather than a solid material. Once the emulsion is removed from its aqueous environment and dehydrated, a rapid decrease in intermolecular chain distance occurs. The rapid decrease in distance between polymer chains, enables the formation of new hydrophobic PDMS side-chain domains, resulting in increased effective crosslinking density and thus decreased swelling ability. Since it is more favoured for the hydrophobic side-chains to interact with each other, rather than the polar surrounding water, the hydrogel will not undergo the same degree of swelling after dehydration.

Table 4-5: Degree of water swelling (Q) of three different samples prepared by film casting and slow precipitation by dialysis, respectively (20 °C, pH 7).

Preparation method			**Film cast**	**Slow precipitation by dialysis**	
PDMS chain length	mol.% PDMS	wt.% PDMS	Swollen (Q)	Swollen (Q)	Rehydrated (Q)
5 000 g/mol	2.9	57.7	1.96	2.95	2.09
10 000 g/mol	2.9	73.2	1.89	2.31	1.97
10 000 g/mol	3.8	82.3	1.72	2.16	1.62

Figure 4-20 shows the difference between the opacity of the slow precipitated swollen hydrogel and the transparency of its dehydrated equivalent. The opacity of the gels may be explained by the collapsed PDMS side-chains forming hydrophobic domains in the less favoured polar solvent. This results in less light being transmitted through the material. During slow precipitation in water, the hydrophobic PDMS segments self-assemble to form hydrophobic clusters. However, since they are covalently grafted to the hydrophilic PNIPAM backbone, precipitation of these clusters does not occur and rather result in the formation of a highly swollen hydrogel material. This preparation technique allows sufficient time to reach maximum equilibrium swelling.

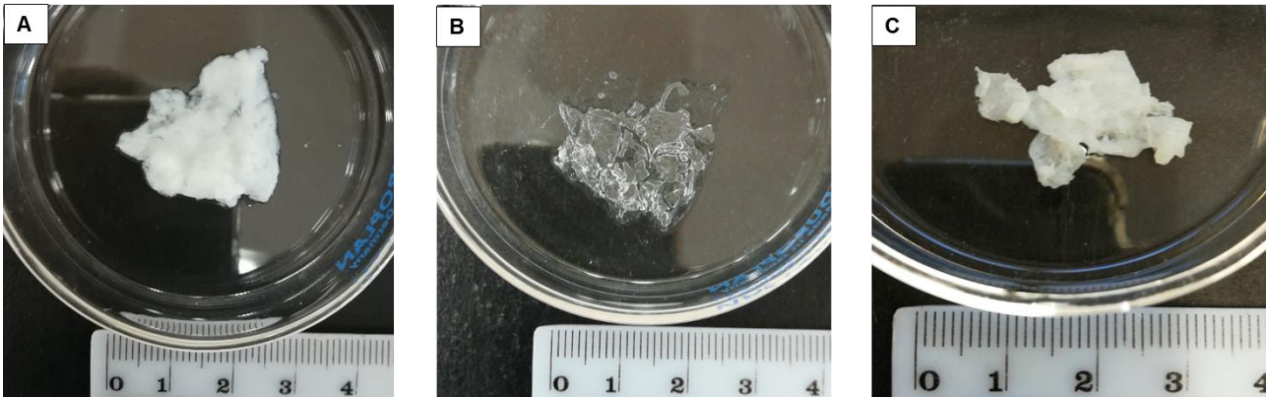

Figure 4-20: 2.9 mol.% 5 000 g/mol PDMS (A) hydrogel prepared by slow dialysis from THF to water, (B) dehydrated hydrogel, and (C) rehydrated hydrogel.

4.5.3. Hydrogel fibres by electrospinning

Electrospinning is considered one of the simplest and most commonly used techniques for the production of nanofibre hydrogels with high surface-to-volume ratios and increased swelling rates and abilities, compared to the bulk material.[18] Hydrogel nanofibres are ideal platforms for rapid response systems since the diffusion distance of molecules are much smaller than that of macroscopic hydrogels, allowing for faster response times in stimuli-responsive materials.[18] The production and use of hydrogel nanofibres are regularly reported throughout literature, most commonly as chemically crosslinked materials where solution or non-solution based post-electrospin crosslinking is required. One of the major advantages of the current copolymer system, is the presence of physical crosslinks within the polymer network, permitting the formation of water-insoluble, mechanical stable crosslinked materials that do not require post-electrospinning processing or further purification. The physically crosslinked copolymer networks allow for solution processing from a common solvent such as THF to facilitate the production of hydrogel nanofibres.

Many different combinations of basic electrospinning parameters such as concentration, solvent systems, flow rate and voltage supply, were tested on a trial-and-error basis until the most appropriate combination was selected for the production of smooth, uniform fibres.

Figure 4-21 shows the effect of electrospinning solution concentration on the fibre morphology for 2.9 mol.% 5 000 g/mol PDMS sample. Particles formed at low solution concentrations in a technique known as electrospraying, as seen in (A). Although interesting, thermo-responsive particles were not the focus of this study, signifying that the solution concentration had to be increased. Incremental increase in solution concentration resulted in the production of particles as well as beaded fibres, as seen in (B) and finally at high solution concentration of 55 % w/v smooth, bead-free fibres were formed (C).

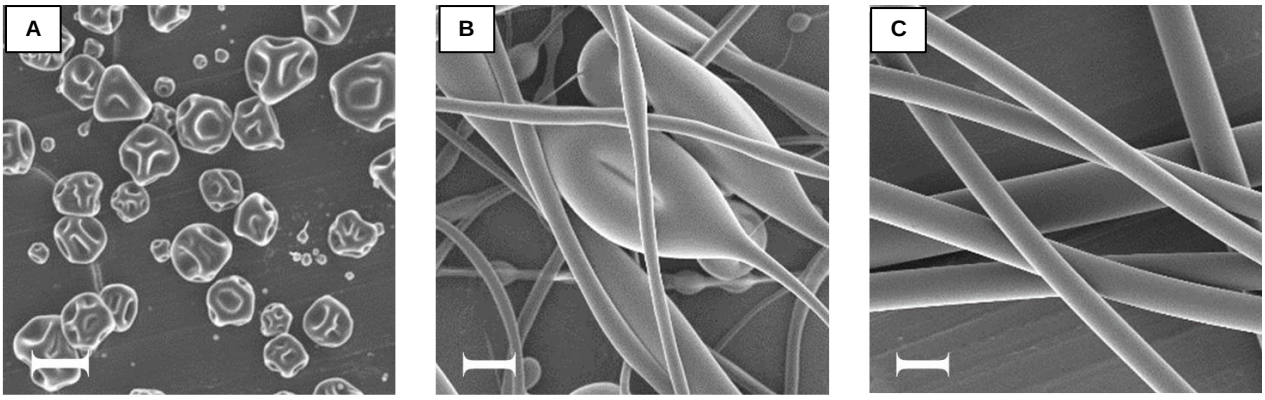

Figure 4-21: SEM images of (A) particles resulted from electrospraying due to low solution concentration (20% w/v), (B) beaded fibres and particle (40% w/v), (C) smooth fibres obtained by electrospinning of high solution concentration of the 2.9 mol.% 5 000 g/mol PDMS sample (55% w/v). Scale bars indicate 2 µm, 2 µm and 10 µm, respectively.

The selected parameters were identified to be a high solution concentration of 55% w/v and 50% w/v for 5 000 g/mol and 10 000 g/mol PDMS samples, respectively, with electrical potential of 5 kV, tip-to-collector distance of 15 cm and a flow rate of 5 µL/min for both sample series. The appearance and physical properties of the different fibre samples varied as a function of PDMS content. The average fibre diameters and distributions thereof are presented in Table 4-6 and Figure 4-22.

Table 4-6: Average fibre diameters (µm) and distributions of a minimum of 200 measurements per sample of the 5 000 and 10 000 g/mol PDMS fibre samples.

5 000 g/mol PDMS		**10 000 g/mol PDMS**	
PDMS content (mol.%)	Average diameter (µm)	**PDMS content (mol.%)**	Average diameter (µm)
1.7	6.9 ± 2.4	**1.2**	2.9 ± 1.3
2.6	4.3 ± 2.2	**2.5**	3.7 ± 1.2
2.9	6.8 ± 2.0	**2.9**	2.6 ± 1.1
3.0	5.4 ± 1.5	**3.8**	3.9 ± 0.9
4.3	6.9 ± 1.5	**4.1**	3.8 ± 1.0

A minimum of 200 measurements per copolymer sample in both series were made. The average fibre diameters of the 5 000 g/mol PDMS series varied greatly and were much larger than the 10 000 g/mol PDMS samples. Although no definitive trend could be observed for average diameters of these fibres, it should be noted that the overall fibre diameter distribution decreased with increasing PDMS, indicating the production of more uniformly sized fibres. Figure 4-22 shows that the fibre diameters of the 10 000 g/mol PDMS series were on average much smaller with smaller fibre distributions than the fibres obtained from the 5 000 g/mol PDMS series, although still quite large in terms of electrospun fibres. Again, a decrease in fibre diameter distribution is observed with increasing PDMS content as fibre uniformity improved. The generally large and increased fibre diameters may be

ascribed to increased viscosity of the spinning solution, which may be indicative of polymer self-assembly in solution.[8,19] The solution concentration of the 5 000 g/mol PDMS series (55% w/v) and the 10 000 g/mol PDMS series (50% w/v) are in both cases regarded high for general electrospinning applications. Increased viscosity of the spinning solution was certainly evident during the electrospinning process, causing intermittent needle tip blockage and hindering the ease of electrospinning. This may be problematic in the case of large-scale electrospinning since the droplet at the needle tip needed to be physically removed to continue fibre production.

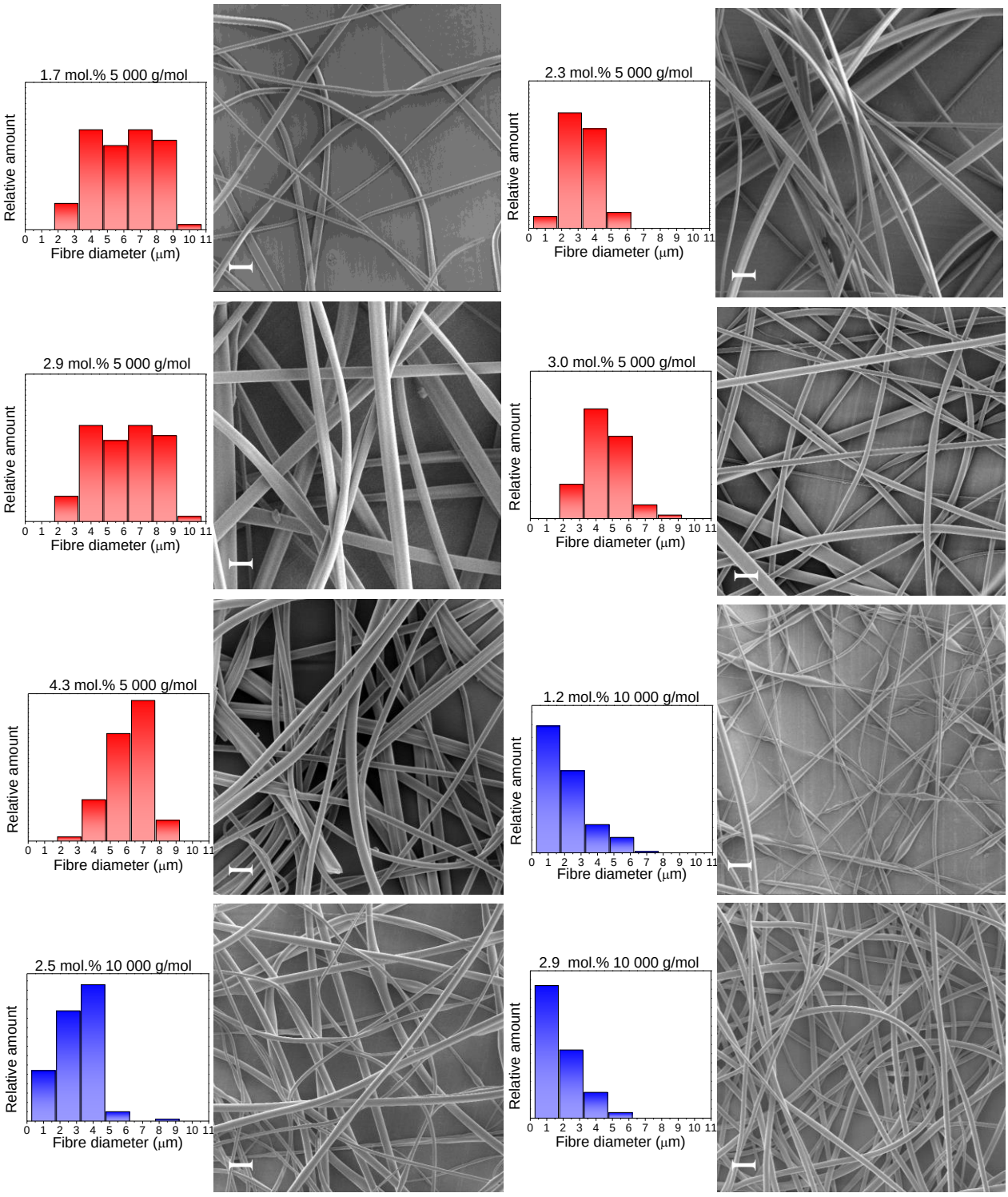

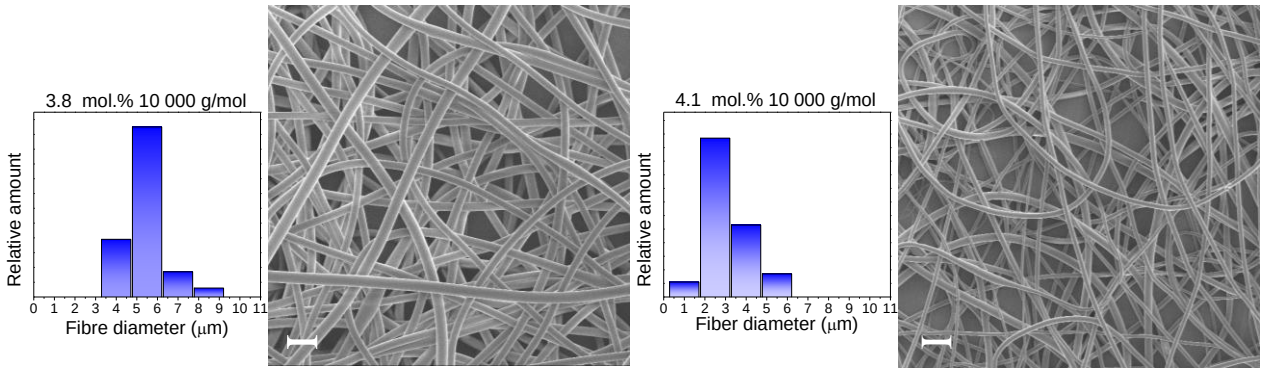

Figure 4-22: Histograms representative of the fibre diameter (μm) distribution of the 5 000 g/mol PDMS (red) and the 10 000 g/mol PDMS (blue) fibre series. A minimum of 200 measurements per sample were made. The SEM fibre images all have scale bars indicating 20 μm.

The large fibre diameters may also be ascribed to the relatively low applied voltage used during the electrospinning process. It is well documented that processing parameters such as applied voltage and flow rate greatly affect fibre diameters.[20] However, in the current study increasing the applied voltage lead to non-continuous electrospinning in the form of sputtering resulting in entangled fibre knots, as seen in (A) in Figure 4-23.

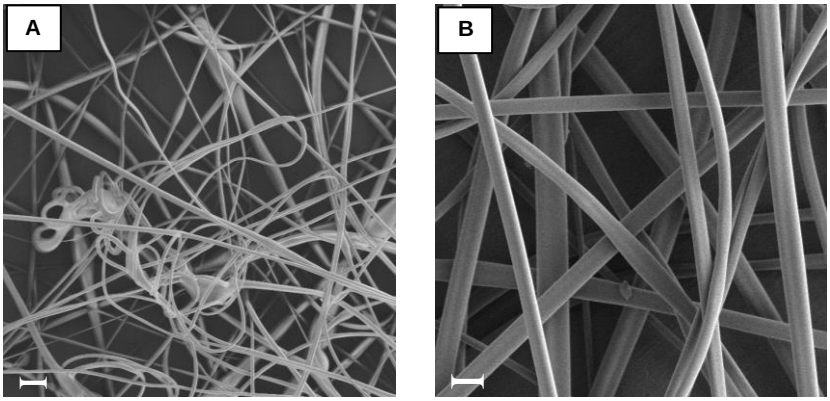

Figure 4-23: SEM images illustrating the effect of flow rate and applied voltage on the 2.9 mol.% 5 000 g/mol PDMS sample where in (A) 10 kV at 10 μL/min and (B) 5 kV at 5 μL/min. Solution concentration and tip-to-collector distance was kept constant (55% w/v and 15 cm).

Another important factor to consider is the physical appearance of the produced fibres. Figure 4-24 below shows the fibre morphology for two selected samples. In (A) the low PDMS content sample produced flat, ribbon-shaped fibres that were very brittle to the touch, whereas (B) the high PDMS content sample produced round, smooth fibres that permitted easy handling without fibre breakage. This is an important factor to keep in mind when considering the viability of these fibres in real-world applications. The varying shapes and sizes of the low PDMS content samples may also be a contributing factor to the larger fibre diameter distribution values of the low PDMS content samples.

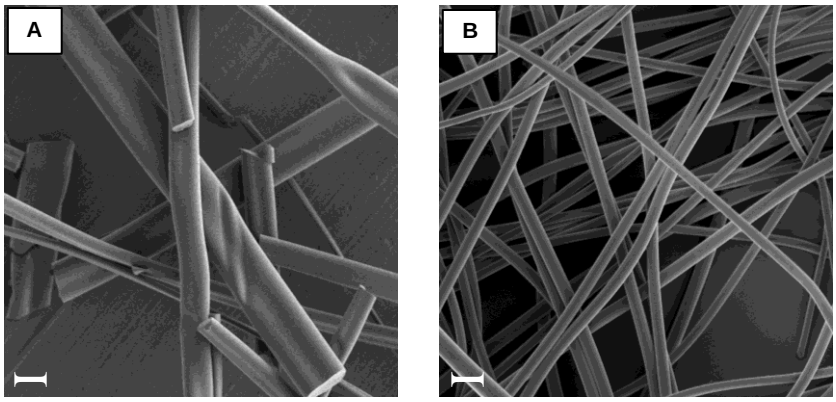

Figure 4-24: SEM images allowing visual comparison between fibre samples made from PNIPAM-*g*-PDMS samples with (A) 2.3 mol.% and (B) 4.3 mol.% 5 000 g/mol PDMS inclusion, respectively. The scale bars indicate 20 µm. (55 % w/v, 5 kV, 15 cm t.c.d., 5 µL/min).

A magnified image of a fractured fibre in Figure 4-25 illustrates the smoothness of the fibre surfaces, verifying that these materials are not porous in nature. No fine structures or pores could be identified on the fractured surface, even though it is speculated that self-assembled structures are present in solution, as deduced from previously discussed analytical techniques. Thus, the swelling mechanism in water occurs via diffusion and hydrogen bonding of water molecules with the hydrophilic NIPAM segments within the copolymer network as opposed to capillary action provided by an interconnected porous structure. In work conducted by Bayley, the effect of PDMS content on the internal fibre morphology was investigated. Porous type fibres were obtained by the incorporation and variation of PDMS content within the PAN-*g*-PDMS copolymer.[8] This was ascribed to the rapid crystallization of the PAN fraction within the copolymer structure. This does not occur in the case of PNIPAM used in this study. Meltz, however, did not observe any particular internal structures within the amphiphilic PMMA-*g*-PDMS fibre samples, although solution self-assembly was present.[19]

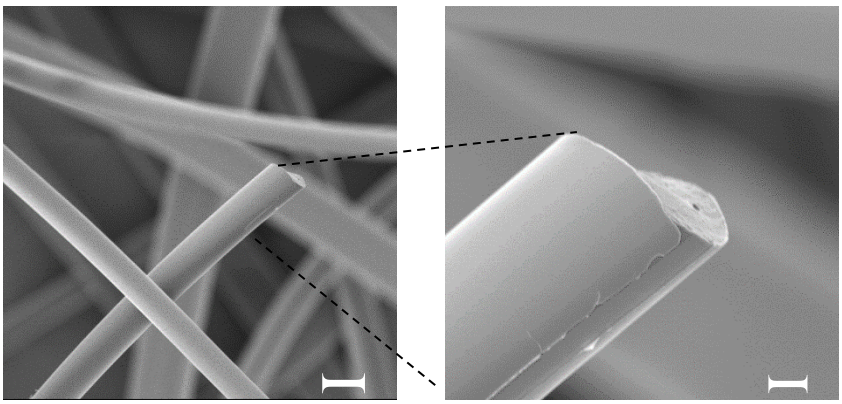

Figure 4-25: Magnified SEM image of 2.3 mol.% PDMS (5 000 g/mol) PNIPAM-*g*-PDMS fibre. Scale bar indicates 10 µm (left) and 2 µm (right), respectively.

4.6. Swelling and water stability of hydrogel nanofibres

Accurate quantification of swollen samples using SEM is not possible since wet samples cannot be evaluated under normal SEM operating conditions due to the high vacuum employed. It does, however, allow visual investigation of fibre morphologies after moisture exposure. Structural integrity and morphological changes of the fibres were investigated under varying humidity conditions and water submersion. All fibres proved to retain structural integrity and dimensional stability after being submitted to 45 % r.H. and 85 % r.H. for 7 days. Figure 4-26 shows the 5 000 g/mol PDMS fibre series after 7 days at 95 % r.H. This figure shows that low PDMS content fibres displayed some swelling and a decrease in fibre roundness after 7 days at 95 % r.H. Yet, all fibres samples remained structurally intact and retained their overall fibrous structure. This may be explained by the fact that PDMS inherently has a low surface tension and therefore tend to segregate to the fibre surface, enhancing the hydrophobic nature of the fibre surface.[10] Therefore, the fibres will not undergo much swelling when subjected to a high moisture environment, but will, however, swell rapidly when the hydrophilic component of the copolymer is in direct contact with water during water submersion. This hypothesis is supported by the SCA measurements discussed in Section 4.8, where low PDMS content fibres initially display highly hydrophobic behaviour after which rapid swelling is observed.

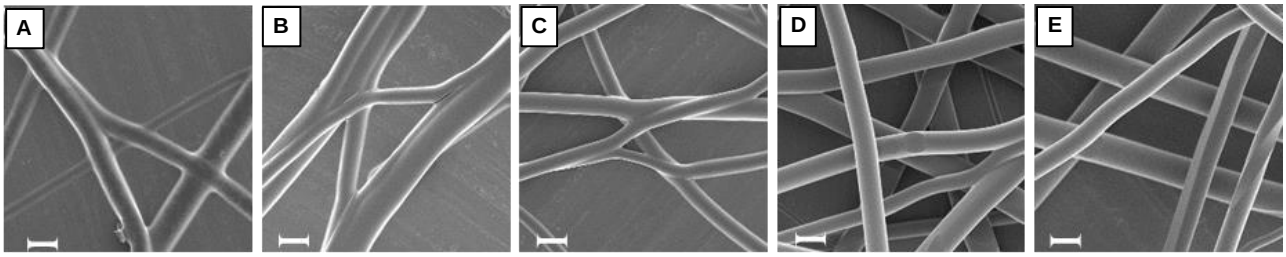

Figure 4-26: A to E are the 1.7 mol.% to 4.3 mol.% 5 000 g/mol PDMS samples at 95 % r.H. for 7 days before drying under vacuum and imaging by SEM. Scale bar indicates 10 µm.

Water stability of the various fibre samples were analysed by submerging the fibres in water with pH 7 at 20 °C for 5 minutes and 1 hour, respectively. The water stability of the fibres was primarily associated with the amount of PDMS incorporated within the copolymer system. Figure 4-27 shows an example of a low PDMS content fibre sample. Low PDMS content samples of both the 5 000 g/mol and 10 000 g/mol series lost structural integrity when submerged in water for several minutes. The amount of incorporated PDMS within these samples were insufficient in maintaining swollen fibrous structures.

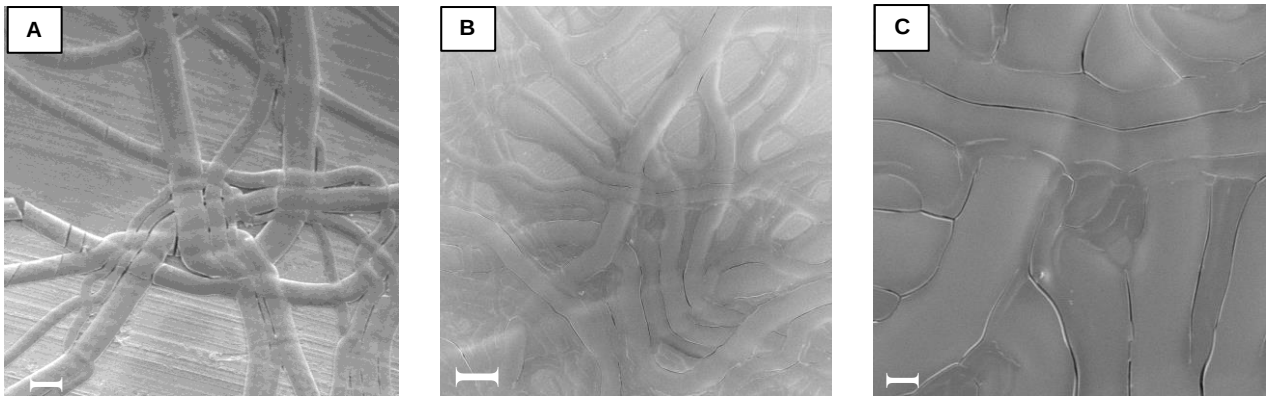

Figure 4-27: Low PDMS content (2.3 mol.% 5 000 g/mol) fibres after submersion in water for 5 min (A) and 1 hour (B), respectively. (C) is a magnified image illustrating fibre fusion after water exposure for 1 hour. All samples were dried under vacuum and visualized by SEM. Scale bar indicates 20 µm, 100 µm and 20 µm, respectively.

Figure 4-28 shows an example of a high PDMS content fibre sample. The high PDMS content samples proved to retain their fibrous structure after 5 minutes in water, however, only the highest PDMS content (4.3 mol.% and 4.1 mol.% PDMS inclusion, respectively) of both the 5 000 g/mol and 10 000 g/mol PDMS series remained structurally intact after 1 hour in water. Although these materials exhibited hydrogel properties and formed stable hydrogels in film form, the water stability experiments showed that the fibres lost their individual fibrous structures and fused together after deswelling. In all cases increased PDMS content resulted in improved film and fibre morphology.

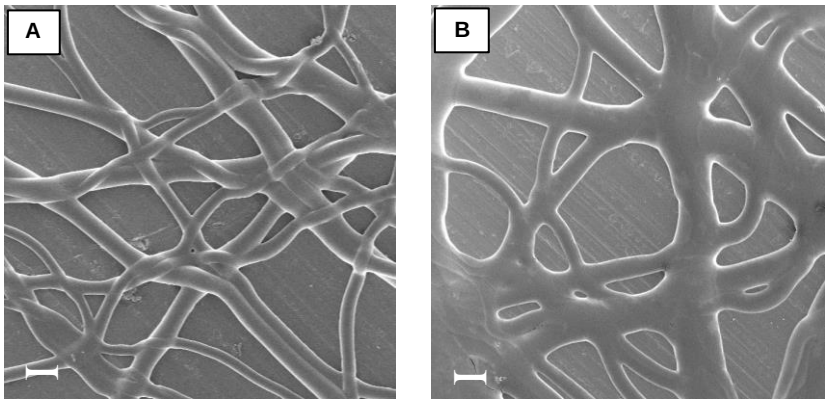

Figure 4-28: High PDMS content (4.3 mol.% 5 000 g/mol) fibres after submersion in water for 5 min (A) and 1 hour (B), respectively. All samples were dried under vacuum visualized by SEM. Scale bar indicates 20 µm.

It is clear that unlike other reported nanofibre hydrogels, some degree of post-electrospin crosslinking is required to maintain the structural integrity of the PNIPAM-*g*-PDMS hydrogel fibres after water swelling. In this case, the longer PDMS side-chains and high PDMS content produced less stable fibre hydrogels. This is most likely due to the formation of larger PDMS domains and the very low glass transition of the PDMS macromonomer. However, this should not necessarily be considered a failure. Some potential applications for these fused fibres may include the fabrication of porous membrane materials that can potentially be used as cell carrier substrates or scaffolds for regenerative tissue structures.[21]

All films, on the other hand, remained structurally intact and water-stable for several hours, some even for days. The fibres could only retain their structure for several minutes before fusion to form a porous membrane structure. This may be due to the rapid swelling rate of the high surface-to-volume fibres, where the hydrophobic PDMS domains could not act as sufficient physical crosslinks to produce completely water-stable hydrogel fibres. This may be attributed to the rapid solvent evaporation, the volatile nature of the electrospinning solvent (THF) and drawing during the electrospinning technique. During the production of the fibres, the polymer solution is rapidly extruded through the needle towards the collector plate. This and the charged nature of the solution and collector plate cause rapid elongation and drying of the fibres while it travels towards the collector plate. All these factors contribute to the short time period available to form the sufficiently large hydrophobic clusters needed to act as physical crosslinks and keep the copolymer network together, resulting in non-equilibrium morphologies. During solvent casting of films, slow solvent evaporation provides polymer chains with sufficient time to reach equilibrium morphology, which will differ from that of the fibre state. Phase segregation occurs in both cases, but not nearly to the extent of slow solvent evaporation film casting. This is again supported by the fact that the film equivalents are much more water-stable than the fibres. Films cast from the same solvent display only small differences in the degree of swelling, thus validating that it is the process of sample preparation, rather than the type of solvent alone that induce changes in sample morphology.

Figure 4-29 and Figure 4-30 show the differences in a low PDMS content sample (2.3 mol.% 5 000 g/mol PDMS) in fibre and film form. It is evident from the figures that the sample preparation method has a significant influence on the physical properties and swelling behaviour of the material when comparing the film and fibre equivalent made from the same sample. Both the film and fibre form of low PDMS inclusion samples were brittle and difficult to handle in dry state. The low PDMS content fibres swelled very rapidly in water and fibre fusion occurred, resulting in a loss of fibrous structure after deswelling.

Figure 4-29: Digital images obtained by optical microscope of (A) brittle, low PDMS (2.3 mol.% 5 000 g/mol PDMS) inclusion fibres in dry state, (B) swollen in water, and (C) dehydrated. These fibres were very brittle to touch in the dry state and fused together after deswelling, thus losing their fibrous structure.

The film equivalent, however brittle, were able to cast into manageable hydrogel shapes for swelling analysis. The films showed sizable swelling in water without undergoing dissolution as well as structural retention after dehydration.

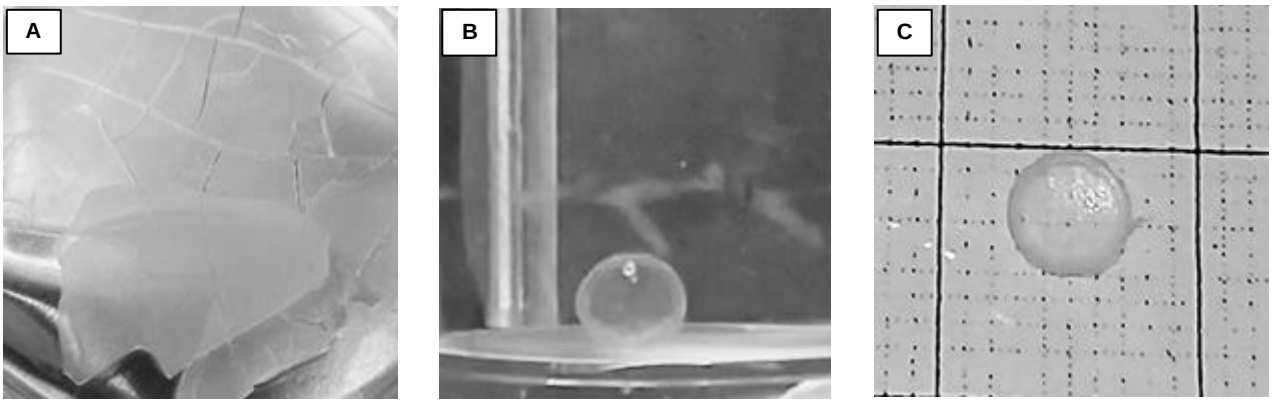

Figure 4-30: Digital images of a (A) brittle, low PDMS inclusion film (2.3 mol.% 5 000 g/mol PDMS) in the dry state, (B) swollen in water and (C) dehydrated. Although brittle, small hydrogel shapes could be cast and swelling behaviour could be analysed. The hydrogel films retained their structure after deswelling.

Higher PDMS inclusion samples produced less brittle, easier to handle materials. Figure 4-28 shows that the fibres of these samples still displayed rapid swelling in water without completely retaining its fibrous structure. The film equivalents, on the other hand, showed greatly improved physical properties, albeit decreased equilibrium swelling. Figure 4-13 shows higher PDMS inclusion films proved to be rubber-like, thus much easier to handle when dry and water-swollen, even when cast into large films. The physical improvement of the materials presents enhanced potential for commercial hydrogel applications.

4.7. Thermo-responsive behaviour and lower critical solution temperature (LCST)

The swelling and thermo-responsive nature of the copolymers in aqueous solution is notably affected by the incorporation of the hydrophobic PDMS side-chains. It is well-documented that the copolymerization of thermo-responsive NIPAM with either hydrophilic or hydrophobic comonomers may result in a modified lower critical solution temperature (LCST) value for the resultant copolymer, due to the altered balance between hydrophilicity and hydrophobicity. The effect of the PDMS on the material's swelling abilities and overall hydrophobicity is comprehensively studied in this work.

To investigate the potential effect of PDMS on the material's thermo-responsive behaviour, two methods of LCST determination were employed since traditional turbidity measurements were not suitable for LCST determination of water-insoluble hydrogel materials. Gravimetric analysis is another frequently used method for hydrogel LCST determination. However, this technique holds many experimental parameters and accurate measurements of saturated hydrogels at exact temperatures are often very challenging and irreproducible. It should also be noted that the determination of the LCST of the electrospun fibres is an additional challenge given their physical form.

The first approach to determine the LCST of the hydrogels involves digital recording of the hydrogel material in water with increasing temperature over time at a constant heating rate. The recorded images are then manually processed using digital image processing software to determine the *L*-value on a given pixel on the hydrogel at a given temperature, where the *L*-value is an indication of the material's opacity. This process is repeated on several pixels on the hydrogel image to obtain an average *L*-value for the hydrogel at that specific temperature. S-shaped curves were obtained and allowed the determination of the transition temperature of the hydrogel material in water. This method proved to be extremely labour intensive and time-consuming, especially since repeated measurements were required to ensure reproducibility. Further information regarding this technique may be found in the Appendix.

A second and simpler approach involved the use of an OptiMelt apparatus which is widely used in laboratories for melting point determination. This specific model was equipped with a digital camera and digital image processing software, allowing the user to observe the melting process while generating a spectroscopically produced curve. This curve plotted intensity versus temperature, producing an S-shaped curve similar to that obtained from method 1. In this case, the change in opacity of the films and fibres in water were monitored at a constant heating rate and plotted as a function of temperature. The data points and curves correlated well between the two methods, however, method two was selected as the method of choice since it was much more robust, easier and proved to be more reproducible.

Table 4-7 presents the data obtained using the OptiMelt instrument and data analysis software. The LCST value and a temperature range (FWHM) over which the transition occurred were obtained for all hydrogels and hydrogel fibres. The LCST values were selected as the midpoint of the Boltzmann fitted S-shaped curves, where the full-width at half maximum of the first derivative of the curve is an indication of a possible temperature range above and below the determined LCST. Details on data processing and curve fitting can be found in the Appendix.

Table 4-7: Lower critical solution temperature (LCST) value determined by two different methods for all films and fibres in the 5 000 g/mol PDMS and 10 000 g/mol PDMS series. The measurements in method 2 includes a full width at half maximum (FWHM) value to quantify the temperature range over which the transition occurs.

		Method 1	Method 2			
LCST (°C)		Films	Films	FWHM	Fibres	FWHM
	PNIPAM	32.7	32.4	± 0.3	-	-
5 000 g/mol series	1.7 mol.%	23.3	29.2	± 0.6	30.4	± 1.2
	2.3 mol.%	27.7	27.9	± 1.0	30.8	± 2.0
	2.9 mol.%	27.8	28.0	± 2.8	30.7	± 1.2
	3.0 mol.%	26.8	28.7	± 2.3	29.5	± 1.3
	4.3 mol.%	26.0	26.7	± 2.9	29.8	± 1.6
10 000 g/mol series	1.2 mol.%	28.1	27.7	± 2.3	30.7	± 1.1
	2.5 mol.%	27.4	28.4	± 3.0	30.8	± 0.6
	2.9 mol.%	26.5	28.8	± 1.8	30.6	± 0.8
	3.8 mol.%	27.9	28.9	± 2.9	31.3	± 4.5
	4.1 mol.%	29.2	28.5	± 2.9	31.2	± 6.9

Figure 4-31 and Figure 4-32 illustrate the change in opacity of a film and fibre sample as a function of temperature.

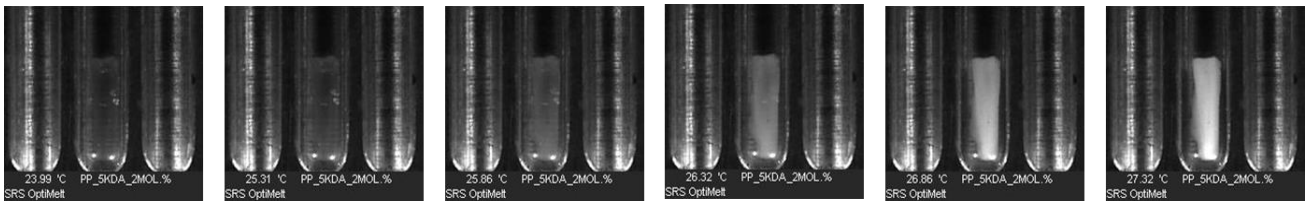

Figure 4-31: Monitoring the change in opacity as a function of temperature for the 2.3 mol.% 5 000 g/mol PDMS film in water (pH 7) using the OptiMelt apparatus. Temperature range presented in the images: 24.0 to 27.3 °C.

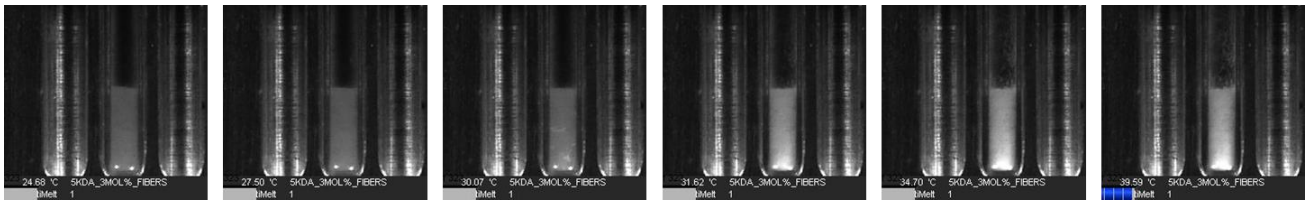

Figure 4-32: Monitoring the change in opacity as a function of temperature for the 2.9 mol.% 5 000 g/mol PDMS fibres in water (pH 7) using the OptiMelt apparatus. Temperature range presented in the images: 24.7 to 39.6 °C.

In all cases, the addition of PDMS resulted in a lower LCST value for the copolymers in water, compared to the PNIPAM homopolymer. It should be noted that the LCST of the material in fibre form was influenced to a lesser extent compared to the films. To rationalise this, the swelling behaviour of the films and fibre equivalents are compared. It was noted that the fibres had a much more significant swelling rate and degree than that of the corresponding films. This was contributed to the fact that the sample preparation method induced different solid-state morphologies within the samples. Since electrospinning promotes rapid solvent evaporation and drawing of the material, less time is allowed for the formation of equilibrium morphologies and thus much smaller hydrophobic domains can be formed. The limited time for PDMS domain formation resulted in less efficient physical crosslink formation and decreased crosslink density, resulting in water-instable fibres. This, in turn, can also be related to the effect of the hydrophobic PDMS incorporation on the material's LCST behaviour. The presence of hydrophobic PDMS domains may not necessarily influence the LCST of PNIPAM directly but may, in fact, cause a disruption of the hydrophobic and hydrophilic balance of the material. In the case of the fibres, much smaller PDMS domains exist compared to the film equivalents, thus disrupting the PNIPAM segments to a lesser extent, resulting in a smaller alteration of the material's LCST. During film preparation, on the other hand, slow solvent evaporation allows more time for equilibrium PDMS domain formation, more efficient physical crosslinks and higher crosslink density within the polymer network. This is evident in the swelling behaviour of the film materials since most of the films are water-stable over long periods of time and swell to a lesser extent than the fibres. Thus, the swelling behaviour of the films can be related to the altered LCST where the larger PDMS domains existing in the films impose a greater disruption within the PNIPAM network, consequently resulting in a greater change in the recorded LCST values.

It should be noted that a very broad temperature range is recorded for the 3.8 and 4.1 mol.% 10 000 g/mol PDMS fibre samples. This is due to the very slight change in opacity observed for these two samples due to the very high PDMS content in these samples, thus producing a broad S-shaped curve. Care should be taken not to misinterpret these results. This is not necessarily a transition over a large temperature range, but rather a less significant transition compared to lower PDMS content samples that undergo a dramatic change from transparent to opaque.

Although the incorporation of the PDMS macromonomer has an observable effect on the material's physical properties and swelling behaviour, a complex relationship exists between the incorporated PDMS and the LCST of the material.

4.7.1. Thermo-responsive swelling and deswelling of fibres

The hydrogel nanofibres in this study displayed a significant swelling ratio compared to the dry state. These fibres were, however, not completely water stable, making conventional swelling studies impossible. Therefore, the fibres were imaged using an optical microscope fitted with a temperature-controlled stage while dry and then after being wetted at different temperatures. This allowed the determination of a swelling ratio between dry and water-swollen fibres at temperatures below and above the material's LCST. Very rapid and significant swelling was observed once wetted. It was a challenging feat to image the wet fibres since they floated in the applied water droplet complicating the visualization of the thermal transition of a single fibre. Therefore, several images of each sample containing numerous fibres in the dry and swollen state were taken and allowed the calculation of an average degree of swelling for each sample at 25 °C (below the material's LCST) and 45 °C (above the material's LCST). Figure 4-33 shows the swollen fibres at 25 and 45 °C. From the figure it can be seen that raising the water temperature to 45 °C, fibre shrinkage, as well as a decrease in transmitted light through the fibres, occurred. This indicated the change in fibre appearance from transparent to opaque. The principle of change in opacity over temperature was employed for the determination of the LCST of these materials.

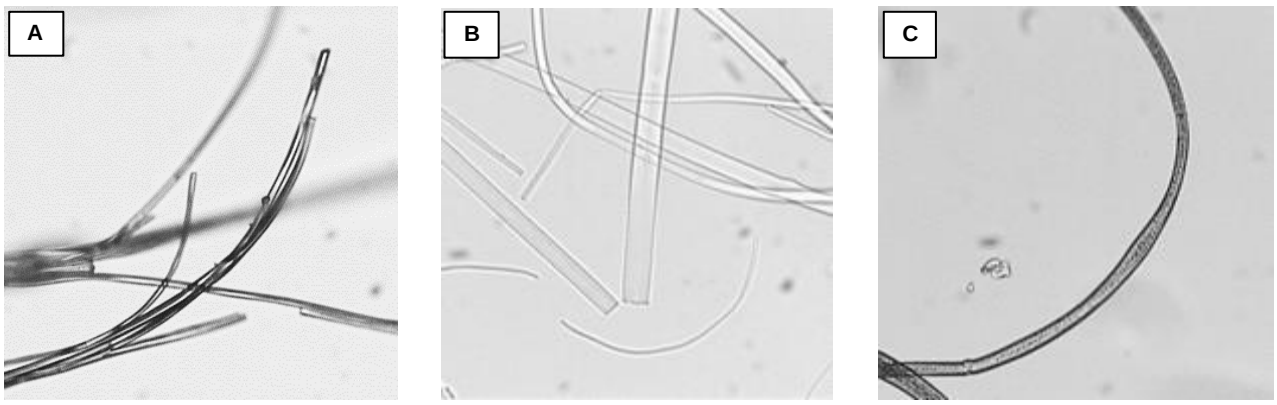

Figure 4-33: Digital images obtained using an optical microscope fitted with a temperature-controlled stage, allowing the visualization of fibre samples when dry and swollen in water at different temperatures. Fibres of 1.7 mol.% PDMS (5 000 g/mol) in (A) dry state, (B) swollen in 25 °C water, and (C) swollen in 45 °C water (ambient conditions of 25 °C, 45% r.H., pH 7).

As previously discussed, this behaviour was also observed for the film equivalents. Deswelling or shrinkage, together with change in opacity, is characteristic to reaching the LCST of the material in water. Figure 4-34 shows the swelling ratios of the different fibre samples of the 5 000 g/mol and 10 000 g/mol PDMS series at temperatures below and above the material's LCST. From the plotted swelling ratios there is a clear correlation between the swelling of the fibres at temperatures below and above the LCST of the material. At 25 °C, all fibre samples reach maximum equilibrium swelling

and are visualised as fully swollen, transparent fibres. This behaviour also corresponds to that of the film equivalents. At 45 °C, the fibres undergo rapid and observable deswelling. Fibre shrinkage is related to decreased swelling ratios and the visible change from transparent to opaque. Some swelling is, however, still observed when compared to the fibres in the dry state. This behaviour again relates to that of the film equivalents. Above the material's LCST, there is a change in the hydrophilic and hydrophobic balance within the material, resulting in the breaking of hydrogen bonding between the hydrophilic moieties and water molecules, resulting in a coil-to-globule transition which causes embedded water to be expelled from within the hydrogel structure. Thus, resulting in the deswelling of the material.

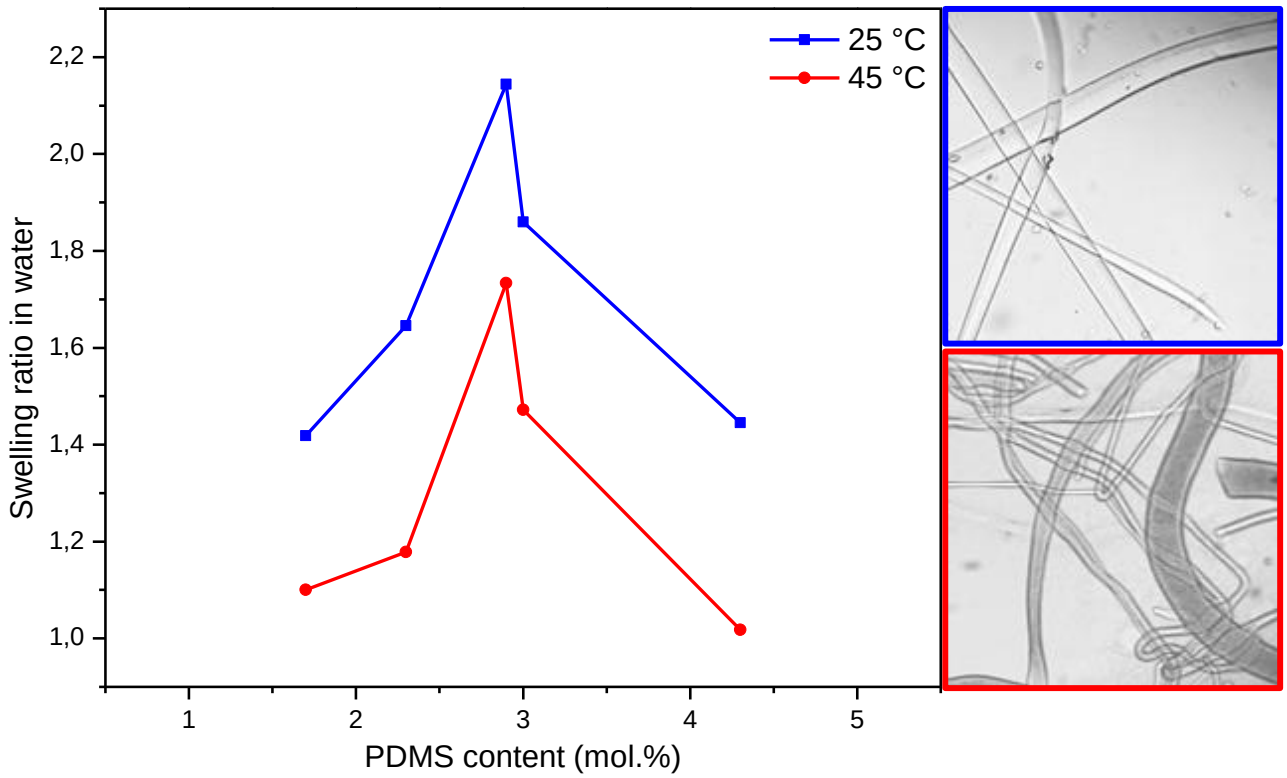

Figure 4-34: Swelling in water (Q) at 25 °C (blue) and at 45 °C (red) of the 5 000 g/mol PDMS fibre series as a function of PDMS content (mol.%).

From Figure 4-34 it may seem that the lower PDMS content samples undergo less swelling than their higher PDMS content counterparts, however, this is not the case. The highly brittle nature of the low PDMS content fibres made the monitoring thereof under an optical microscope very difficult. The transfer and handling caused fibre breakage and thus only small pieces could be observed. This was not fully representative of the sample. Nevertheless, a change in swelling behaviour below and above the LCST could be observed for all fibre samples, concluding that the material is thermo-responsive in nature and that its swelling behaviour was indeed altered by the incorporation of the hydrophobic PDMS macromonomer.

Figure 4-35 shows fused fibres after deswelling from water. It shows that very thick swollen fibres may not be representative of a single fibre since fibre fusion occurred after deswelling. Thus, care should be taken not to include these multi-fibres in fibre thickness measurements. It is therefore imperative to take a large number of measurements on a variety of different samples.

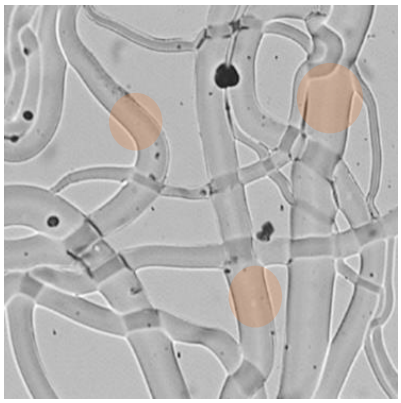

Figure 4-35: Fused fibres of the 2.3 mol.% 5 000 g/mol PDMS sample highlighted after water exposure and drying.

The resolution of the images obtained by the optical microscope was not nearly as high as that obtained by SEM but did allow for the visualization of the fibres in their swollen state while submerged in water, which is not possible with conventional SEM operation. The ideal technique for the visualization of individual fibres in their swollen state at different temperatures would be the use of atomic force microscopy (AFM) in a temperature-controlled solution cell. This technique was, however, not available at the time, but would provide valuable insight in future studies.

Direct comparison of swelling between films and fibres cannot be made since the swelling ratios of the films were obtained gravimetrically, whereas the fibres were analysed based on dimensional swelling. However, by visual comparison fibre equivalents underwent rapid and significant swelling compared to the corresponding films. An increased swelling ratio is to be expected for the fibres due to their greatly enhanced surface-to-volume ratios.

4.7.2. Reversible thermo-responsiveness

To investigate the reversible nature of the hydrogel's thermo-responsiveness in water, the swelling ratios of different film samples were recorded gravimetrically in 20-minute intervals at temperatures above and below its LCST in repeated cycles. Figure 4-36 illustrates the rapid swelling of the hydrogel materials at 20 °C (below its LCST) and deswelling at 60 °C (above its LCST). The swelling and deswelling behaviour of the hydrogel were monitored over 400 minutes, undergoing 4 temperature cycles of 100 minutes each.

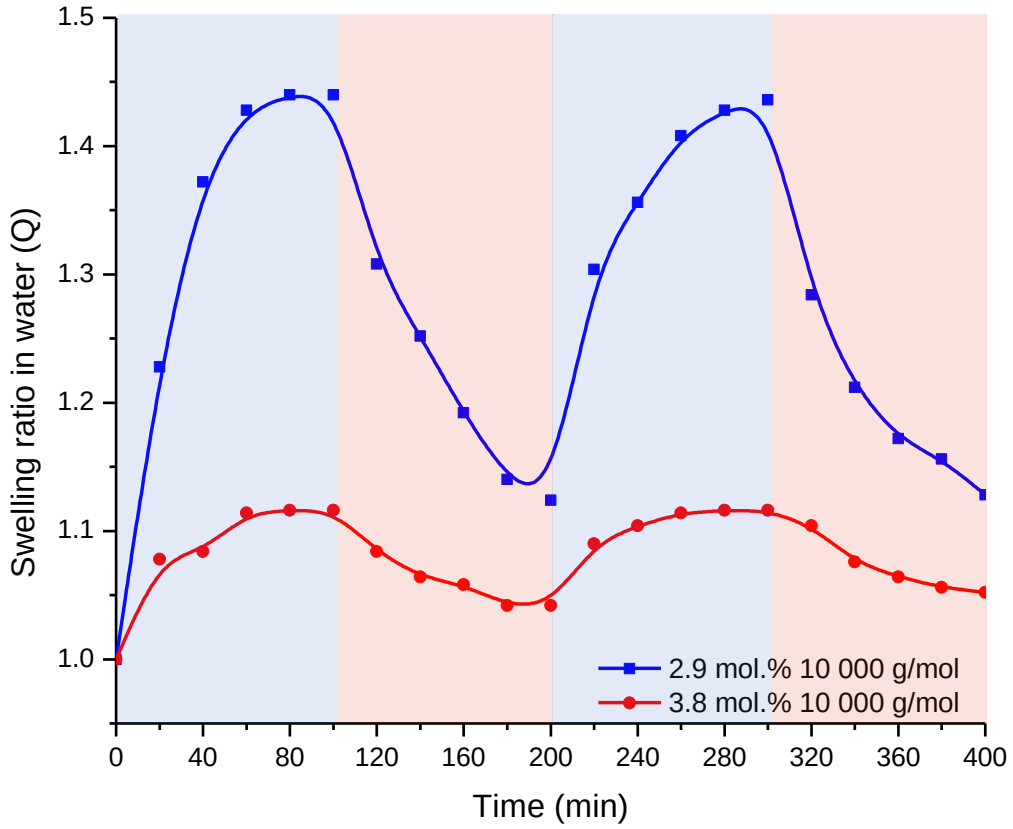

Figure 4-36: Reversible thermo-responsiveness of lower and higher PDMS inclusion samples below and above their LCST values in water (pH 7) undergoing several temperature cycles.

Below the material's LCST at 20 °C, the hydrogel rapidly swelled and was allowed a total of 100 minutes at the specific temperature. Then it was deswelled by immediate transfer to water of 60 °C (above its LCST) for five consecutive 20-minute intervals. From Figure 4-36, a difference between the swelling and deswelling rates of the material was observed. The swelling rate at 20 °C was faster than the deswelling rate at 60 °C. This may be explained by the fact that the already swollen gel has higher free-volume and thus water molecules can easily pass through the material, increasing the water diffusivity. When the hydrogel rapidly deswells at 60 °C, the hydrogel structure collapses and inevitably the free volume decreases, resulting in increased resistance to mass transfer, thus making it difficult for sorbed water molecules to pass through the shrunken outer layer of the hydrogel. This explains why the transport of water molecules is faster in the swelling cycle than in the deswelling cycle. The visual appearance of the hydrogel films changed when transferred between temperatures below and above its LCST. Not only did the films almost instantly change from transparent to opaque after transfer, but the films also floated to the top of the reaction vessel at 60 °C where it sunk to the bottom at 20°C. This behaviour can be rationalized by bearing in mind the principles of the LCST transition. The LCST is induced by a specific balance between hydrophilicity and hydrophobicity within the copolymer system. When the temperature is increased above the critical solution temperature, this balance is altered and ultimately hydrophobic interactions dominate, inducing a coil-to-globule transition, rendering the system more hydrophobic. The physical effect thereof on the hydrogel material is that the material shrinks and thus less light is transmitted through the collapsed

structure, rendering it an opaque, white colour. The collapse also results in any embedded water to be expelled due to the breaking of hydrogen bonds present between the hydrophilic segment of the copolymer and the surrounding water molecules with an increase in temperature. The expelling of water and collapse of polymer chains renders the material more hydrophobic, thus causing it to float to the surface of the reaction vessel.

As previously discussed, the swelling behaviour of the hydrogel materials are significantly influenced by the amount of incorporated PDMS. In Figure 4-36 above, two samples with varying amounts of PDMS were analysed for their reversible thermo-responsiveness. The overall degree of swelling of the higher PDMS content sample is less than that of the lower PDMS content sample. Furthermore, the incorporation of PDMS allows for the alteration of the material's hydrophobicity, where increased PDMS incorporation results in decreased swelling due to increased non-swellable, hydrophobic domains within the copolymer structure. Although to a lesser extent for the higher PDMS sample, both samples exhibited hydrogel properties as well as reversible thermo-responsive behaviour.

4.8. Static contact angle (SCA) measurements

The static contact angle (θ) between the surface of the liquid and the outline of the contact surface, is a measure of the wettability of a solid by a liquid and therefore serves as an indication of a surface's hydrophilicity/hydrophobicity. The hydrophobicity of the copolymers was evidently altered by the incorporation of varying amounts of PDMS. The PDMS chain length did not only have an observable effect on the appearance of the hydrogel materials, but also a significant effect on the degree of hydrophobic alteration. Figure 4-37 shows the instantaneous SCA of all copolymer samples in film and fibre form. It is evident from the plotted data that there is a significant difference in the SCA of the bulk films versus their corresponding hydrogel fibres. In all cases, the fibres had a much larger instantaneous SCA when compared to the films. This may be due to the characteristic large surface-to-volume ratio of the fibres, as well as the contribution of interstitial air-filled spaces between fibres and the applied water droplet. This resulted in decreased initial wetting of the fibres. Additionally, the large initial SCA may be attributed to the low surface tension of PDMS, which causes it to segregate to the material's surface and render the surface more hydrophobic. The surface segregation of PDMS is possibly the main contributing factor since both films and fibres of all samples displayed increased instantaneous SCA with increased PDMS content.

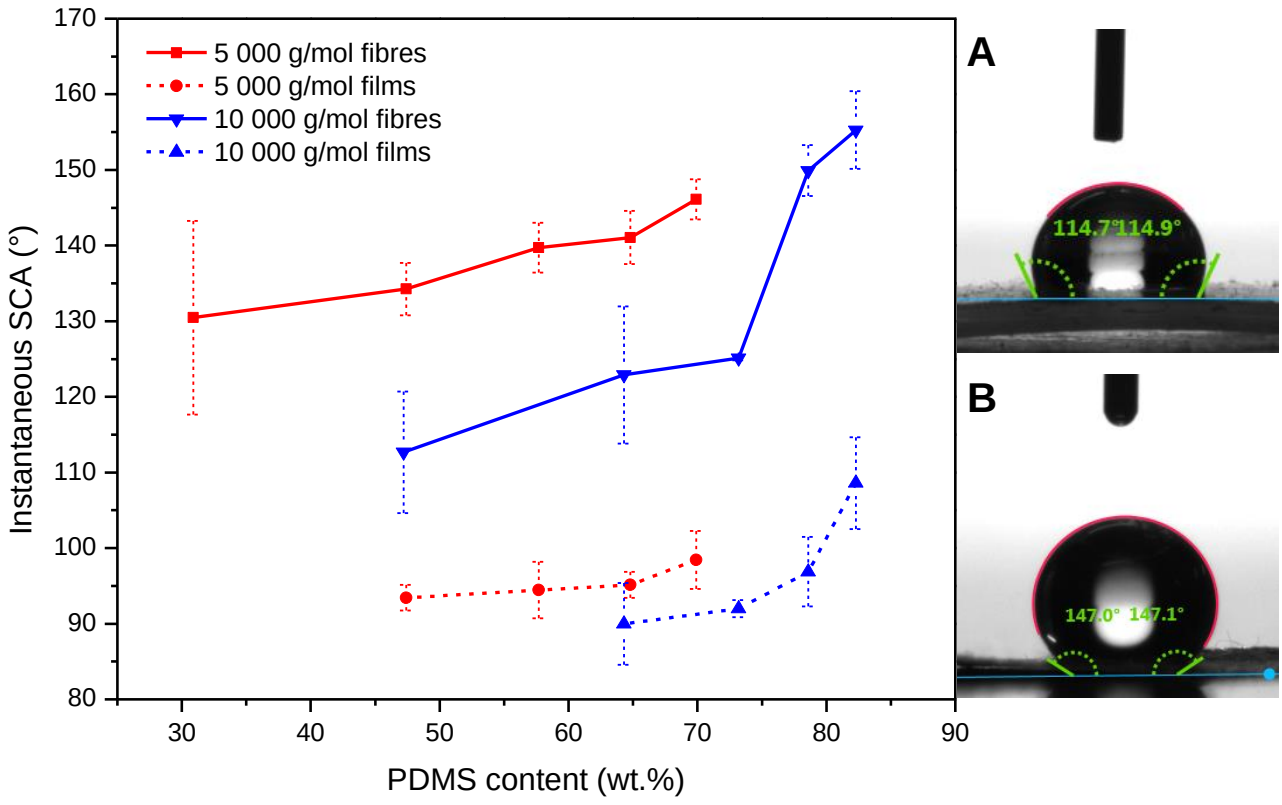

Figure 4-37: Instantaneous SCA (°) as a function of PDMS content (wt.%) for films and fibres of both copolymer series (25 °C, 45% r.H.). Illustration of the SCA determination of a droplet on (A) the film surface and (B) the fibre surface.

Figure 4-37 shows that in all cases, the addition of water to the fibre surface presented surprisingly large instantaneous SCA of >110°, resembling that of a highly hydrophobic surface. All film samples

are also by definition considered hydrophobic since they display contact angles above 90°. A slight increase in initial SCA can be seen for the 5000 g/mol PDMS film series with increasing PDMS content. For both the films and fibres of the 10 000 g/mol PDMS samples a much more dramatic increase in initial SCA with increasing PDMS content occurs. This may be related to the chain length of the included PDMS, where small increases in the amount of PDMS have a large effect on the effective physical crosslinking within the polymer network. This hypothesis is supported by the greatly enhanced physical properties and slightly lower overall swelling capabilities of the 10 000 g/mol samples as a function of PDMS content, compared to the 5 000 g/mol PDMS series.

Figure 4-38 shows the decay in SCA as a function of time on the various fibre surfaces. From the plotted data, there is an evident difference in the SCA decay over time when comparing the low to high PDMS content fibre samples of both copolymer series. Wetting of the low PDMS content fibre surfaces occurred much more rapidly and displayed a much faster decrease in SCA, as these samples are inherently more hydrophilic than their high PDMS content counterparts.

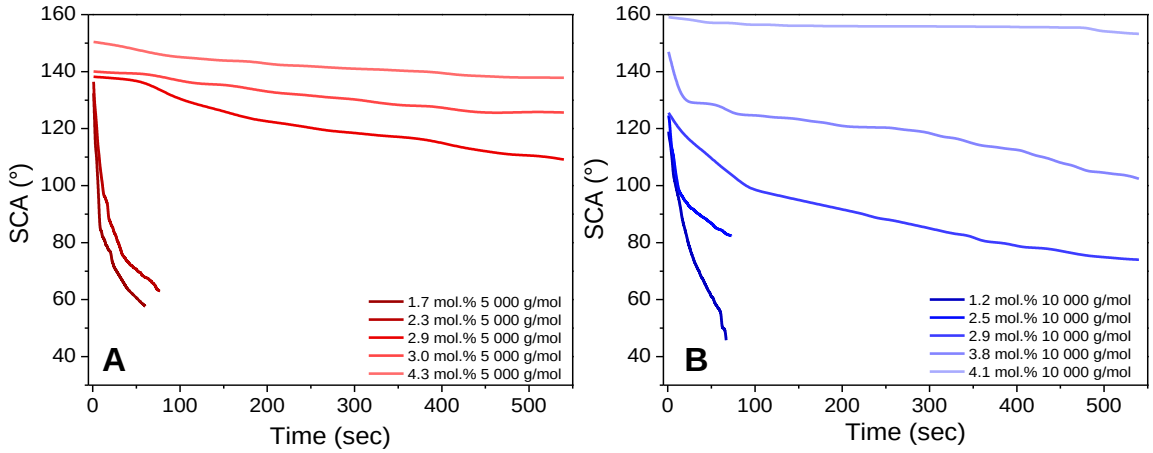

Figure 4-38: SCA (°) decay over time for (A) 5 000 g/mol PDMS fibre samples and (B) 10 000 g/mol PDMS fibre samples (25 °C, 45% r.H.).

Figure 4-39 shows the decay in the SCA on the 2.3 mol.% 5 000 g/mol PDMS fibre sample surface over time. The SCA of the low PDMS content fibre samples of both copolymer series decrease by about 55% within 90 seconds, after which the fibre surface was completely wetted. As PDMS content is increased, the initial SCA is also increased and an observable decrease in the rate of SCA decay is apparent. High 10 000 g/mol PDMS content samples display almost superhydrophobic characteristics with initial SCA of >150 °. The initial contact angle of the highest PDMS content fibre samples of both copolymer series decreased by less than 10 ° after 9 minutes. These materials do, however, still display hydrogel properties when completely wetted, thus making these materials interesting candidates for applications where the initial hydrophobic behaviour of the materials may be manipulated by varying PDMS content and sample preparation.

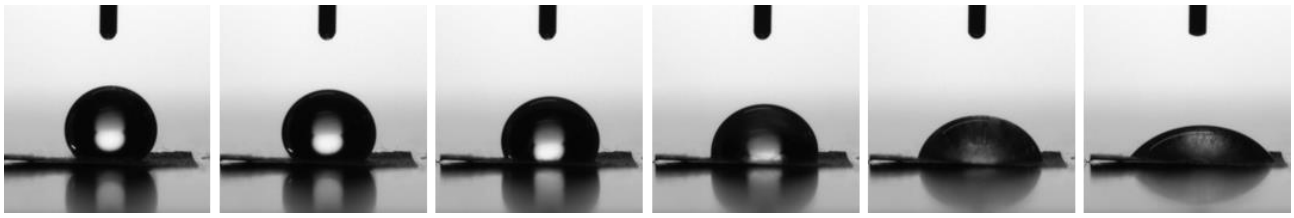

Figure 4-39: An illustration of the decrease in SCA over 90 seconds on the surface of the 1.7 mol.% (30.9 wt.%) 5 000 g/mol PDMS fibre mat (25 °C, 45% r.H.).

Figure 4-40 shows the decrease in SCA of the film samples of both copolymer series as a function of time. There is a much more gradual, almost linear decline in the contact angles of the film surfaces. As with the fibre samples, the rate of SCA decay on the low PDMS content film samples of both copolymer series is faster than that of the high PDMS content film samples. This is due to the increased hydrophobic PDMS content within the copolymer which resulted in increased overall hydrophobicity of the sample surface due to the surface segregation of PDMS.

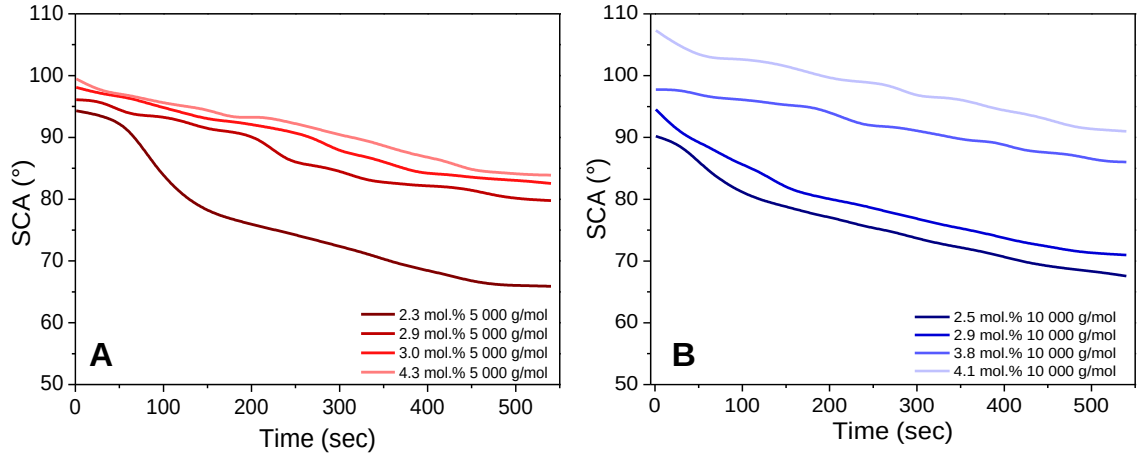

Figure 4-40: SCA (°) decay over time for (A) 5 000 g/mol PDMS film samples and (B) 10 000 g/mol PDMS film samples (25 °C, 45% r.H.).

The large difference in initial SCA of the fibres compared to the films can be rationalized by considering the physical form and solid-state morphology of the samples. By now it has been thoroughly verified that the surface segregation of PDMS is the main contributing factor to the apparent increase in initial SCA as a function of PDMS content in both film and fibre samples. Therefore, the initial SCA of the fibres is evidently much larger than that of the film equivalents due to the high-surface-to-volume ratio and air-filled interstitial spaces between the fibres that act as a preliminary impediment between the hydrophilic segments of the material and the water droplet. No such barrier exists for the film equivalents, resulting in a smaller initial SCA since some of the hydrophilic segments are in direct contact with the applied droplet.

4.9. Reference

1 J. F. Lutz, *J. Polym. Sci. Part A Polym. Chem.*, 2008, **46**, 3459–3470.

2 M. J. Owen, in *Encyclopedia of Materials: Science and Technology*, Elsevier, 2004, pp. 2480–2482.

3 Wako, *Azo Polymerization Initiators Comprehensive Catalog*, Wako Pure Chamical Industries, Ltd., 2016.

4 S. Wagenaar, Stellenbosch : Stellenbosch University, 2017.

5 K. Ito and S. Kawaguchi, in *Branched Polymers I*, Springer Berlin Heidelberg, Berlin, Heidelberg, 1999, pp. 129–178.

6 P. F. Rempp and P. J. Lutz, in *Comprehensive Polymer Science and Supplements*, Pergamon, 2012, pp. 403–421.

7 A. Siewing, B. Lahn, D. Braun and H. Pasch, *J. Polym. Sci. Part A Polym. Chem.*, 2003, **41**, 3143–3148.

8 G. M. Bayley and P. E. Mallon, *Polymer (Guildf).*, 2012, **53**, 5523–5539.

9 A. C. Sutherland, Stellenbosch : University of Stellenbosch, 2010.

10 M. Swart and P. E. Mallon, in *Pure and Applied Chemistry*, 2009, vol. 81, pp. 495–511.

11 R. Fleet, E. T. A. Van Den Dungen and B. Klumperman, *Macromol. Chem. Phys.*, 2011, **212**, 2191–2208.

12 T. Ohshima, Y. Hayashi, K. Agura, Y. Fujii, A. Yoshiyama and K. Mashima, *Chem. Commun.*, 2012, **48**, 5434–5436.

13 A. C. M. Kuo, in *Polymer Data Handbook*, ed. J. E. Mark, Oxford University Press, New York, 2nd edn., 2009, pp. 539–561.

14 F. Ganji, S. Vasheghani Farahani and E. Vasheghani-Farahani, *Iran. Polym. J.*, 2010, **19**, 375–398.

15 Z. Xia, M. Patchan, J. Maranchi, J. Elisseeff and M. Trexler, *J. Appl. Polym. Sci.*, 2013, **127**, 4537–4541.

16 C. Nakamoto, T. Kitada and E. Kato, *Polym. Gels Networks*, 1996, **4**, 17–31.

17 L. R. G. Treloar, *The Physics of Rubber Elasticity*, Oxford University Press, Oxford, UK, 3rd edn., 1975.

18 A. Gestos, P. G. Whitten, G. M. Spinks and G. G. Wallace, *Soft Matter*, 2010, **6**, 1045–1052.

19 F. Meltz, Stellenbosch University, 2014.

20 M. H. A. Zanin, N. N. P. Cerize and A. M. de Oliveira, in *Nanocosmetics and Nanomedicines*, 2011, pp. 311–332.

21 D. Kai, M. P. Prabhakaran, B. Stahl, M. Eblenkamp, E. Wintermantel and S. Ramakrishna, *Nanotechnology*, 2012, **23**, 095705.

Chapter 5

Conclusions & Recommendations

5.1. Conclusions

5.1.1. Overall conclusion

The thermo-responsive *N*-isopropyl acrylamide (NIPAM) monomer was copolymerized via the grafting-through with poly(dimethyl siloxane) (PDMS) in an attempt to synthesize novel physically crosslinked amphiphilic copolymers for the fabrication of solution processible hydrogel materials. PDMS macromonomers of varying chain lengths were investigated and it was found that macromonomers of 5 000 g/mol and 10 000 g/mol yielded the most interesting and useful physical properties. A series of copolymers containing various amounts of these macromonomer lengths were investigated for their hydrogel as well as thermo-responsive behaviour. Comprehensive molecular weight data could be obtained by AF4 analysis, allowing the detailed characterization of these copolymers in solution. The range of coupled detectors allowed for the determination of absolute molecular weights varying between 53 000 and 280 000 g/mol with dispersity values ranging between 1.1 and 1.8. Successful copolymerization and macromonomer incorporation were confirmed by ATR-FTIR spectroscopy and quantified by ^{1}H-NMR spectroscopy. ^{1}H-NMR kinetic studies allowed for monitoring of monomer consumption throughout homopolymerization reactions as well as PDMS incorporation during the copolymerization reaction. It was found that NIPAM was the more reactive comonomer. NIPAM reactivity was reiterated by HPLC analysis which revealed that both PNIPAM homopolymer and PNIPAM-*g*-PDMS copolymer was present within samples, with the PNIPAM homopolymer fraction diminishing with increasing PDMS content within the copolymer. Increased PDMS content resulted in longer retention times during analysis which correlated well with the increased hydrophobic character of the copolymer.

Copolymerization with hydrophobic PDMS macromonomer proved to be an effective means of physical crosslinking for the production of water-insoluble hydrogel materials. The materials were optically transparent when dry and ranged from brittle to rubber-like with increasing PDMS content. The materials were readily soluble in certain organic solvents such as THF, chloroform, DCM, and MEK, yet remained insoluble in water and hexane. The non-covalent or physical crosslinked system and the sufficiently high molecular weights rendered these copolymers suitable for solution processing. Hydrogel fibres of these copolymers were fabricated by the electrospinning technique for the first time. Fibre diameters ranged from 2.6 to 6.9 µm. The micron-scale fibre diameters were attributed to the high viscosity of the spinning solution as well as the relatively low voltage applied to the electrospinning process. Although fibre diameters increased with increasing PDMS content, the fibre diameter distribution decreased due to the higher PDMS content fibres being less brittle and more uniform in shape and size. Moisture exposure experiments in varying humidity conditions showed that low PDMS content samples mostly retained their fibrous structure over the range of humidity conditions but did show some swelling at 95% r.H. The high PDMS content samples swelled to a much lesser extent than the low PDMS content equivalents. Swelling in water for the films

occurred relatively fast and reached 50% saturation within 10 to 15 minutes. The fibres, however, swelled at a very rapid rate, some swelling nearly 115% after only 1 to 2 minutes in water. While most of the films remained structurally stable after repeated swelling cycles, the fibre equivalents lost their fibrous structure and fused together after deswelling. All dry film and fibre surfaces were determined as hydrophobic as static contact angle (SCA) measurements showed that all copolymers had an instantaneous contact angle exceeding 90°. The SCA increased as a function of PDMS content. This highlighted the material's capability for tunable hydrophobicity. The instantaneous contact angles of the fibres were much greater than those of the films, although the SCA decay over time of the fibre surfaces generally occurred at a faster rate than the film equivalents.

A combined approach of swelling and water stability testing, thermo-response studies, FE-SEM, and optical microscopy was used to investigate the morphology of the system, specifically in terms of phase segregation of the PDMS domains. The swelling studies showed that as PDMS content in the copolymers is increased, the degree of swelling in the non-polar hexane increased. From the hexane swelling data, it was shown that in low PDMS content samples the PDMS domains were mostly present in isolated clusters. The physical appearance of the materials changed as a function of PDMS content from brittle to more rubber-like while also increasing the overall hydrophobic character of the material. This highlighted the enhanced phase segregation of the hydrophobic PDMS domains. The differences in the solid-state morphologies were mainly ascribed to the sample preparation methods, even though solvent effects play an important role in the copolymer's solution behaviour. Large differences exist in the stability and swelling behaviour of the materials as films and fibres. This may be ascribed to the time permitted for molecular rearrangement and effective domain formation during the two sample preparation techniques.

All materials displayed thermo-responsive behaviour in water. This was characterized by shrinkage and change in physical appearance from transparent to opaque. The films showed reversible thermo-responsiveness after several temperature cycles. The lower critical solution temperature (LCST) in water was determined by the OptiMelt apparatus for all copolymers in the film and fibre form and ranged between 26 and 31 °C. It was determined that although complex, the incorporation of PDMS had an effect on the LCST of the copolymers, which were in all cases lower than that of the water-soluble PNIPAM homopolymer. It was also observed that the LCST values of the fibres were higher than that of their film equivalents.

Finally, the key objective was to produce a *smart* hydrogel capable of responding to surrounding temperature variations while also presenting the option for tunable hydrophobic character. Not only did these materials display thermo-responsive behaviour but were also solution-processable and allowed for the production of microfibre hydrogels. Hydrophobicity of the material could be altered by varying the amount and chain length of PDMS incorporated, as well as the physical form of the material i.e. film or fibre. These novel materials proved to be highly functional and will likely be useful in a variety of practical applications.

5.1.2. Conclusion on morphology:

The morphology, specifically the phase segregation of the PDMS domains of the system was investigated by a combined approach of swelling and water stability testing, thermo-response studies, FE-SEM, and optical microscopy. A clear trend was observed when considering the water stability and swelling experiments done on these materials. Copolymerization of PNIPAM with PDMS macromonomers of varying lengths resulted in a physically crosslinked phase segregated system. The amount of PDMS inclusion, as well as the sample preparation technique, had a significant effect on the domain formation. It was necessary to relate the physical properties of the copolymer materials to the structure thereof. Increased incorporation of PDMS resulted in less brittle, rubber-like transparent materials with overall improved physical properties. The improved physical appearance and water stability of the materials were ascribed to the effective physical crosslinking provided by the intra- and interpolymer hydrophobic domain formation induced by the PDMS side-chains. The increased PDMS content did, however, affect the degree of water swelling. It resulted in increased apparent crosslink density and thus decreased equilibrium swelling. Higher PDMS inclusion and longer side-chain lengths resulted in the formation of larger and more defined non-swellable hydrophobic domains. Therefore, high PDMS content samples displayed a greater degree of swelling in non-polar hexane than their low PDMS content counterparts. This again emphasized the presence of a more phase segregated system with enhanced hexane-swellable domains.

Although the processing solvent plays an important role in the solution behaviour of these copolymers, sample preparation methods were determined to be the main contributing factor to the differences in the induced solid-state morphologies. Large differences exist in the stability and swelling behaviour of the materials in the form of films and fibres. This may be ascribed to the time allowed for molecular rearrangement and effective domain formation during the two sample preparation techniques. The low water stability and greatly enhanced swelling abilities of the nanofibres compared to the film equivalents prepared from the same solvent was ascribed to the electrospinning process. During the electrospinning process, a charged polymer solution is rapidly extruded, causing drawing of the polymer chains and rapid solvent evaporation. This process does not afford much time for molecular rearrangement and effective domain formation. Thus, the resulting material has a lower apparent crosslink density and enhanced swelling capabilities. Rapid swelling in water and ineffective crosslinking resulted in decreased water stability and ultimately fibre fusion occurred.

Conversely, films of the same material cast from the same solvent were much more dimensionally stable. Although low PDMS content films were brittle and produced weak swollen hydrogels, small hydrogel shapes could still be obtained for effective swelling measurements. As PDMS content increased, physical properties and water stability drastically improved. This was ascribed to more effective domain formation attributed to the time allowed for molecular rearrangement during slow solvent evaporation. Enhanced physical properties were attributed to large, more defined domains

and resulted in increased apparent crosslink density. This consequently resulted in decreased swelling capabilities of these materials in water, as a function of PDMS content. Effective domain formation was reiterated by the improved hexane swelling capabilities of the high PDMS content film samples compared to the low PDMS content samples.

As discussed and demonstrated throughout this work, the solution behaviour of graft copolymers is substantially more complicated than well-defined block copolymers. A variety of morphologies and aggregated structure may exist within a single sample. Therefore, the purpose of this work was not necessarily to visualize or isolate the domains responsible for the physically crosslinked system, but rather to rationalize the material's thermo-responsive hydrogel abilities based on the physical properties while bearing in mind domain size and distribution.

5.2. Recommendations

The investigation of the material's thermo-responsive and hydrogels properties provided a basic understanding of the material's solid-state morphology. The next step would be to investigate phase segregated domains within the differently prepared samples by solid-state NMR, advance confocal microscopy and small-angle X-ray scattering (SAXS).

Preliminary DSC and TGA experiments were conducted, however, the interpretation thereof proved to be challenging and thus more comprehensive techniques such as temperature modulated DSC and DMA should be explored. This would allow for detailed thermal analysis and detection of potentially overlapping thermal transition.

AF4 channel-based fractionation proved to be a comprehensive analytical technique and provided valuable information. Method optimization of this technique, as well as exploring the possibility of thermal field flow fractionation (TFFF) techniques may provide valuable information regarding the solution behaviour of these copolymers.

The biocompatible nature of these copolymers should be assessed in order to explore the field of biomedical applications, such as drug delivery systems in the form of topical applications. The thermo-responsive and amphiphilic nature of these materials are desirable traits in various drug delivery systems. Thus, drug loading and release studies would be highly beneficial to determine the feasibility of these materials in such applications. Mechanical testing of the materials should be conducted to assert the viability of these materials as functional hydrogels.

Electrospraying of low solution concentrations allowed for the production of particles. The effect of different solvents and preparation conditions may be explored for particle optimization which may also be applied for interesting applications.

The viability of the fused fibre membranes could be explored as thermo-responsive porous membranes for applications such as cell culture substrates. The use of thermo-responsive hydrogel materials for cell culture is often reported and this may be an interesting option for such applications.

The easily altered hydrophobic nature of the material make it suitable for a wide range of applications. Especially in the case of the fibres where it initially presented a highly hydrophobic surface after which hydrogel character was observed.

Atomic force microscopy (AFM) in a temperature-controlled solution cell would be the ideal technique for the visualization of individual fibres in their swollen state at different temperatures. This will allow detailed characterization and the fibres' thermo-responsive behaviour.

Challenges encountered throughout this study may be ascribed the uncontrolled free radical polymerization used to produce these graft copolymers with undefined grafting densities and amphiphilic character. Therefore, controlled polymerization techniques such as ATRP or SET-LRP

could be explored and potentially compared to the current system for the production of the optimum physical hydrogel materials.

These copolymers displayed thermo-response behaviour in water, however, co-nonsolvency may occur in certain solvent combinations, this opens up a whole new avenue for exploration.

Finally, it is clear that although some degree of fibre stability when swollen was achieved by the inclusion of the PDMS, overall the materials formed weak hydrogel fibres. For the production of fibres with a higher degree of dimensional stability during swelling, some additional crosslinking may be needed. In the case of electrospun fibres this implies that some post-electrospin crosslinking is necessary. This would be an interesting study since such hydrogel fibres would be highly amphiphilic in nature with the addition of tunable hydrophobicity based on PDMS content. These materials may also offer the opportunity for inclusion of hydrophobic compounds within the PDMS domains which may have interesting possibilities in for example drug delivery applications.

Appendix

Appendix

4.2.2. ^{1}H-NMR

Determination of the mole fraction of PDMS in each sample by the appropriate peak integrations:

$$mol.\%\ PDMS = \frac{\left(\frac{Peak\ integral}{Number\ of\ protons\ associated}\right)^{PDMS}}{\left(\frac{Peak\ integral}{Number\ of\ protons\ associated}\right)^{PDMS} + \left(\frac{Peak\ integral}{Number\ of\ protons\ associated}\right)^{Acrylamide}}$$

Table A-1: Example of actual PDMS content using ^{1}H-NMR peak integrations of three 1 000 g/mol PDMS samples with varying amounts of PDMS in the feed ratio.

Sample	mol. % PDMS in feed	Acrylamide peak integral [a]	Number of protons associated [b]	PDMS peak integral [c]	Number of protons associated [d]	Actual PDMS content	mol.%
1KDa_3%	3	1	6	0.41	70	0.0339	3.4
1KDa_5%	5	1	6	0.57	70	0.0466	4.7
1KDa_8%	8	1	6	1.03	70	0.0811	8.1

[a] Acrylamide peak integral of the peak found at 1.2 ppm.

[b] Number of associated protons refers to the 6 isopropyl protons of the acrylamide.

[c] PDMS peak integral of the peak found at 0.1 ppm.

[d] Number of associated protons refers to the calculated ^{1}H-NMR peak integral of the pure macromonomer (600 MHz, $CDCl_3$) and refers to the methyl protons attached to the siloxanes.

.4.1. General swelling behaviour

Water-swellable fraction (Q_s):

$$Q_s = \left(\frac{Q-1}{1-wt.\%\ PDMS}\right) + 1$$

Hexane-swellable fraction (Z_s):

$$Z_s = \left(\frac{Z-1}{wt.\%\ PDMS}\right) + 1$$

Appendix

4.4.2. Crosslink density

Calculation of polymer volume fraction using the following equation:

$$v_p = \frac{\rho_{\text{polymer}}}{[(Q_s - 1)\rho_{\text{water}}] + \rho_{\text{polymer}}}$$

Where Q_s values are listed, PNIPAM density (ρ_{polymer}) of 1.116 g/cm^3 and water density of (ρ_{water}) 1.0 g/cm^3 (at ambient conditions).

4.7. Thermo-responsive behaviour and lower critical solution temperature (LCST)

Method 1:

1. Apparatus and set-up:

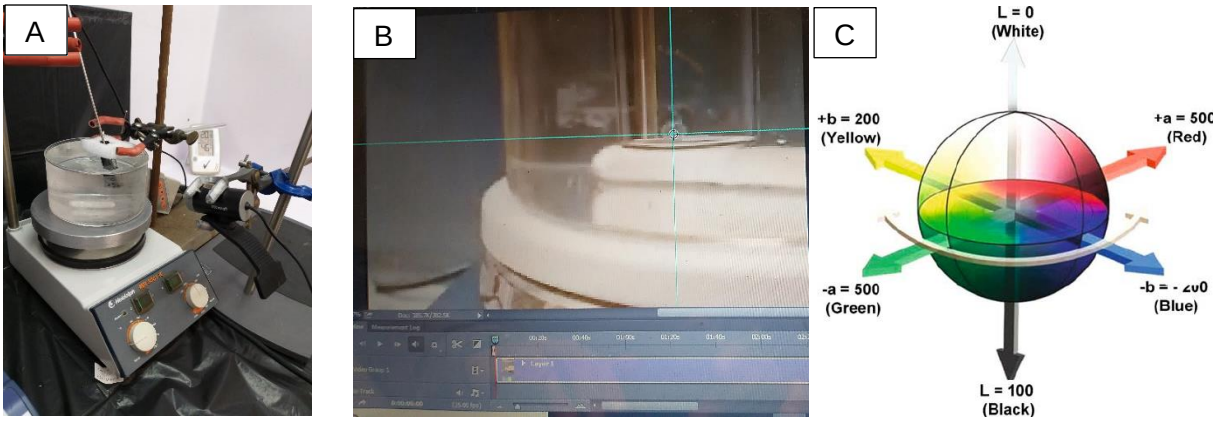

Figure A-1: (A) Set-up containing of water bath, heating and stirrer plate, digital thermometer, and digital camera. (B) Selection of a single pixel on the hydrogel image at temperatures well below the LCST, using image processing software. (C) Illustration of the L-value used to plot the transition from transparent to opaque in the hydrogel materials.

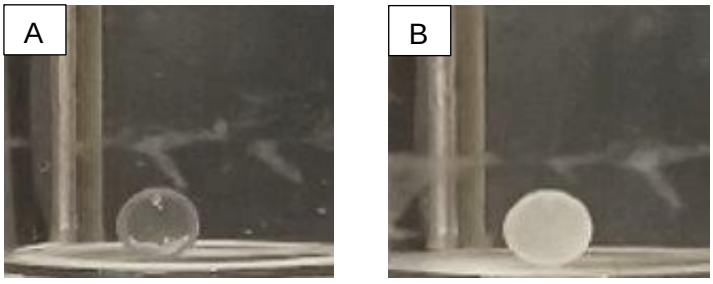

Figure A-2:Digital images of a hydrogel sample (2.9 mol.% 5 000 g/mol PDMS) in water and digital thermometer below (A) and above (B) the LCST value.

2. Data processing:

The *L*-value obtained by Method 1 was plotted against temperature. This produced an S-shaped curve of which the second derivative of its fitted curve was taken. The second derivative allowed the determination of the curve's inflection point which was identified as the LCST of the specific sample.

Appendix

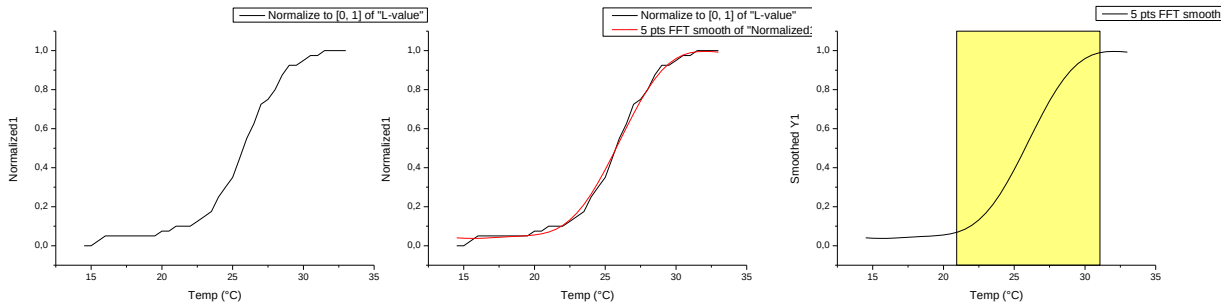

Figure A-3 Fitted S-shaped curve and highlight derivation region of the 4.3 mol.% 5 000 g/mol PDMS hydrogel sample.

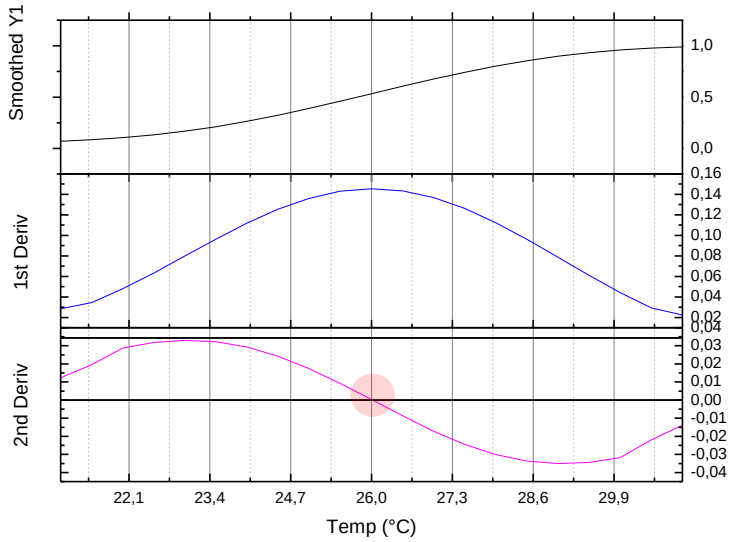

Figure A-4: The second derivative of the S-shaped curve in Figure 3. The inflection point of is highlighted and identified as the LCST in water of the 4.3 mol.% 5 000 g/mol PDMS hydrogel sample.

Appendix

Method 2:

1. Apparatus and set-up:

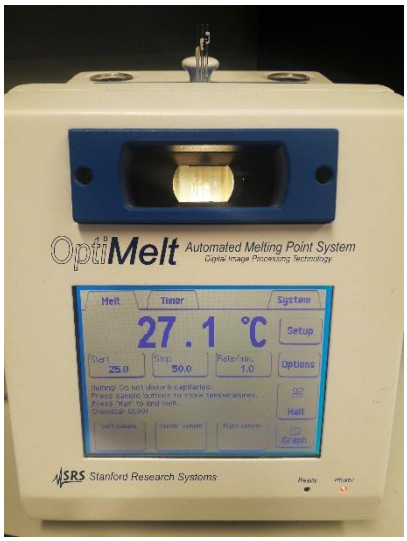

Figure A-5: SRS OptiMelt apparatus with three samples in glass capillaries inserted at the top.

2. Data processing:

The apparatus produced a spectroscopicaaly generated curve which was sigmoidal fit using a Boltzmann fit and the following equation:

$$y = A2 + \frac{A1 - A2}{1 + e^{\left(\frac{x-x0}{dx}\right)}}$$

The LCST value for each sample was selected as the midpoint of the curve, while the first derivative of the fitted curve was used to determine the FWHM. The FWHM served as temperature transition range.

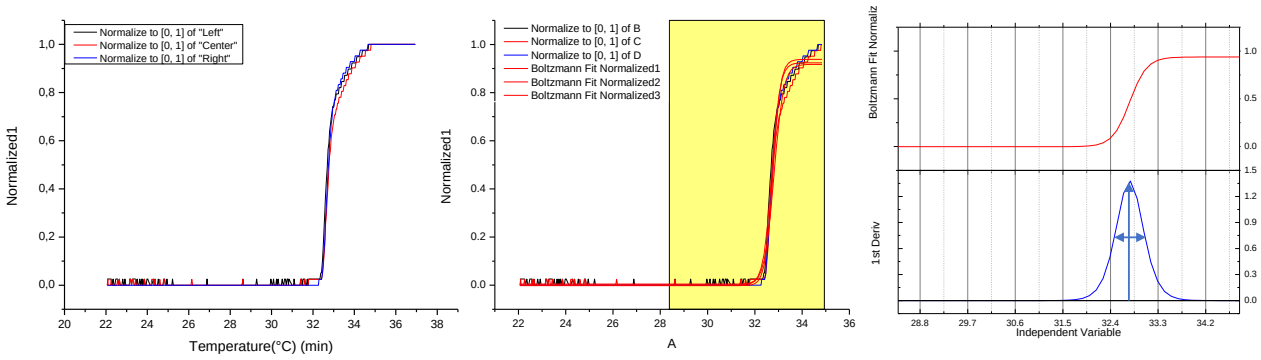

Figure A-6: Boltzmann fitted curves, highlighted derivation region and first derivative of three PNIPAM homopolymer samples in water.

Appendix

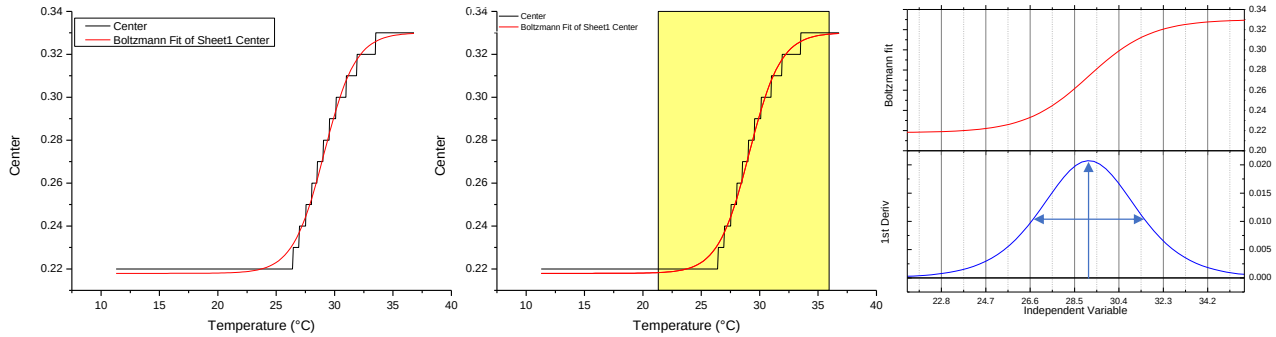

Figure A-7: Boltzmann fitted curve, highlighted derivation region and first derivative of a copolymer sample (2.3 mol.% 5 000 g/mol PDMS) in water.

Table A-2: Summary of the LCST values obtained from the OptiMelt method as well as the curve fitting parameters (R^2) and the full width at half maximum (FWHM).

		Method 2					
	LCST (°C)	**Films**	**R^2**	**FWHM**	**Fibres**	**R^2**	**FWHM**
	PNIPAM	**32.4**	0.996	± 0.3	-	-	-
5 000 g/mol series	1.7 mol.%	29.2	0.995	± 0.6	30.4	0.995	± 1.2
	2.3 mol.%	27.9	0984	± 1.0	30.8	0.984	± 2.0
	2.9 mol.%	28.0	0.997	± 2.8	30.7	0.983	± 1.2
	3.0 mol.%	28.7	0.998	± 2.3	29.5	0.992	± 1.3
	4.3 mol.%	26.7	0.997	± 2.9	29.8	0.997	± 1.6
10 000 g/mol series	1.2 mol.%	27.7	0.971	± 2.3	30.7	0.989	± 1.1
	2.5 mol.%	28.4	0.996	± 3.0	30.8	0.996	± 0.6
	2.9 mol.%	28.8	0.996	± 1.8	30.6	0.989	± 0.8
	3.8 mol.%	28.9	0.993	± 2.9	31.3	0.993	± 4.5
	4.1 mol.%	28.5	0.995	± 2.9	31.2	0.993	± 6.9